

Authors' response to Anonymous Referee #1:

We, the authors, are very thankful for the detailed and constructive comments and greatly appreciate the willingness to review our manuscript. Please find our responses below. The original comments are shown in **bold** with the respective answers below. Excerpts of the manuscript are shown in *italic writing*, whereas additions are written in **blue** and deleted parts in **red**.

Please note that the format of citations in manuscript excerpts might be changed.

Thank you very much for your efforts,

Jannik Schottler on behalf of all authors

---

1)

**Main comment is on the impact to loads. In the introduction, and later in the paper, references to past literature documenting that there is a connection between velocity increments and loads, but the nature of the connection is not elaborated on. Could some of the findings of those papers be summarized for context? For example, are the impacts more important for fatigue loads or extreme loads? In the companion paper, figure 11 shows a reduction in TKE during wake steering. If one is considering wake steering, to what extent would a reduction in TKE counter-balance a change in increment velocity? Is there a method to weigh these two changes? Is there a connection to loads on specific components (blades, drivetrain) or failure modes? Details in this regard would help to contextualize the findings.**

Thank you very much for this constructive comment. We want to answer the different aspects separately, for better clarity. Afterwards, we give some more details for completeness of the discussion.

**In the introduction, and later in the paper, references to past literature documenting that there is a connection between velocity increments and loads, but the nature of the connection is not elaborated on. Could some of the findings of those papers be summarized for context?**

To what extent intermittent characteristics of atmospheric turbulence transfer to turbine data such as torque, moments, power, etc has been investigated experimentally and numerically. Details are subject of discussion within the research community, however, relevant studies are summarized here: Milan et al. [9] analyzed power data of full scale wind turbines and of a whole wind farm, finding heavy-tailed power increments on time scales of the order seconds, suggesting intermittency is transferred from wind to power. In a wind tunnel experiment using an active grid and a model wind turbine [1], we showed that non-Gaussianity of velocity increments was transferred to power, torque and thrust data of the model turbine on the lab scale (that is the same model wind turbine as denoted *ForWind* turbine in the manuscript).

In a numeric study, Mücke et al. [10] found that intermittent flow conditions result in similarly intermittent torque increments using FAST [11] in combination with Aero-

Dyn [12]. In the manuscript, we suggest to summarize this in the introduction:

p.2, ll.25 ff:

*[...]. To what extent statistical characteristics of velocity increments are transferred to wind turbines is of current interest throughout the research community [14]. ~~We Schottler et al. [1] found a transfer of intermittency from wind to torque, thrust and power data in a wind tunnel experiment using a model wind turbine. Similarly, Mücke et al. [10] found a transfer of intermittency to torque data using a generic turbine model. Milan et al. [9] reported intermittent power data in a full-scale wind farm. We thus believed that distributions of velocity increments in wakes are of importance for potential downstream turbines as ~~extreme events non-Gaussian characteristics~~ are likely to be transferred to wind turbines in terms of fluctuating loads and power output. ~~Studies show this for a generic turbine model [10], in a wind tunnel experiment [1] and by analyzing field data of a full-scale wind farm [9]. Those findings make an investigation of~~ Consequently, investigations of velocity increments in wakes become extremely relevant for active wake control concepts as well as for wind farm layout approaches. A further elaboration on the connection of non-Gaussian velocity increments and loads as well of power fluctuations is given in Section 4. This work is organized as follows. [...]~~*

**For example, are the impacts more important for fatigue loads or extreme loads?**

Despite the above findings (intermittency is transferred to turbine data), the question remains to what extent intermittent, non-Gaussian force statistics influence common ways to calculate fatigue and extreme loads. Berg et al. [15] reported a vanishing effect of non-Gaussian turbulence on extreme and fatigue loads based on an LES wind field in combination with HAWC2 [16]. However, in numeric studies the challenge is to generate synthetic wind field featuring correct statistics of both, velocity increments and velocity values. At ForWind, we use the Continuous Time Random Walk (CTRW) model, which is known e.g. from electron transport and molecular movement, in combination with LES to generate synthetic wind fields. An early version of this approach was used in [10], showing insignificant effects. Recent improvements allow for a more realistic generation of synthetic wind fields in the sense of one- and two-point statistics. Those wind fields were used by Schwarz et al. [17] in combination with a Blade Element Momentum approach and the NREL 5MW reference turbine in order to quantify the effects of non-Gaussian velocity increments on fatigue load calculations. Figure 1 shows the equivalent fatigue loads based on a rainflow counting. Results should be seen as preliminary and are taken from [17].

Clearly, the inflow conditions featuring intermittent velocity increments result in increased fatigue loads relative to the reference case featuring Gaussian statistics.

Summarizing, we believe that the non-Gaussian character of atmospheric velocity increments, on time scales affecting the rotor, do impact loads of wind turbines. However, it is important to notice that it is today not clear and a current research question, how intermittency affects common ways of load calculations (rainflow counting for example). This possibly strongly depends on details such as time scales etc. Proper numeric and experimental tools for investigations are being developed and so-

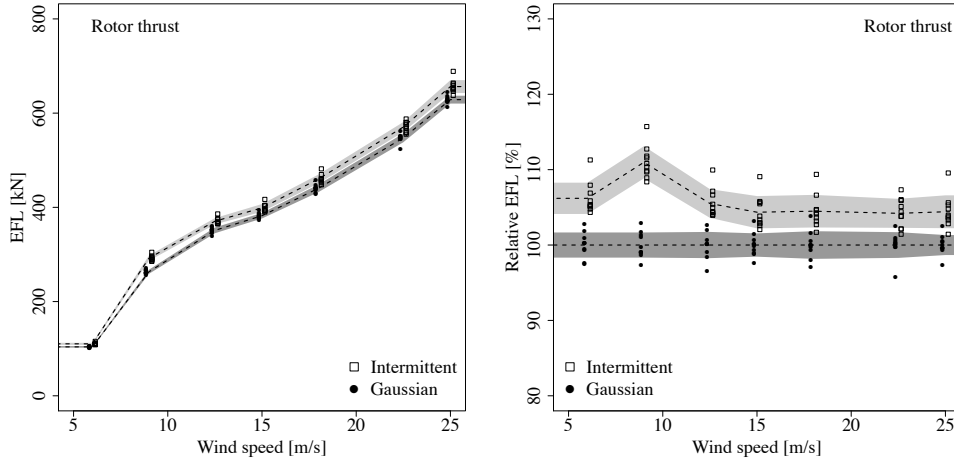


**Figure 1.** Effective fatigue loads, absolute (left) and relative (right) of the NREL 5MW reference turbine exposed to Gaussian and non-Gaussian wind fields generated with the CTRW model. Taken from [17].

phisticated studies are limited. Therefore, a complete and conclusive answer is not within the scope of this manuscript. Nevertheless, we do agree that this should be stated more clearly in the manuscript and that it should be elaborated in more detail. We suggest to update the discussion section as follows:

p.15, ll. 5 ff:

*This becomes important when assessing the applicability of active wake steering approaches, as a gain in power has to be balanced with a potential load increase, affecting maintenance costs and the lifetime of turbines overall.*

*It should be noted that it is to date not clear to what extent high TKE levels and intermittent force data are affecting common ways of fatigue and extreme load calculations. This important aspects needs to be addressed in future works. Possibly, it strongly dependents on details such as considered time scales. In our opinion, it is likely that non-Gaussian inflow is linked to drive train, gear box or pitch systems failures, especially because those inflow characteristics are not accounted for in standard models used in the design process. The velocity deficit [...]*

**In the companion paper, figure 11 shows a reduction in TKE during wake steering. If one is considering wake steering, to what extent would a reduction in TKE counter-balance a change in increment velocity? Is there a method to weigh these two changes?**

We believe that a quantification of the impact of the inflow’s TKE on e.g. fatigue loads of a turbine is a challenging tasks. To our knowledge a direct method is yet to be found. The same holds for intermittency. Thus, there is not a method to weigh both flow situations in terms of loads quantitatively. However, we do agree that some speculation about these questions can improve the discussion section of the manuscript. Please refer to the above changes (p.15,ll 5 ff).

### Further Details:

It is a well-known feature of the atmospheric boundary layer that velocity increments (time scale: order  $\sim$  seconds) feature non-Gaussian characteristics. This has been summarized in [1], Figure 2 of this reply shows a screen shot. In the wind energy con-

linked to torque fluctuations (e.g., Musial et al., 2007; Feng et al., 2013). Next, turbulent wind affects extreme and fatigue loads, which is clearly related to the lifetime of WECs (Burton et al., 2001).

Wind dynamics in the atmospheric boundary layer have been investigated extensively. Here, one has to differentiate between analyses concerning the statistics of the wind speed values and velocity increments. The wind velocities might become anomalously distributed due to large-scale meteorological events like downbursts or thunderstorms (De Gaetano et al., 2014). Velocity increments, on the other hand, statistically characterize the temporal aspect of fluctuations, whose non-Gaussian statistics are well-known from small-scale turbulence (Frisch, 1995). Active systems, like wind turbines discussed here, adapt to actual wind situations. Thus, in this paper we focus on wind speed changes within seconds, i.e., by the corresponding increments. Numerous studies have reported on non-Gaussian characteristics of wind speed increments; see, e.g., Boettcher et al. (2003), Liu et al. (2010), Morales et al. (2012), and Wächter et al. (2012). Furthermore, findings of non-Gaussian wind statistics have been implemented in simulations by a variety of methods; see, e.g., Nielsen et al. (2007), Mücke et al. (2011), and Gong and Chen (2014).

**Figure 2.** Screen shot taken from [1]. The highlightes references are [2, 3, 4, 5, 6].

text, this is of particular interest because those characteristics are not implemented in standard wind field models such as the Kaimal model, which is suggested to be used in the design process by the norm IEC 61400-1. Figure 3 shows a screen shot taken from [1], showing distributions of velocity increments of two time series, one is based on offshore measurements in the north sea (FINO1 measurement platform), the other one is based on a synthetic wind field based on the Kaimal model [7], generated in TurbSim [8]. Both time series are equal regarding mean values and turbulence intensity, however, as the graph shows, the distributions of velocity increments are not grasped correctly by the Kaimal model, which features purely Gaussian statistics. So far, it is clear that atmospheric wind features non-Gaussian increment statistics on small scales.

**Table 1.** First two statistical moments and turbulence intensities of a synthetic wind speed time series based on the **Kaimal model and offshore data (FINO1)**. Values are rounded to two decimal places.

Time series	$\langle u \rangle$ [ $\text{m s}^{-1}$ ]	$\sigma_u$ [ $\text{m s}^{-1}$ ]	TI [%]
<b>Kaimal</b>	<b>7.51</b>	<b>0.54</b>	<b>7.21</b>
<b>FINO1</b>	<b>7.50</b>	<b>0.54</b>	<b>7.18</b>

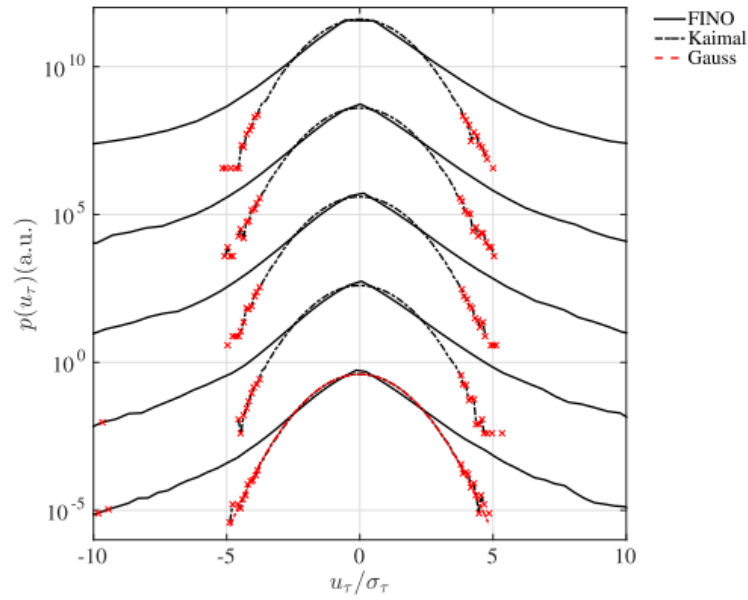


**Figure 1.**  $p(u_\tau)$  for data sets based on the **Kaimal model (dashed black line)** and for offshore measurements, conditioned so that  $\langle u \rangle = 7.5 \pm 0.5 \text{ m s}^{-1}$  (solid black). The PDFs for each scale are shifted vertically for better comparison, which is done throughout this paper. Scales from top to bottom  $\tau = \{1, 5, 10, 30, 60 \text{ s}\}$ .

**Figure 3.** Screenshot taken from [1]. FINO1 refers to offshore measurement data, Kaimal is a synthetic wind field based on the Kaimal model, generated by TurbSim.

---

2)

Could the authors elaborate further on the connections to the companion paper. Would it make sense to bring the TKE analysis of the companion paper into this paper, and move the analysis of wake position to the companion paper? Feel free to reject this suggestion if I misunderstand the distinctions between the papers, My thinking is just that, for example, if only one of the papers dealt with estimating wake position, then this could make each of the papers more focused on specific effects. But, it would also be acceptable to further elaborate on the focus of the two papers, where they overlap and where they diverge.

Thank you very much for pointing this out and adding these constructive ideas to the discussion. Generally, the idea of dividing both manuscripts is the following: This paper here compares both turbines. Therefore, the turbine is the changing variable and we limited examined cases to one downstream distance ( $6D$ ) and one inflow condition (uniform turbulence/grid). Comparing data of 2 turbines, 3 yaw angles, 2 distances and multiple inflow conditions would simply be too much for one manuscript. The means of comparison are the velocity deficit, the TKE and the intermittency parameter  $\lambda^2$ . The companion paper focuses on the impact of different inflow conditions. Therefore, the changing variable is the turbulence grid (no grid, uniform grid, shear grid) and therewith the inflow. The turbine was limited to one turbine only to keep the focus. Although both papers investigate the TKE in the wake, one main point in this manuscript is how findings are different/similar regarding both turbines, while the main point in the companion paper is how the findings change with different inflow conditions. Because of that, we would like to keep the distinctions as done in the discussion papers. However, we think it adds clarity to mention parts of this discussion in the introduction and suggest to reformulate more clearly:

p. 3, ll. 1 ff.

*This work is part of a joint experimental campaign by the NTNU in Trondheim and ForWind in Oldenburg. ~~A~~ While this paper compares the wakes behind two different model wind turbines during one inflow condition, a second paper by [18] examines the influence of varying inflow conditions on the wake of one model wind turbine.*

---

3)

Finally, the difference in rotation direction between the turbine models is very interesting. The authors use this difference to explain the asymmetries in vertical transport and tilt, could it also explain differences in displacement for positive vs negative yaw observed in the companion paper? Does the size of observed vortices vary with whether the vortex shed by misalignment is rotating in the same direction as the wake?

Thank you very much for bringing up this interesting aspect. To address the first question, Figure 4 of this document shows the results of the wake center quantification as proposed in Section 2.2 of the manuscript. The figure is the basis of Table 2 of the

manuscript. As Table 2 of the manuscript and Figure 4 of this document show, the same deflection magnitude for either direction of yaw misalignment was found for the ForWind turbine. Differences occur behind the NTNU turbine only using the method described in Section 2.2 of the manuscript. Therefore, we cannot conclude with certainty that the direction of rotation is the reason for asymmetric deflections. If that hypothesis held, one would expect that the deflections behind the ForWind turbine would be asymmetric as well but the other way round, which it is not. Consequently, one can only speculate about the reasons for the distinctions between the turbines in terms of asymmetric deflection regarding  $\gamma = \pm 30^\circ$ . Intuitively, one would assume reasons are connected to the differences amongst the turbines, being:

- blockage
- geometry (tower, nacelle)
- rotor (airfoil, rotor tips,...)

In my opinion it is important that blockage/wind tunnel effect are more influential using the NTNU turbine, especially during yaw misalignment with a wake deflection. Wind tunnel effects might play a role regarding the distinctions between both turbines shown in Figure 4 of this document.

However, the data does not allow a certain reasoning, so its all a bit speculative.

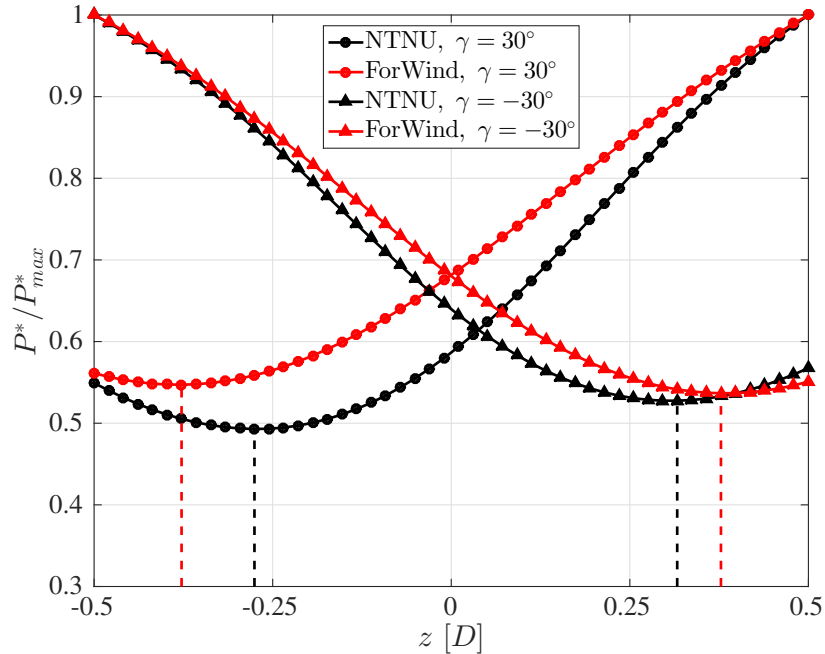


**Figure 4.** Potential power  $P^*$  as described in Section 2.2 of the manuscript for varying horizontal positions  $z$ .  $x/D = 6$ .

At the same, a "wake center" is somewhat a vague term. We use the method of a potential downstream turbine's power because we believe it is closest to the potential application of wake deflection studies. We only considered variations in  $z$  direction, which should be kept in mind.

Regarding the second question, I think this is a very interesting train of thought. Ideally, one would have to consider all three flow components for a proper interpretation of the evolving vortex pairs. However, only two components were recorded for the majority of this campaign. Those ( $u(t)$  and  $v(t)$ ) are shown in Figures 5 and 6 of this document for the ForWind turbine and the NTNU turbine, respectively. Showing both turbines (and thus both rotational directions), both yaw angles and both flow components, one can compare as much as the data allows. However, as the third flow component was not recorded, some speculation about the vortex pair is probably inevitable. Starting with the ForWind turbine (Fig. 5 of this document), we believe the plots show quite symmetric situations comparing positive and negative yaw misalignment. Confirming Table 2 of the manuscript, also the  $v$  component shows very symmetric contours, regarding position, shape and magnitude of the dipoles. One expects a strong horizontal velocity component at hub height towards positive  $z$  direction for  $\gamma = -30^\circ$  and in negative  $z$  direction for  $\gamma = +30^\circ$ , resulting in two counter rotating vortex pairs (cf. Fig.6 of the companion paper). As the contours for  $\gamma = -30^\circ$  and  $\gamma = +30^\circ$  look very symmetric regarding  $u(t)$  and  $v(t)$ , one cannot conclude that the shed vortices are much different regarding the direction of yaw misalignment. Looking at Figure 6 of this document, contours behind the NTNU rotor are slightly asymmetric, which is expected based on Figure 4 of this document.

I believe, similarly as for the first question, one has to think about the differences listed above and some speculation is inevitable. To me, it is more likely that those asymmetries are caused by wind tunnel/blockage effects. Consequently, we do not believe that there is a clear connection between the size of the vortex pair and the direction of yawing / the direction of rotation.

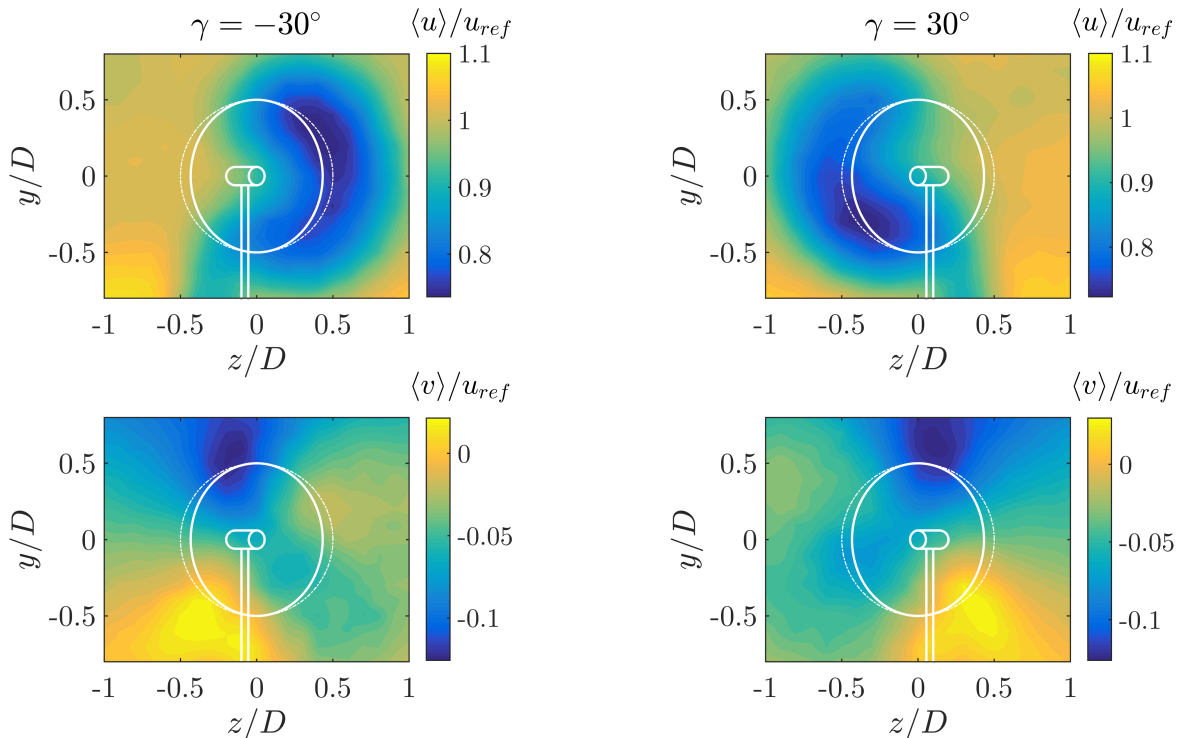


**Figure 5.** Wakes behind the ForWind turbine at  $x/D = 6$ . Left column:  $\gamma = -30^\circ$ , right column:  $\gamma = +30^\circ$ . Top row:  $\langle u \rangle / u_{ref}$ , bottom row:  $\langle v \rangle / u_{ref}$ .



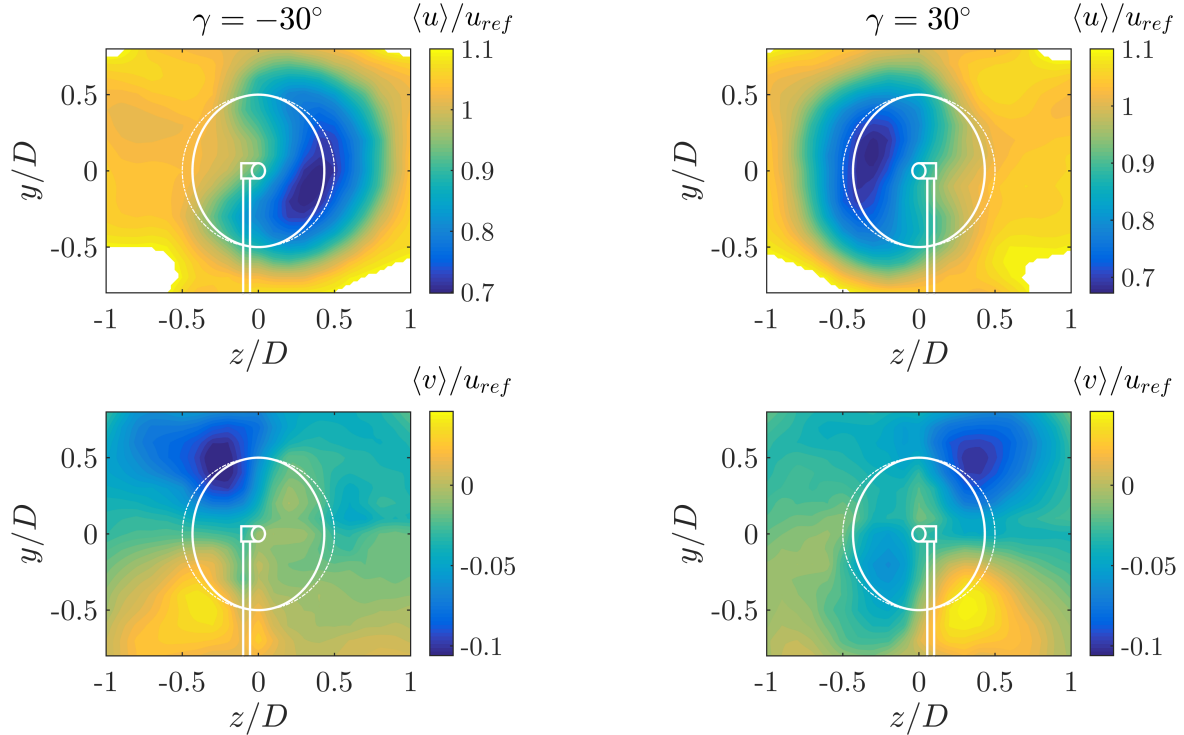


**Figure 6.** Wakes behind the NTNU turbine at  $x/D = 6$ . Left column:  $\gamma = -30^\circ$ , right column:  $\gamma = +30^\circ$ . Top row:  $\langle u \rangle / u_{ref}$ , bottom row:  $\langle v \rangle / u_{ref}$ .

## References

- [1] Schottler, J., Reinke, N., Hölling, A., Whale, J., Peinke, J., and Hölling, M., “On the impact of non-Gaussian wind statistics on wind turbines – an experimental approach,” *Wind Energy Science*, Vol. 2, No. 1, jan 2017, pp. 1–13.
- [2] Frisch, U., *Turbulence : the legacy of A.N. Kolmogorov*, Vol. 1, Cambridge university press, 1995.
- [3] Boettcher, F., Renner, C., Waldl, H. P., and Peinke, J., “On the statistics of wind gusts,” *Boundary-Layer Meteorology*, Vol. 108, No. 1, 2003, pp. 163–173.
- [4] Liu, L., Hu, F., Cheng, X.-L., and Song, L.-L., “Probability Density Functions of Velocity Increments in the Atmospheric Boundary Layer,” *Boundary-Layer Meteorology*, Vol. 134, No. 2, 2010, pp. 243–255.
- [5] Morales, A., Wächter, M., and Peinke, J., “Characterization of wind turbulence by higher-order statistics,” *Wind Energy*, Vol. 15, No. 3, 2012, pp. 391–406.
- [6] Wächter, M., Heißelmann, H., Hölling, M., Morales, A., Milan, P., Mücke, T., Peinke, J., Reinke, N., and Rinn, P., “The turbulent nature of the atmospheric boundary layer and its impact on the wind energy conversion process,” *Journal of Turbulence*, Vol. 13, 2012, pp. N26.
- [7] Kaimal, J. C. J., Wyngaard, J. C. J., Izumi, Y., Coté, O. R., and Cote, O. R., “Spectral Characteristics of Surface-Layer Turbulence,” *Quarterly Journal of the ...*, Vol. 98, No. 417, 1972, pp. 563–589.

- [8] Jonkman, B. J., “TurbSim user’s guide: Version 1.50,” 2009.
- [9] Milan, P., Wächter, M., and Peinke, J., “Turbulent character of wind energy,” *Physical Review Letters*, Vol. 110, No. 13, 2013, pp. 1–5.
- [10] Mücke, T., Kleinhans, D., and Peinke, J., “Atmospheric turbulence and its influence on the alternating loads on wind turbines,” *Wind Energy*, Vol. 14, No. 2, 2011, pp. 301–316.
- [11] Jonkman, J. M. and Buhl Jr, M. L., “FAST user’s guide,” *National Renewable Energy Laboratory, Golden, CO, Technical Report No. NREL/EL-500-38230*, 2005.
- [12] Moriarty, P. J. and Hansen, A. C., *AeroDyn theory manual*, Citeseer, 2005.
- [13] Tavner, P., Qiu, Y., Korogiannos, A., and Feng, Y., “the Correlation Between Wind Turbine Turbulence and Pitch Failure,” *Euro. Wind Energy Conf.*, 2011, pp. 2–6.
- [14] van Kuik, G. A. M., Peinke, J., Nijssen, R., Lekou, D., Mann, J., Sørensen, J. N., Ferreira, C., van Wingerden, J. W., Schlipf, D., Gebraad, P., Polinder, H., Abrahamsen, A., van Bussel, G. J. W., Sørensen, J. D., Tavner, P., Bottasso, C. L., Muskulus, M., Matha, D., Lindeboom, H. J., Degraer, S., Kramer, O., Lehnhoff, S., Sonnenschein, M., Sørensen, P. E., Künneke, R. W., Morthorst, P. E., and Skytte, K., “Long-term research challenges in wind energy – a research agenda by the European Academy of Wind Energy,” *Wind Energy Science*, Vol. 1, No. 1, 2016, pp. 1–39.
- [15] Berg, J., Natarajan, A., Mann, J., and Patton, E. G., “Gaussian vs non-Gaussian turbulence: impact on wind turbine loads,” *Wind Energy*, Vol. 17, No. April 2013, 2016, pp. n/a–n/a.
- [16] Larsen, T. J. and Hansen, A. M., *How 2 HAWC2, the user’s manual*, Risø National Laboratory, 2007.
- [17] Schwarz, C. M., Ehrich, S., Martín, R., and Peinke, J., “Fatigue load estimations of intermittent wind dynamics based on a Blade Element Momentum method,” *The Science of Making Torque from Wind 2018 (to be submitted)*, 2018.
- [18] Bartl, J., Mühle, F., Schottler, J., Sætran, L., Peinke, J., Adaramola, M., and Hölling, M., “Wind tunnel experiments on wind turbine wakes in yaw: Effects of inflow turbulence and shear,” *Wind Energy Science Discussions*, , No. January, jan 2018, pp. 1–22.

Authors' response to Anonymous Referee #2:

We, the authors, are very thankful for the detailed and constructive comments and greatly appreciate the willingness to review our manuscript. Please find our responses below. The original comments are shown in **bold** with the respective answers below. Excerpts of the manuscript are shown in *italic writing*, whereas additions are written in blue and deleted parts in ~~red~~.

Please note that the format of citations in manuscript excerpts might be changed.

Thank you very much for your efforts,

Jannik Schottler on behalf of all authors

---

1)

**Although the title clearly mentions the paper deals with a wind tunnel test, it would be good to exercise some caution in the text on the application of the results to the 'real world'.**

Thank you very much for this valuable input to the discussion. We do agree that it is important discuss real life application of the findings and want to adapt the manuscript accordingly.

Generally the (scientific) interest in wind turbine wakes is closely related to the 'real world' as wake effects are known to cause an increase in the cost of energy. Therefore, a mitigation of wake effects would be economically beneficial for wind farm operators and turbine manufacturers. As described in the introduction, wake steering through intentional yaw misalignment is one concept potentially capable of mitigating wake effects in wind farms, however, prior to applying the concept, the effects have to be studied carefully in numeric simulations, experimentally and in field tests, all of which are currently done. Going towards the concrete finding of this study that are summarized in the conclusion, we think the formation of a curled wake during yaw misalignment is important when assessing the applicability of wake steering concept. Those flow conditions become inflow conditions for downstream turbines, therefore an inhomogeneous flow field is an important feature for resulting loads which need to be investigated when judging active wake steering methods. Similarly, the curled shape shows that line measurements at hub height are not sufficient when quantifying wake deflection magnitudes. This is stated in p.15, ll. 6-8 in the manuscript.

Next, a ring of super-Gaussian velocity increment surrounding the velocity deficit of a wake, thus having a significantly larger diameter than the rotor, is one main finding of this paper. The importance of those statistical characteristics are potential load increases. For a more detailed elaboration, please refer to comment/answer #1 of the Referee #1. In a 'real world' scenario, the applications are two folded:

- In wind farm layout optimization, the width of of a wake is a crucial parameter, especially for lateral turbine spacing. Our results suggest the width of a wake significantly increases when taking two-point quantities into account (here:  $\lambda^2$ ). Exemplary, in a (laterally) densely spaced wind farm, a turbine might operate in free stream condition considering the velocity deficit, but might be affected

by the ring of high  $\lambda^2$  values shown in Fig. 7 of the manuscript. This difference becomes more clear looking at Fig. 10. Power *and* loads are being considered when optimizing a layout, loads are potentially strongly affected by the findings of the paper.

- As stated in the introduction, wake steering approaches through yaw misalignment are heavily discussed in the research community. The idea is to steer a wake away from a potential downstream turbine to mitigate power losses through wakes, thus gaining net power. Just as in layout optimizations, not only power but also loads have to be considered, which again might be affected by our findings: Looking at Fig. 13 for example at  $z = -0.5, y = 0$  a potential in-line downstream turbine would experience more free stream velocity, thus a power increase. Taking two-point statistics into account however shows that the exact same location would experience flows featuring high  $\lambda^2$  values. Please refer to comment #1 of referee #1 for a more detailed elaboration about the connection between loads and intermittency.

We suggest to formulate more clearly in the updated discussion section:

p.14, ll.8 ff:

*Consequently, our findings should be considered in wind farm layout optimization approaches, where a wake's width ~~affects~~ is a crucial parameter for radial turbine spacing. As layouts are being optimized regarding power and loads, the latter might be significantly affected by taking into account intermittency and the resulting increased wake width. Possibly, the ring of non-Gaussian velocity increments [...].*

2)

**The reported high thrust coefficients corresponds to rather high axial induction factors towards the turbulent wake state, in how far is this representative for real life turbines nowadays and how would this affect the observed wake shapes? Has there been any attempt to clarify the effect of operational conditions on observations (partial load. full load)**

Thank you very much to pointing the attention to the high thrust for the ForWind turbine. We noticed a non-consistency here and want to correct it: Regarding Table 1 of the manuscript, the thrust coefficient of the NTNU turbine was calculated with subtracting the thrust caused by the tower. For the ForWind turbine, the value is based on the total turbine thrust, including the tower structure. This should be corrected in the manuscript and clearly stated. We apply the following correction of the ForWind thrust coefficient:

The tower structure of the ForWind turbine is simplified as a cylindrical structure of 4cm diameter. At the inflow velocity of  $\langle u(t) \rangle = 7.5 \text{ m s}^{-1}$ , the resulting Reynolds number is  $Re_{tower} \approx 2.1 \times 10^4$ . Based on Figure 1, the resulting drag coefficient of a circular cylinder and thus the tower is

$$c_{T,tower} \approx 1.2. \tag{1}$$

With the thrust on the tower being

$$F_{T,tower} = 2c_{T,tower}/u^2 \rho A_{tower}, \quad (2)$$

we can now calculate the corrected thrust coefficient to be

$$c_T^* = 2(F_{tot} - F_{tower})/u^2 \rho A_{rotor} \quad (3)$$

$$c_T^* \approx 0.87. \quad (4)$$

Therewith, the thrust coefficient is the same for both turbines. We want to correct this is in the manuscript as follows:

p. 3, Table 1:

Table 1: Summary of main turbine characteristics. The tip speed ratio (TSR) is based on the free stream velocity  $u_{ref}$  at hub height. The Reynolds number at the blade tip,  $Re_{tip}$ , is based on the chord length at the blade tip and the effective velocity during turbine operation. The blockage corresponds to the ratio of the rotor's swept area to the wind tunnel's cross sectional area. The direction of rotation refers to observing the rotor from upstream, with (c)cw meaning (counter)clockwise. The thrust coefficients were measured at  $\gamma = 0^\circ$  [and corrected for thrust on the tower and support structure.](#)

Turbine	Rotor diameter	Hub diameter	Blockage	TSR	$Re_{tip}$	Rotation	$c_T$
ForWind	0.580 m	0.077 m	5.4 %	6	$\approx 6.4 \times 10^4$	cw	<del>0.97</del> <a href="#">0.87</a>
NTNU	0.894 m	0.090 m	13 %	6	$\approx 1.1 \times 10^5$	ccw	0.87

p.11, l.20:

*In [1], where the same setup was used, the skew angle for the NTNU rotor decreased from  $x/D = 3$  to  $x/D = 6$ , which is a further indication for wall effects due to blockage, especially during yaw misalignment. Furthermore, both values show smaller angles as for the ForWind turbine. ~~In addition to the blockage effects, this is much likely caused by differences in thrust coefficient, cf. Table 1.~~*

p.12, l.11:

*As already seen in Figure 11, the wakes behind the ForWind turbine are deflected further and the curled shape is pronounced stronger, which can be attributed to ~~the larger thrust coefficient and~~ blockage effects. Figure 12(b) also shows that the wakes behind both turbines are slightly tilted. Looking at the black curves (ForWind turbine), an asymmetry can be noticed as the curves are tilted towards the left, while the red curves are tilted towards the right.*

Barthelmie et al. report a thrust coefficient of  $c_T \approx 0.8$  for Siemens 2.3-MW and 2.0MW Vestas V80 turbines. Trujillo et al. show a  $c_T$  of 0.77 for Adwen AD 5- 116 turbines, formerly called M5000-116. This list shows a bit more quantitatively, that a value of 0.87 is slightly high, although the theoretical optimum is at  $c_T = 8/9 \approx 0.89$  [3]. When discussing the effect on our observations, one has to distinguish between

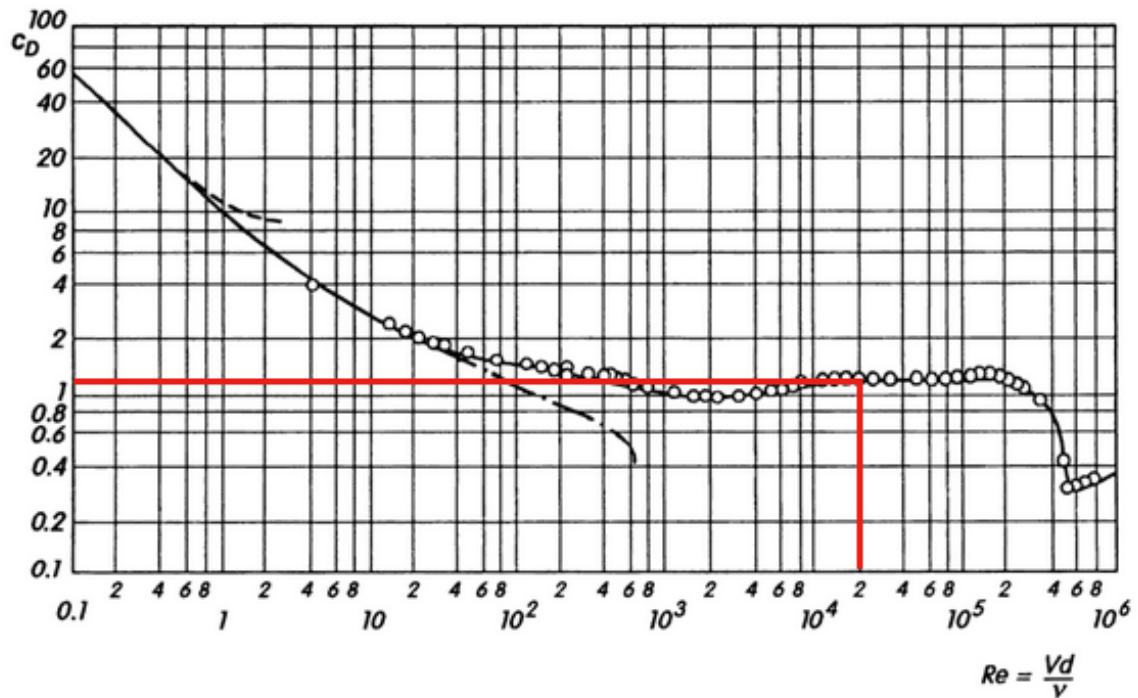


**Fig. 1.12.** Circular cylinder: drag coefficient vs. Reynolds number  
 ○ measurements by C. Wieselsberger, see H. Schlichting (1982), p. 17  
 - - - - asymptotic formula for  $Re \rightarrow 0$ :  $c_D = \frac{8\pi}{Re} [\Delta - 0.87 \Delta^3 + \dots]$ ,  
 with  $\Delta = [\ln(7.406/Re)]^{-1}$ ,  $Re = Vd/\nu$ ,  $c_D = 2D/(\rho V^2 bd)$   
 - · - · - numerical results by A.E. Hamielec; J.D. Raal (1969) and  
 B. Fornberg (1985) for steady flow  
 Re = 300: steady:  $c_D = 0.729$ , after B. Fornberg (1985)  
 unsteady:  $c_D = 1.32$ , after R. Franke; B. Schönung (1988)

**Figure 1.** Screenshot taken from [2], drag coefficient over Reynolds number for a circular cylinder.

the different findings as done below:

CURLES WAKE DURING YAW MISALIGNMENT:

Two further experimental studies report on a curled wake shape during yaw misalignment. Bastankhah & Porté Agel [4] use a small turbine model of  $c_T = 0.82$ , while Howland et al. [5] use a drag disc of  $c_T = 0.75$ . Similarly, Berdowski et al. [6] simulated an actuator disc of  $c_T = 0.89$ . All three studies report the same general effect of a curled wake shape during yaw misalignment. Thus we think, qualitatively the effect does not depend on the thrust coefficient significantly.

AREAS OF HIGH  $\lambda^2$  VALUES SURROUNDING THE VEL. DEFICIT:

To our knowledge, the ring of intermittent flow structures surrounding a velocity deficit of a wind turbine's wake as shown in Figure 7 of the manuscript, has not been reported before. Therefore, the effect of different thrust coefficients is hard to predict. However, speculating that the picture of the origin as described in the discussion section (p. 14, ll. 9-13) is correct, I would suspect a variation of the thrust coefficient would not affect the qualitative effect significantly. Of course the thrust has to be high enough to create a wake in the first place. In fact, during yaw misalignment the thrust in main flow direction is decreased and we do observe the same effect there, which supports the above speculation.

---

3)

**Blockage. Referred paper on tunnel effects refers to blockage correction (to correct free stream velocity and modify power and loads). Does the same conclusion hold for measured wake velocities or are they more sensitive to tunnel effects? Is there an influence of the asymmetry of the test section on the measured wake shape at 6D in yaw?**

Thank you for the comment. We assume the referred paper on wind tunnel effects is Chen and Liou (2011) [7]. Unfortunately, it is not really clear which conclusion is meant in the referee comment, we assume the assumption of neglect-able blockage effects for a cross-sectional blockage ratio of  $\leq 10\%$  is meant here.

We do believe that our results support the assumption of 10% blockage ratio being a good estimation for neglect-able blockage effects, even for wake velocity measurements 6D downstream. Figures 5 and 11 of the manuscript do not show any speed up effects behind the ForWind turbine (ratio  $< 10\%$ ), which are visible behind the NTNU turbine (ratio  $> 10\%$ ). Further, the wake center position based on the approach described in Section 2.2 of the manuscript result in symmetric values for positive and negative angles of yaw misalignment and slightly asymmetric values for the NTNU turbine. Thus, we conclude that the suggested 10% is a good estimation of blockage effects becoming noticeable. We stated this in the result (p. 7, ll. 26-27) and in the conclusions (p. 15, ll. 25-27) of the manuscript, however we suggest to reformulate more clearly:

p.15, ll.25 ff:

*Minor differences could be ascribed to the more prominent blockage (12.8% vs 5.4%) in the NTNU setup, confirming findings by Chen et al. [7] even for wake velocity measurements, who state blockage effects can be neglected for a blockage ratio  $\leq 10\%$ .*

We assume that 'asymmetric test section' refers to the test section having different extensions in  $y$  than in  $z$  direction. We believe that during yaw misalignment and the resulting wake deflection in  $z$  direction, the tunnel width ( $z$  direction) is the parameter potentially affecting the wake extension, especially for the larger rotor as previously discussed. For both directions, larger measures would be of advantage, however, we do not believe that both extensions being asymmetric cause specific effects.

---

4)

**2.1 pp3 Please state the cause/reason for the different TI. How was the homogeneity verified, do I understand correctly that standard deviation of flow velocity was the same in all three directions??**

We certainly agree that the difference in TI is well worth discussing, thank you very much for pointing it out. The reasons for the different values in inflow turbulence intensity are wind tunnel limitations, unfortunately. The same turbulence grid at the test section inlet was used for both turbines. However, at first, the stream wise position of the smaller ForWind turbine was chosen as a compromise of two aspects: on the one hand, the position should be at a sufficiently large distance from the turbulence grid to allow turbulent mixing. On the other hand, the position should enable a traversing of the LDA system 6 rotor diameters downstream of the turbine.

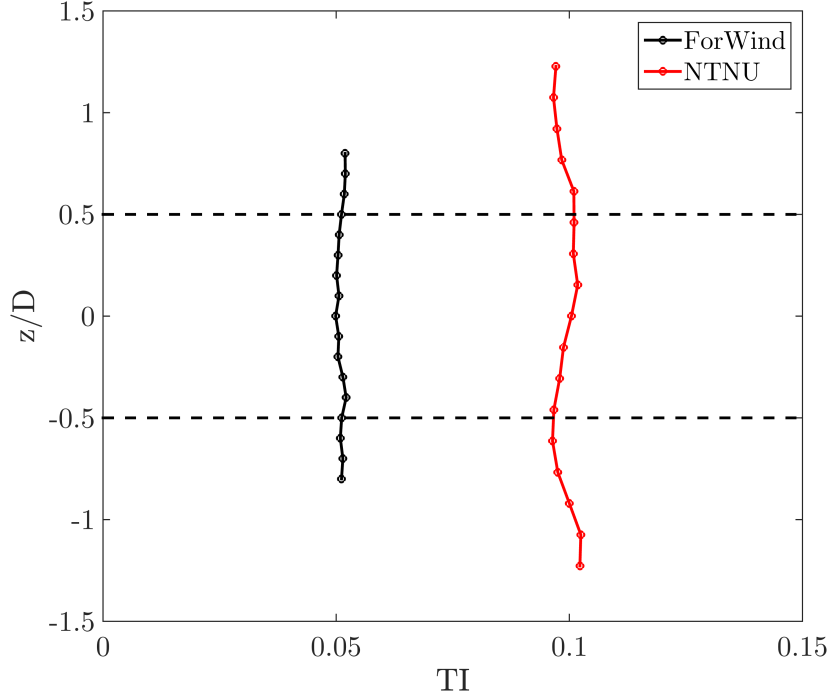
As the NTNU rotor is larger than the ForWind rotor, the NTNU turbine had to be installed closer to the turbulence grid and therewith to the inlet to the test section, to allow wake measurements 6 rotor diameters downstream of the turbine in the test section of 11.15 m length. The traversing system in the NTNU wind tunnel is permanently installed, so moving the turbine was the only way to access downstream distances of 6D. Consequently, the grid generated turbulence did not decay to the same extent as for the ForWind turbine, unfortunately resulting in different turbulence intensities in the inflow.

Figure 2 of this document shows the resulting values of turbulence intensities,

$$TI := \sigma_u / \langle u \rangle , \quad (5)$$

over height, measured at a vertical line at the respective turbine's position, without the turbine being installed. Vertically, deviations in TI are within  $\pm 1.7\%$  for the ForWind turbine and within  $\pm 3\%$  for the NTNU turbine. Equation 5 states that only the stream wise flow component  $u$  was used, as not all three flow components were recorded.





**Figure 2.** Turbulence intensity (TI) of the inflow for both turbines, measured in one vertical line at the turbine position without the turbine being installed.

We suggest to add the information about the turbulence intensity to the caption of Table 1 of the manuscript:

p.3, ll. 16 ff:

*For the NTNU turbine, the reference velocity measured in the empty wind tunnel was  $u_{ref,NTNU} = 10 \text{ m s}^{-1}$  at a turbulence intensity of  $TI = \sigma_u / \langle u \rangle = 0.1$ . For the ForWind turbine, the inflow velocity was  $u_{ref,ForWind} = 7.5 \text{ m s}^{-1}$  and  $TI = 0.05$ . In both cases, ~~the inflow  $u(t)$~~  was homogeneous within  $\pm 6\%$  and the TI within  $\pm 3\%$  on a vertical line at the turbine's position.*

5)

## 2.2 pp4 motivate choice for $x/D=6$

Thank you for this comment. As previously mentioned in the answer to comment #4), six rotor rotor diameters is the upper limit that can be realized at the wind tunnel facility, setting the upper boundary of possible downstream distances. Within the project, we decided to measure two downstream positions to get an insight in downstream wake development. As  $6D$  is the upper limit we chose this distance along with  $3D$  as second distance, which was investigated in previous studies using a comparable setup [8, 9]. This manuscript here focuses on the comparison of both turbines. Therefore, the turbine is the changing variable and we limited examined cases to one downstream distance ( $6D$ ) and one inflow condition (uniform turbulence/grid) as comparing data of 2 turbines, 3 yaw angles, 2 distances and multiple inflow conditions would be too much for one manuscript. In the companion paper (Bartl et al. 2018 [10]), only one turbine was investigated, however, during different inflow conditions and both downstream distances.

wind farm	Horns Rev 1	Rødsand	Lillgrund	North Hoyle	Nysted
spacing [D]	7	5.2–7.8	3.3–4.4	4.4–10	5.8–10.4

Table 2: Overview of wind farm spacings as stated in [11].

The study by Walker et al. (2016) [11] uses measurement data from five offshore wind farms: Horns Rev 1, Rødsand II, Lillgrund, North Hoyle and Nysted, listed in Table 2. Averaging all values results in  $\approx 6.47D$  as average turbine spacing. We thus conclude that the (somewhat forced) choice of  $6D$  is a downstream distance relevant to consider.

6)

### 5 pp15, does blockage also depend on $C_t$ ?

In this study, we did not investigate how varying the thrust coefficient affects blockage effects on the wake velocities. In our opinion, it would be very hard to isolate the effect of  $c_T$  on the blockage effect as varying the  $c_T$  would affect the wakes regardless of blockage effect. One study examining blockage effects during wind tunnel experiments using model wind turbines is Chen and Liou (2011) [7], although the focus is on turbine performance rather than wake measurements. Nevertheless, Figure 3 of this document shows that blockage effects (on performance) are dependent on the tip speed ratio. Thus, the  $c_T$  should impact blockage effects on performance.

## 4. Conclusions

This research provides quantitative results for the effects of tunnel blockage on the power coefficients of small horizontal-axis wind turbines in wind tunnel tests under different tip speed ratios (TSR), rotor pitch angles ( $\beta$ ), tunnel blockage ratios (BR), and air freestream velocities ( $U_\infty$ ). Results indicate that the tunnel blockage effects and, thus, the blockage factor (BF) are largely dependent on TSR, BR, and  $\beta$ , and weakly dependent on  $U_\infty$ . The blockage effects increase as TSR and BR increase, and as  $\beta$  decreases. The

Figure 3. Screen shot taken from [7].

7)

5 pp15 It is stated that another paper "Bartl, J., Mühle, F., Schottler, J., Sætran, L., Peinke, J., Adaramola, M., and Hölling, M.: Experiments on wind turbine wakes in yaw: Effects of inflow turbulence and shear, Wind Energy Science, submitted, 2017." discusses the effect of inflow TI. " Since the differences between the measurements on the 2 turbines are discussed in the conclusions, what would be the effect of the different inflow TI for the 2 campaigns on the measured differences?

Thank you very much for this constructive point. I think to answer this question, one has to distinguish between the different findings/distinctions and discuss them separately as done below:

## WAKE DEFLECTION

The manuscript reports different wake deflection magnitudes for both turbines (cf. Table 2 of the manuscript). The companion paper Bartl et al. (2018) [10] discusses differences in the wakes during yaw misalignment for the NTNU turbine and turbulence intensities of about 0.23% and 10%. Figure 4 shows the wakes behind the NTNU turbine for both angles of yaw misalignment and both turbulence intensities. [10] shows detailed elaboration on the differences, some of which I summarize here

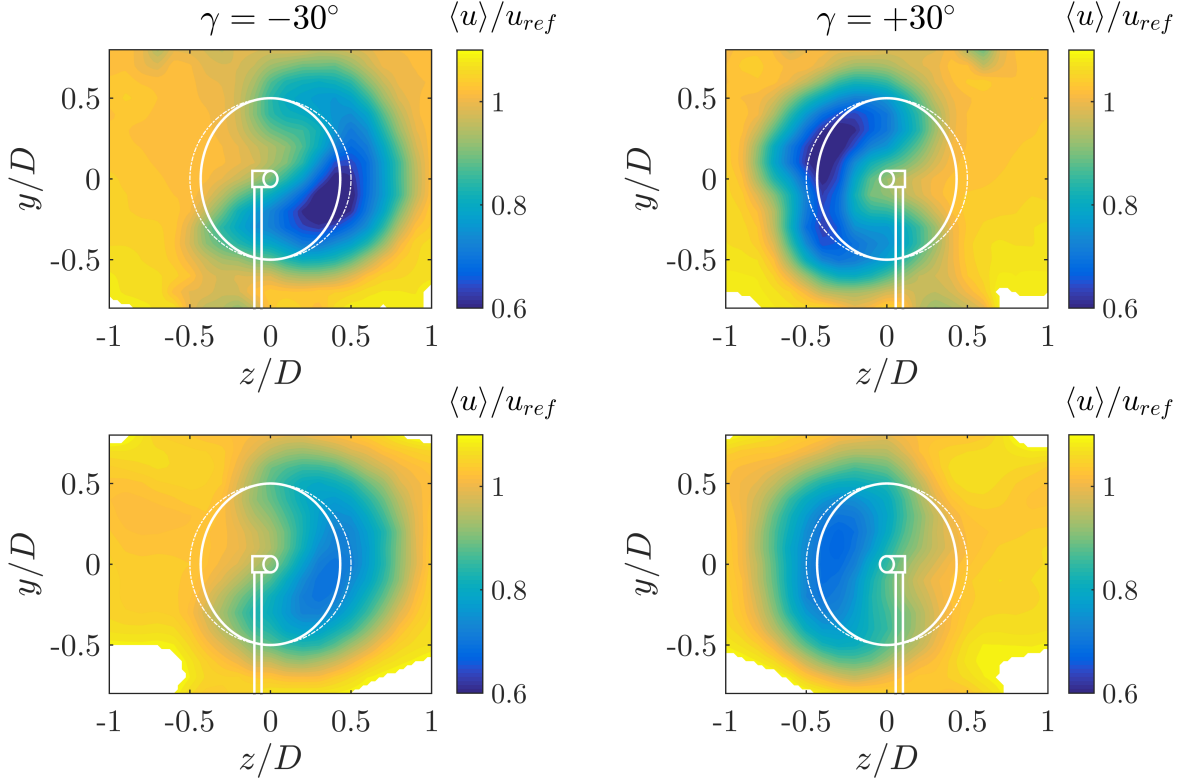


**Figure 4.**  $\langle u \rangle / u_{ref}$  behind the NTNU turbine at  $x/D = 6$ . Left column:  $\gamma = -30^\circ$ , right column:  $\gamma = +30^\circ$ . Top row: inflow  $TI = 0.23\%$ , bottom row: inflow  $TI = 10.0\%$ . The same data was used in [10].

with regard to the referee comment.

In [10], we apply the same method for wake center detection as described in the manuscript. Figure 5 of this document shows a screen shot taken from [10], comparing the wake deflection magnitudes for different inflow conditions, inflow A and B being 0.23% and 10% inflow TI. As further discussed in the companion paper, the different inflows show only very small distinctions regarding wake deflection.

Further, the maximum velocity deficit is pronounced much stronger at low inflow turbulence. This is expected since higher TI enhances turbulent mixing with the free stream and thus wake recovery. Next, the (curled) wake shape appears to be more 'stable'/defined with higher TI. In my opinion, this effect is due to the *very* low TI of 0.23% (top row), and similar distinctions would not be observable comparing 5% and 10% inflow TI using the same turbine. In fact, the result of this manuscript do show a rather smooth shape for both turbines and thus both inflow TI values.

We suggest to point the reader's attention to the companion paper regarding the issue of 2 different inflow TIs by adding to the discussion of the manuscript:

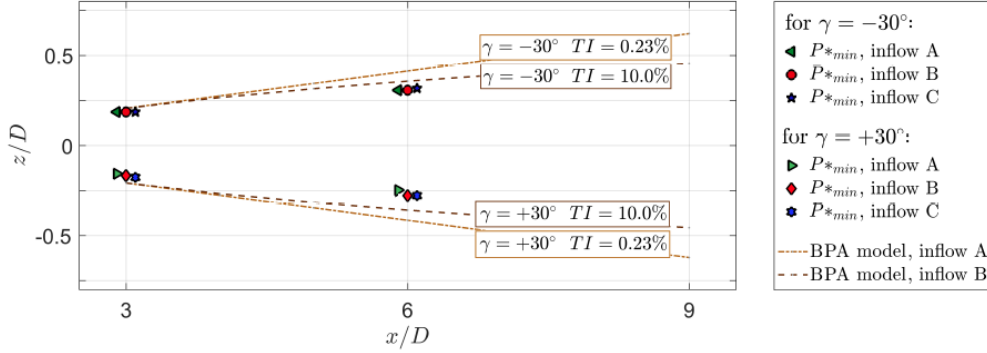


**Figure 9.** Calculated wake deflection  $\delta(z/D)$  at  $x/D=3$  and  $x/D=6$  for three different inflow conditions A, B and C compared to TI-dependent deflection predictions by Bastankhah and Porte-Agél’s wake deflection model. Note that a small offset in  $x/D$  of the measured values was chosen for better visibility.

**Figure 5.** Screenshot taken from [10], showing the wake deflection for different in flow conditions.

p.15, 20.ff:

*This confirms findings by [12] and [9], reporting an asymmetric power output of a two-turbine case with respect to the upstream turbine’s angle of yaw misalignment. One should bear in mind that the inflow turbulence intensities are different regarding both turbines. We want to point out that the influence of inflow turbulence on the wake deflection is studied in [10], showing no significant effects.*

#### RING OF HIGH $\lambda^2$ VALUES

Regarding the ring of high  $\lambda^2$ , we see a strong influence of the free stream TI on the magnitude of  $\lambda^2$  values. As can be seen in Figure 7 of the manuscript, the  $\lambda^2$  values within the ring are considerably higher behind the ForWind turbine and thus for lower free stream turbulence. This connection is further supported by Figure 6 of this document, showing  $\lambda^2$  contours behind the NTNU turbine for two different inflow conditions (TI=0.23% and TI=10.0%). Notice that the scale is different in both cases, showing that the values of  $\lambda^2$  are higher for the low turbulent case, thus supporting the previous statement. Based on those two comparisons, we assume that a larger gradient in TI (or TKE) between wake and free stream leads to higher  $\lambda^2$  values and thus more heavy-tailed increment PDFs on scales comparable to the rotor. This also fits to our interpretation that the ring of high  $\lambda^2$  values arises from a transition zone, switching between wake state and free stream state, please see p. 14 ll. 9-12 of the manuscript.

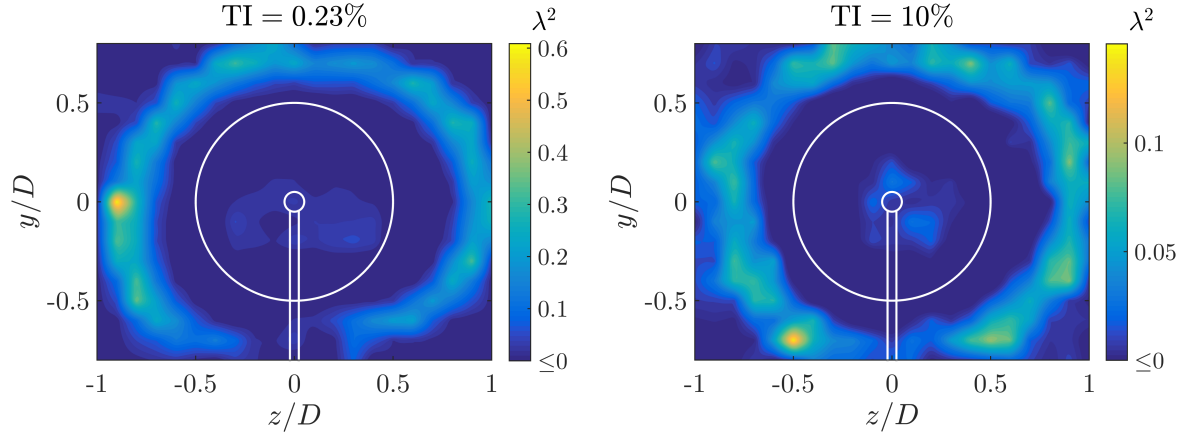


**Figure 6.** Shape parameter  $\lambda^2$  at  $x/D = 6$  behind the NTNU turbine. Left: free stream TI=0.23%, right: free stream TI=10.0%.

## References

- [1] Schottler, J., Mühle, F., Bartl, J., Peinke, J., Adaramola, M. S., Sætran, L., and Hölling, M., “Comparative study on the wake deflection behind yawed wind turbine models,” *Journal of Physics: Conference Series*, Vol. 854, may 2017, pp. 012032.
- [2] Schlichting, H. and Gersten, K., *Boundary-Layer Theory*, Vol. 102, Springer Berlin Heidelberg, Berlin, Heidelberg, 2017.
- [3] Manwell, J. F., McGowan, J. G., and Rogers, A. L., *Wind energy explained: theory, design and application*, 2009.
- [4] Bastankhah, M. and Porté-Agel, F., “Experimental and theoretical study of wind turbine wakes in yawed conditions,” *Journal of Fluid Mechanics*, Vol. 806, No. 1, nov 2016, pp. 506–541.
- [5] Howland, M. F., Bossuyt, J., Martínez-Tossas, L. A., Meyers, J., and Meneveau, C., “Wake structure in actuator disk models of wind turbines in yaw under uniform inflow conditions,” *Journal of Renewable and Sustainable Energy*, Vol. 8, No. 4, 2016.
- [6] Berdowski, T., “Three-Dimensional Free-Wake Vortex Simulations of an Actuator Disc in Yaw and Tilt,” *2018 Wind Energy Symposium*, No. January, American Institute of Aeronautics and Astronautics, Reston, Virginia, jan 2018.
- [7] Chen, T. and Liou, L., “Blockage corrections in wind tunnel tests of small horizontal-axis wind turbines,” *Experimental Thermal and Fluid Science*, Vol. 35, No. 3, apr 2011, pp. 565–569.
- [8] Schottler, J., Hölling, A., Peinke, J., and Hölling, M., “Wind tunnel tests on controllable model wind turbines in yaw,” *34th Wind Energy Symposium*, , No. January, 2016, pp. 1523.

- [9] Schottler, J., Hölling, A., Peinke, J., and Hölling, M., “Brief Communication : On the influence of vertical wind shear on the combined power output of two model wind turbines in yaw,” , No. 2016, 2017, pp. 1–5.
- [10] Bartl, J., Mühle, F., Schottler, J., Sætran, L., Peinke, J., Adaramola, M., and Hölling, M., “Wind tunnel experiments on wind turbine wakes in yaw: Effects of inflow turbulence and shear,” *Wind Energy Science Discussions*, , No. January, jan 2018, pp. 1–22.
- [11] Walker, K., Adams, N., Gribben, B., Gellatly, B., Nygaard, N. G., Henderson, A., Marchante Jiménez, M., Schmidt, S. R., Rodriguez Ruiz, J., Paredes, D., Harrington, G., Connell, N., Peronne, O., Cordoba, M., Housley, P., Cussons, R., Håkansson, M., Knauer, A., and Maguire, E., “An evaluation of the predictive accuracy of wake effects models for offshore wind farms,” *Wind Energy*, Vol. 19, No. 5, may 2016, pp. 979–996.
- [12] Fleming, P., Gebraad, P. M., Lee, S., Wingerden, J.-W., Johnson, K., Churchfield, M., Michalakes, J., Spalart, P., and Moriarty, P., “Simulation comparison of wake mitigation control strategies for a two-turbine case,” *Wind Energy*, 2014.

Authors' response to Anonymous Referee #3:

We, the authors, are very thankful for the detailed and constructive comments and greatly appreciate the willingness to review our manuscript. Please find our responses below. The original comments are shown in **bold** with the respective answers below. Excerpts of the manuscript are shown in *italic writing*, whereas additions are written in blue and deleted parts in **red**.

Please note that the format of citations in manuscript excerpts might be changed.

Thank you very much for your efforts,

Jannik Schottler on behalf of all authors

---

1)

**The anonymous referee #2 has commented on the high induction factors and the choice of position of measurement plane, the different TI, Ct and blockage ratios for the two turbines tested, and the possible impact on the measured wake velocities. I understand that the wake effects are more easily studied at high induction factors, relatively close to the rotor, but I also share ref #2's curiosity about how this relates to real wind farms. I suggest a section showing the Ct vs. wind speed curve for a large modern wind turbine, and a few sentences about typical wind turbine spacings in recently built wind farms (along and across the main wind direction).**

Thank you very much for this comment and the suggestions. The agreement with referee #2 shows that this is indeed an aspect that should be further elaborated on in the manuscript. We kindly ask you to refer to comment/answer #2 of referee #2, where we discussed the thrust coefficient, as well as comment/answer #5, where we discuss the choice of 6D and typical turbine spacings.

---

2)

**The anonymous referee #1 main comment is on the impact of inflow velocity increments on the loads for a wind turbine. I would like to add a few comments on this topic. Figure 5 shows the mean velocity deficit at 6D behind the rotor. As expected, the wake (in terms of velocity deficit) has expanded somewhat, but at  $y/D$  and  $z/D$  of 1, we have more or less free stream conditions. Figure 6 shows the influence of the rotor in terms of TKE. Again we see that the wake has expanded, but at  $y/D$  and  $z/D$  of 1, we are almost at free-stream. Figure 7 is intriguing. Although the wake in terms of mean velocity deficit and TKE is hardly present at  $y/D$  and  $z/D$  of 1, the shape parameter here shows a strong signal, close to the maximum value across the measurement plane. My main comment is that the shape parameter can be high, but the velocity fluctuations may be too small to affect the loads. I therefore appreciate that the authors in the following figures try to present the results in different ways, but in my opinion, some more figures should be added here. In figure 8, the**

probability density functions at the two points are normalized in different ways to be compared with the same Gauss distribution. What is the ratio of velocity increment standard deviations at the two positions? How would a plot look if the results were normalized in the same manner? In figure 9, the velocity increments at the two positions are again normalized with different standard deviations. I would like to see the corresponding plots also normalized with the standard deviation at  $D/2$ .

Thank you very much for this very constructive criticism and interest. I do understand that several questions are posed and details asked for in this comment. Nevertheless, I think it makes sense and adds clarity to answer the aspects mentioned in this comment in one answer as they are closely related. I will refer to specific aspects of the comment throughout the answer in bold writing.

To begin with, I think one has to pay attention to the term 'fluctuations'. Often in literature, fluctuations refer to

$$u'(t) = u(t) - \langle u(t) \rangle, \quad (1)$$

see equation 3 of the manuscript. When stating '**the shape parameter can be high, but the velocity fluctuations may be too small to affect the loads**', we assume that not fluctuations in the sense of Eq. (1) but velocity increments are meant:

$$u_\tau(t) := u(t) - u(t + \tau), \quad (2)$$

which is statistically different as fluctuations are one-points quantities and increments two-point quantities. For a detailed elaboration we refer to Morales et al. [1].

**'In figure 8, the probability density functions at the two points are normalized in different ways to be compared with the same Gauss distribution.'**

This is not entirely correct and we want to clarify: the PDFs  $u_\tau$  are indeed normalized by the standard deviation  $\sigma_\tau$  and therewith by different values. This is not done to be compared to the same Gaussian. The normalization allows to purely compare the shape of the individual PDFs. The Gaussian is added to guide the eye as normally one is familiar with the Gaussian shape. As mentioned in the manuscript (p.14, ll. 14 ff),  $\lambda^2$  is an indicator for a PDFs shape. Because of that, we normalize the PDFs in Fig. 8 to purely compare the shape and thus visualizing what is expressed by  $\lambda^2$ .

We fully agree and really appreciate the hint, that for a connection to loads, the absolute values of  $u_\tau [ms^{-1}]$  are much more intuitive. However, we want to clearly distinguish this and order it the following way:

1. we find a ring of high  $\lambda^2$  values (Fig. 7). This parameter expresses the *shape* of a pdf.
2. we show 2 exemplary increment PDF, normalized, in order to actually show the shape that is expressed by  $\lambda^2$ . We believe the shape is best compared by normalizing by the standard deviation
3. Fig. 10 shows that  $\lambda^2$  is high where  $\langle u \rangle$  would indicate free steam conditions



4. Now, we think it would be nice to show non-normalized plots, but comparing positions within the ring of high  $\lambda^2$  values and the *free stream*. That way, we show much more intuitively that strong velocity jumps (increments) in short time scale happen significantly more often in the ring than in the free stream. Thus, we show that the ring is indeed no free stream as (falsely) suggested by defining a wake width by the velocity deficit in the wake. We show that it is significantly different regarding velocity increments, and therewith of importance.

For the above points 1. and 2., we think Fig. 7 and 8 should stay in the manuscript. Point 3. is expressed by Fig. 10. We suggest to add the following plots to bring across point 4.:

In order to comment on the impact on loads, or at least get a feeling for the potential impact, we agree that a non-normalized presentation is very beneficial. Figure 1 of this document shows the increment time series  $u_\tau$  in free stream condition (a) and within the ring of high  $\lambda^2$  values (b). One can clearly see that jumps exceeding 2.5m/s happen frequently in (b), and are non-existent in the free stream. Hereby we show that this radial position of the wake features significantly different flows than the free stream. To show this more clearly, Figure 2 shows the corresponding increment PDFs,  $p(u_\tau)$  of the absolute values. Clearly, one sees the same thing as in Fig. 1 (of this document):

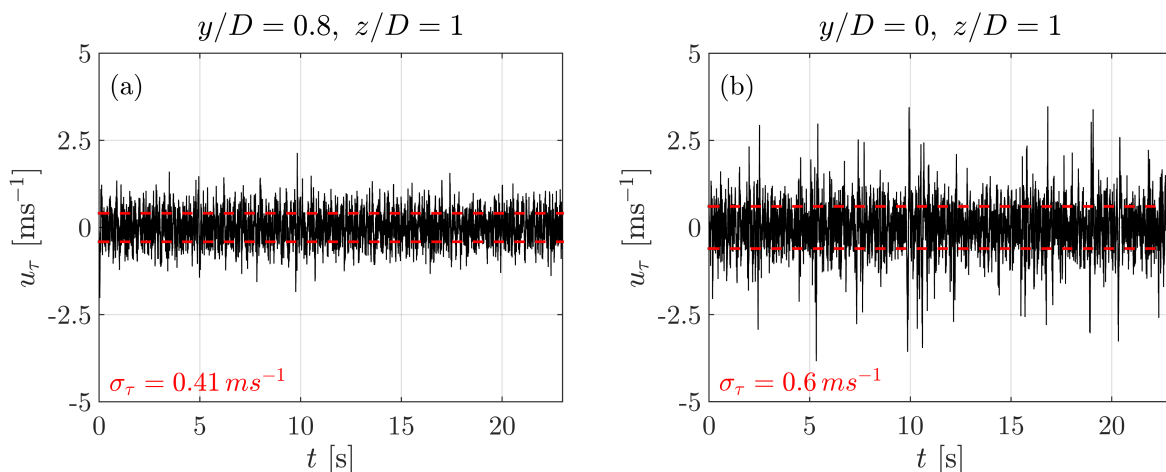


**Figure 1.** Time series of increments  $u_\tau(t)$  for the positions  $y/D = 0.8$ ,  $z/D = 1$  (free stream, a) and  $y/D = 0$ ,  $z/D = 1$ . The standard deviations  $\sigma_\tau$  are indicated in red.

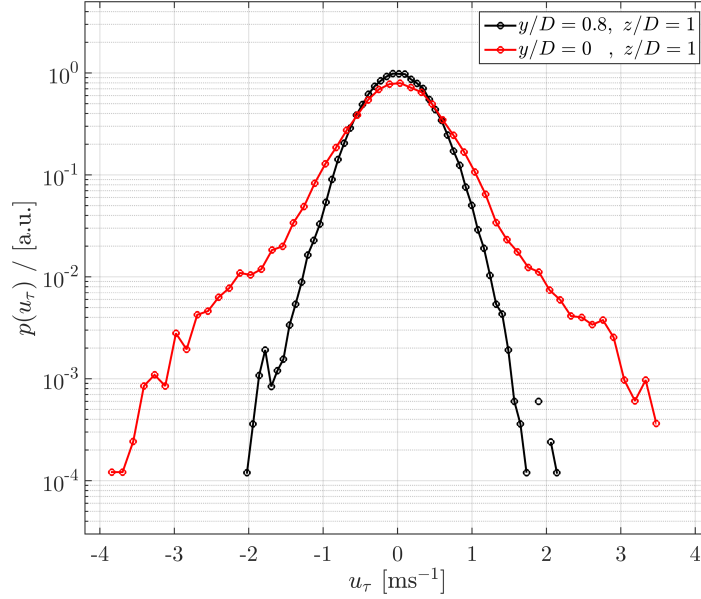


**Figure 2.**  $p(u_\tau)$  of the free stream at  $y/D = 0.8$ ,  $z/D = 1$  and of  $y/D = 0$ ,  $z/D = 1$ , exemplary for the ForWind turbine.

We suggest to update the Results-section of the manuscript the following way:

p.9 ll. 4 ff:

*For  $z = D$ , which lies within the ring of large  $\lambda^2$  values,  $p(u_\tau)$  strongly deviates from a Gaussian, showing a heavy-tailed distribution, indicating more frequent occurrences of extreme events. Exemplary, in both cases an event of  $5\sigma_\tau$  is underestimated by multiple orders of magnitude comparing a Gaussian distribution to the PDFs at  $z = D$ . Figure 8 further shows  $p(u_\tau)$  based on the model proposed by [2]. Those distributions were evaluated based on the  $\lambda^2$  values computed by Equation (6) at  $z = D$ , visualizing exemplary how well the distributions' shapes are grasped by  $\lambda^2$ . To show the difference in  $p(u_\tau)$  more intuitively, Figure 9 shows the increment time series  $u_\tau(t)/\sigma_\tau$  at  $z = D/2$  and  $z = D$ , exemplary for the ForWind turbine. It can be seen how Figure 9(a) is characterized by noisy fluctuations while Figure 9(b) shows sudden jumps e.g. extreme events  $u_\tau(t)$  at  $z = D/2$  (a) and  $z = D$  (b) behind the ForWind turbine, cf. Figures 7(b) and 8(b).  $\sigma_\tau$  is the standard deviation of  $u_\tau$ . Our results show that, depending on[...].*

p.11, ll. 3ff:

*For illustration, the dotted lines in Figure 10 mark the respective locations. It is shown that the radial areas of TKE and  $\lambda^2$  can be related in this way to the velocity deficit. To get a feeling of the impact on potential downstream turbine, Figure \*2 of this response\* compares  $p(u_\tau)$  in absolute terms at a free stream position,  $y/D = 0.8$ ,  $z/D = 1$ , and at a position featuring high  $\lambda^2$  values,  $y/D = 0$ ,  $z/D = 1$ , exemplary for the ForWind turbine. It becomes clear that velocity increments exceeding  $3\text{ms}^{-1}$  occur much more frequent within the ring of high  $\lambda^2$  values than in three free stream. Hereby we show that this radial position of the wake features significantly different flows than the free stream. To compare more visually, Figure \*1 of this response\* shows the corresponding time series  $u_\tau(t)$ . Clearly, the spiky signature of extreme events become obvious in Figure*

1(b), confirming that no free stream condition is reached at  $z/D = 1$ .

p.14, ll.2 ff:

*We find heavy-tailed distributions of velocity increments in a ring area surrounding the velocity deficit and areas of high TKE in a wind turbine wake. Thus, the definition of a wake width strongly depends on the quantities taken into account as the ring area features significantly different statistics than the free stream. The heavy-tailed distributions are [...]*

We further suggest to delete Figure 9 of the manuscript. I think Figure 1 of this reply is more valuable and both might be a bit too much.

---

3)

**Caption of Table 1, pg. 3: Is the effective velocity during turbine operation the relative wind speed with respect to the rotor tip? The blade tip of the ForWind turbine looks like it has a rounded shape. Where is the tip chord defined?**

Thank you for pointing out that we should be a bit more precise here. As correctly described, the effective velocity  $vel_{eff}$  during operation is the wind speed the airfoil experiences at the tip. Indeed, the tip of the ForWind blades are somewhat round. To account for this we calculated the effective velocity and Reynolds number at  $r \approx 96\%$  blade radius  $R$  and not at 100%. At  $r = 0.96R$ , the cord length is  $c_{96\%} \approx 20mm$  and we can calculate the Reynolds number:

$$\omega = \lambda u / R \quad (3)$$

$$vel_{rot} = \omega r = \lambda u \cdot r / R \quad (4)$$

$$vel_{rot} = \lambda u \cdot 0.96 \quad (5)$$

$$vel_{eff} = \sqrt{u^2 + vel_{rot}^2} \quad (6)$$

$$vel_{eff} \approx 45.6m/s. \quad (7)$$

$$\Rightarrow Re \approx 6.42 \times 10^4 . \quad (8)$$

I think it is still fair to call it  $Re_{tip}$  and suggest to clarify this in the updated manuscript by adding to the caption of Table 1:

p.3, Tab.1 (caption):

*Summary of main turbine characteristics. The tip speed ratio (TSR) is based on the free stream velocity  $u_{ref}$  at hub height. The Reynolds number at the blade tip,  $Re_{tip}$ , is based on the chord length at the blade tip and the effective velocity during turbine operation. For the ForWind turbine,  $0.96R$  was chosen as radial position to account for the rounded blade tips. The blockage corresponds to the ratio of the rotor's swept area to the wind tunnel's cross sectional area. The direction of rotation refers to observing the rotor from upstream, with (c)w meaning (counter)clockwise. The thrust coefficients were measured at  $\gamma = 0^\circ$  and corrected for thrust on the tower and support structure.*

4)

**2.3, page 6: Please mention if measurements support the assumption about vertical vs transversal fluctuations. I assume you mean  $\langle w^2 \rangle$  vs.  $\langle w'^2 \rangle$ .**

Thank you for this hint. In fact, we mean  $\langle v'(t)^2 \rangle \approx \langle w'(t)^2 \rangle$  so the approximation of the TKE is satisfied:

$$k = 0.5 (\langle u'(t)^2 \rangle + \langle v'(t)^2 \rangle + \langle w'(t)^2 \rangle) \quad (9)$$

$$\approx 0.5 (\langle u'(t)^2 \rangle + 2\langle v'(t)^2 \rangle). \quad (10)$$

We did do measurements supporting this is a fair assumption. We suggest to add this information to the manuscript:

p.6, l. 6 ff:

*For brevity, we write  $\langle u \rangle$  instead of  $\langle u(t) \rangle$ . As the third flow component  $w$  was not recorded, we assume  ~~$w'(t) \approx v'(t)$~~   $\langle w'(t)^2 \rangle \approx \langle v'(t)^2 \rangle$  so that Equation (2) becomes*

$$k = 0.5 (\langle u'(t)^2 \rangle + 2\langle v'(t)^2 \rangle), \quad (11)$$

*which will be used in further analyses. Measurements were performed validating this approximation. For a thorough analysis[...]*

---

5)

**Caption, Figure 3: Consider adding something like: For the NTNU turbine, the wind tunnel walls are located at  $z/D = \pm 3.03$  and  $y/D = \pm 2.02$ . For the ForWind turbine, the wind tunnel walls are located at  $z/D = \pm 4.67$  and  $y/D = \pm 3.12$**

We agree that this is helpful information and will add it as suggested in the updated manuscript. Thank you for the suggestion. We believe a factor 0.5 is missing in the suggested values, so we would like to edit the caption of Fig. 3 as follows:

p. 5, Fig 3(caption):

*Non-dimensional measurement grid behind the rotor for  $\gamma = 0^\circ$ . The respective contours of the turbines are shown in black (ForWind) and red (NTNU). For the NTNU turbine, the wind tunnel walls are located at  $z/D = \pm 1.5$  and  $y/D = \pm 1.0$ , for the ForWind turbine at  $z/D = \pm 2.34$  and  $y/D = \pm 1.56$ .*

---

6)

**Caption, Figure 11, pg. 12: Bottom row.**

Thank you for this hint, it will be corrected.

---

7)

**Caption, Figure 13: The red marks show the approximation of the respective parameter's radial extension based on  $\mu \pm 1\sigma$  and  $\mu \pm 2\sigma$  as described**

in Section 3.1. But I see only two red lines, is it at one or two sigma?

Thank you for pointing this out. In the TKE contour plots (center column), the red lines correspond to  $\mu \pm 1\sigma_\mu$  and in the  $\lambda^2$  contours (right column), the red lines correspond to  $\mu \pm 2\sigma_\mu$ . We suggest to state this more clearly in the caption:

p.14, Fig 13, caption:

*$\langle u \rangle / u_{ref}$  (left column), TKE (center column) and  $\lambda^2$  (right column) for  $\gamma = -30^\circ$  behind the NTNU turbine (top row) and the ForWind turbine (bottom row). The time scale for  $\lambda^2$  corresponds to the length scale of the rotor diameter. The red marks show the approximation of the respective parameter's radial extension based on  $\mu \pm 1\sigma_u$  (TKE, middle column) and  $\mu \pm 2\sigma_u$  ( $\lambda^2$ , left column) as described in Section 3.1.*

## References

- [1] Morales, A., Wächter, M., and Peinke, J., “Characterization of wind turbulence by higher-order statistics,” *Wind Energy*, Vol. 15, No. 3, 2012, pp. 391–406.
- [2] Castaing, B., Gagne, Y., and Hopfinger, E. J., “Velocity probability density functions of high Reynolds number turbulence,” *Physica D: Nonlinear Phenomena*, Vol. 46, No. 2, 1990, pp. 177–200.

# Wind tunnel experiments on wind turbine wakes in yaw: Redefining the wake width

Jannik Schottler<sup>1</sup>, Jan Bartl<sup>2</sup>, Franz Mühle<sup>3</sup>, Lars Sætran<sup>2</sup>, Joachim Peinke<sup>1,4</sup>, and Michael Hölling<sup>1</sup>

<sup>1</sup>ForWind, University of Oldenburg, Institute of Physics, Oldenburg, Germany

<sup>2</sup>Department of Energy and Process Engineering, Norwegian University of Science and Technology, Trondheim, Norway

<sup>3</sup>Faculty of Environmental Sciences and Natural Resource Management, Norwegian University of Life Sciences, Ås, Norway

<sup>4</sup>Fraunhofer IWES, Oldenburg, Germany

Correspondence to: Jannik Schottler (jannik.schottler@forwind.de)

**Abstract.** This paper presents an investigation of wakes behind model wind turbines, including cases of yaw misalignment. Two different turbines were used and their wakes are compared, isolating effects of boundary conditions and turbine specifications. Laser Doppler Anemometry was used to scan a full plane of a wake normal to the main flow direction, 6 rotor diameters downstream of the respective turbine. The wakes of both turbines are compared in terms of the time averaged main flow component, the turbulent kinetic energy and the distribution of velocity increments. The shape of the velocity increments' distributions is quantified by the shape parameter  $\lambda^2$ .

The results show that areas of strongly heavy-tailed distributed velocity increments are surrounding the velocity deficit in all cases examined. Thus, a wake is significantly wider when two-point statistics are included as opposed to a description limited to one-point quantities. As non-Gaussian distributions of velocity increments affect loads of downstream rotors, our findings impact the application of active wake steering through yaw misalignment as well as wind farm layout optimizations and should therefore be considered in future wake studies, wind farm layout and farm control approaches. Further, the velocity deficits behind both turbines are deformed to a kidney-like curled shape during yaw misalignment, for which parameterization methods are introduced. Moreover, the lateral wake deflection during yaw misalignment is investigated.

## 1 Introduction

Due to the installation of wind turbines in wind farm arrangements, the turbine wakes become inflow conditions of downstream rotors, causing *wake effects*. Those include a reduced wind velocity and increased turbulence levels. The former cause power losses of up to 20% (Barthelmie et al., 2010) in wind farms, while the latter are linked to increased loads of downstream turbines, affecting fatigue and life time (Burton et al., 2001). In order to mitigate wake effects, various concepts of active wake control strategies have been proposed and investigated. One concept is an active wake steering by an intentional yaw misalignment, where the velocity deficit behind a rotor is deflected laterally by misaligning it with the mean inflow direction. The possibility of wake re-direction by yawing was observed and investigated by means numeric simulations (e.g. Jiménez et al., 2010; Fleming et al., 2014b), in wind tunnel experiments (e.g. Medici and Alfredsson, 2006; Campagnolo et al., 2016) and in full-scale field measurements by Trujillo et al. (2016). Further, the potential of increasing the power yield in a wind farm

configuration was explored experimentally (Schottler et al., 2016), numerically (e.g. Fleming et al., 2014b; Gebraad et al., 2014) and in a field test in a full-scale wind farm (Fleming et al., 2017), showing promising results as the total power yield could be increased in the mentioned studies.

As the applicability of the concept to future wind farms require a thorough understanding of the wakes behind yawed wind turbines, this study examines the wakes behind model wind turbines during yaw misalignment. Experimental studies are necessary to validate numeric results, to tune engineering models and to gain a deeper understanding of the present effects in a controlled laboratory environment. However, when examining wake effects experimentally, varying turbine models are used. Those models strongly differ in their complexity and design, including blade design, geometry or control concepts. The simplest model is a drag disc concept, where a wind turbine is modeled by a porous disk in the flow as done by España et al. (2012) or Howland et al. (2016). Moreover, rotating turbine models have been used in numerous studies, where the design and complexity of the models vary significantly. Examples include (Medici and Alfredsson, 2006), (Bottasso et al., 2014), (Abdulahim et al., 2015), (Rockel et al., 2016) or (Bastankhah and Porté-Agel, 2016). In contrast to numerical studies, where the vast majority of the research community uses consistent turbine models (NREL 5 MW (Jonkman et al., 2009) or DTU 10 MW (Bak et al., 2013) reference turbines for example), experiments lack certain systematics and comparability due to varying turbine models, facilities and measurement techniques. The present study aims to compare the wakes of two different model wind turbines in the same facility, using comparable boundary conditions as far as possible. Therewith, a separation between general wake effects and turbine specific observations can be achieved.

We present wake analyses ranging from mean quantities to higher order statistics. Average mean flow components are of relevance when assessing the energy yield of potential downstream turbines. An investigation of turbulence parameters such as the turbulent kinetic energy (TKE) is linked to fluctuating inflow conditions, which is important for loads of downstream turbines and therewith their lifetime (Burton et al., 2001). To gain a deeper insight, we extend our analyses to two-point statistics. More precisely, velocity increments are analyzed, allowing for a scale dependent analysis of flows. Non-Gaussianity of the distributions of velocity increments has been reported not only in small scale turbulence (Frisch, 1995), but also in the atmospheric boundary layer (e.g. Boettcher et al., 2003; Liu et al., 2010; Morales et al., 2012). To what extent statistical characteristics of velocity increments are transferred to wind turbines is of current interest throughout the research community (van Kuik et al., 2016). We Schottler et al. (2017c) found a transfer of intermittency from wind to torque, thrust and power data in a wind tunnel experiment using a model wind turbine. Similarly, Mücke et al. (2011) found a transfer of intermittency to torque data using a generic turbine model. Milan et al. (2013) reported intermittent power data in a full-scale wind farm. We thus believed that distributions of velocity increments in wakes are of importance for potential downstream turbines as **extreme events non-Gaussian characteristics** are likely to be transferred to wind turbines in terms of fluctuating loads and power output. **Studies show this for a generic turbine model (Mücke et al., 2011), in a wind tunnel experiment (Schottler et al., 2017c) and by analyzing field data of a full-scale wind farm (Milan et al., 2013). Those findings make an investigation of** Consequently, investigations of velocity increments in wakes become extremely relevant for active wake control concepts as well as for wind

**Table 1.** Summary of main turbine characteristics. The tip speed ratio (TSR) is based on the free stream velocity  $u_{ref}$  at hub height. The Reynolds number at the blade tip,  $Re_{tip}$ , is based on the chord length at the blade tip and the effective velocity during turbine operation. [For the ForWind turbine,  \$0.96R\$  was chosen as radial position to account for the rounded blade tips.](#) The blockage corresponds to the ratio of the rotor’s swept area to the wind tunnel’s cross sectional area. The direction of rotation refers to observing the rotor from upstream, with (c)cw meaning (counter)clockwise. The thrust coefficients were measured at  $\gamma = 0^\circ$  [and corrected for thrust on the tower and support structure.](#)

Turbine	Rotor diameter	Hub diameter	Blockage	TSR	$Re_{tip}$	Rotation	$c_T$
ForWind	0.580 m	0.077 m	5.4 %	6	$\approx 6.4 \times 10^4$	cw	<del>0.97</del> 0.87
NTNU	0.894 m	0.090 m	13 %	6	$\approx 1.1 \times 10^5$	ccw	0.87

farm layout approaches. [A further elaboration on the connection of non-Gaussian velocity increments and loads as well of power fluctuations is given in Section 4.](#)

This work is organized as follows. Section 2 introduces the methods used throughout the study, including the experimental methods, a concept for quantifying a wake’s deflection and a definition of the examined parameters. Section 3 shows the result of the study. First, results of the non-yawed rotors are investigated and compared in Section 3.1. Wakes during yaw misalignment are analyzed in Section 3.2, including a quantification of the wake deflection. Section 4 discusses the findings before Section 5 summarizes this work and states the conclusions. This work is part of a joint experimental campaign by the NTNU in Trondheim and ForWind in Oldenburg. [While this paper compares the wakes behind two different model wind turbines during one inflow condition,](#) a second paper by Bartl et al. (2017) examines the influence of varying inflow conditions on the wake of one model wind turbine.

## 2 Method

### 2.1 Experimental methods

The experiments were performed in the wind tunnel of the Norwegian University of Science and Technology (NTNU) in Trondheim, Norway. The closed-loop wind tunnel has a closed test section of  $2.71\text{ m} \times 1.81\text{ m} \times 11.15\text{ m}$  (width  $\times$  height  $\times$  length). The inlet to the test section was equipped with a turbulence grid having a solidity of 35% and a mesh size of 0.24 m. Further details about the grid are described by Bartl and Sætran (2017). Two different model wind turbines were used that vary in geometry, blade design and direction of rotation. Those deliberate distinctions allow for an isolation of general effects of wake properties. The turbines will be denoted *NTNU* and *ForWind*, respectively. Table 1 summarizes the main features and differences of both turbines, further details are described by Schottler et al. (2017b). Figure 1 shows technical drawings. As can be seen, the ForWind turbine was placed on four cylindrical poles to lift the rotor above the wind tunnel boundary layer to the same hub height as the NTNU turbine, being 820 mm above the wind tunnel floor. One turbine at a time was placed on a turning table allowing for yaw misalignment, denoted by the angle  $\gamma$ , which is positive for a clockwise rotation of the rotor when observed from above as sketched in Figure 2. For the NTNU turbine, the reference velocity measured in the empty



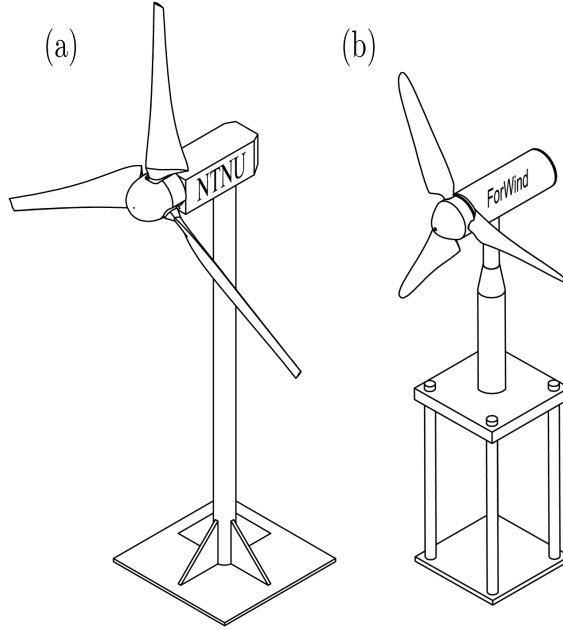


**Figure 1.** Technical drawings of the NTNU turbine (a) and the ForWind turbine (b).

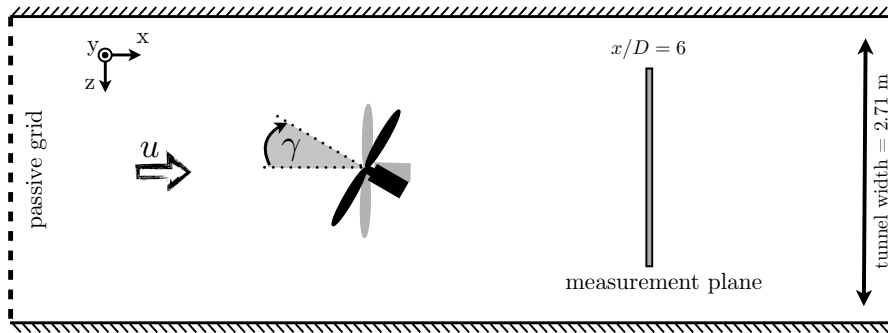


**Figure 2.** Sketch of the setup, top view.  $D$  denotes the respective rotor diameter as listed in Table 1.

wind tunnel was  $u_{ref,NTNU} = 10 \text{ m.s}^{-1}$  at a turbulence intensity of  $TI = \sigma_u / \langle u \rangle = 0.1$ . For the ForWind turbine, the inflow velocity was  $u_{ref,ForWind} = 7.5 \text{ m.s}^{-1}$  and  $TI = 0.05$ . In both cases, ~~the inflow  $u(t)$~~  was homogeneous within  $\pm 6\%$  and the  $TI$  within  $\pm 3\%$  on a vertical line at the turbine's position.

In this study we consider two-dimensional cuts through the wake, normal to the main flow direction at a downstream distance of  $x/D = 6$  for both turbines as illustrated in Figure 2. Data were acquired using a Dantec FiberFlow two-component Laser Doppler Anemometer (LDA) system, recording the  $u$ - and  $v$ -component of the flow. The accuracy is stated to be 0.04% by the manufacturer. During turbine operation, the LDA system was traversed in the  $yz$ -plane, normal to the main flow direction. Each

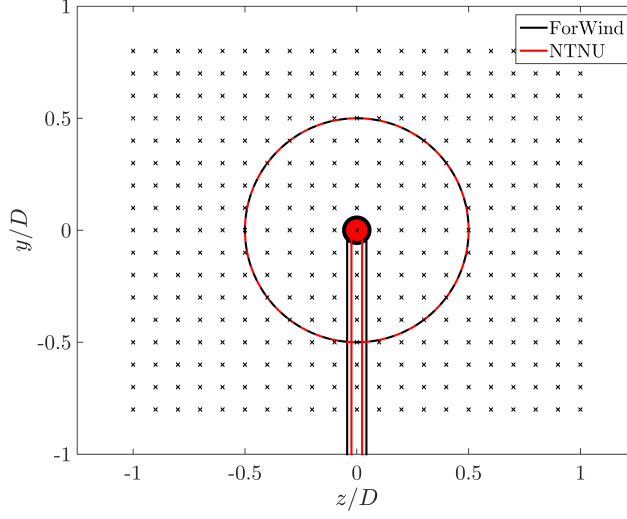


**Figure 3.** Non-dimensional measurement grid behind the rotor for  $\gamma = 0^\circ$ . The respective contours of the turbines are shown in black (ForWind) and red (NTNU). For the NTNU turbine, the wind tunnel walls are located at  $z/D = \pm 1.5$  and  $y/D = \pm 1.0$ , for the ForWind turbine at  $z/D = \pm 2.34$  and  $y/D = \pm 1.56$ .

measured plane consists of 357 points, 21 in  $z$ -direction ranging from  $-D$  to  $+D$  and 17 points in  $y$ -direction, ranging from  $-0.8D$  to  $0.8D$ , see Figure 3. The resulting distance separating two points of measurement is thus  $0.1D$ . For one location,  $5 \times 10^4$  samples were recorded, resulting in time series of varying lengths of approximately 30 s. As can be seen, the NTNU turbine has a slimmer tower and nacelle relative to its rotor diameter when compared to the ForWind turbine. The grid of physically measured values was interpolated to a grid of  $401 \times 321 \approx 129000$  points for further analyses. The distance between the interpolated grid points is therewith reduced to  $0.005D$ . Natural neighbor interpolation is used, resulting in a smoother approximation of the distribution of data points (Amidror, 2002).

## 2.2 Wake center detection

In order to quantify the lateral wake position, we compute the power of a potential downstream turbine as described by Schottler et al. (2017b). A similar approach was shown by Vollmer et al. (2016). We define the potential power of a downstream turbine to be

$$P^* = \sum_{i=1}^{10} \rho A_i \langle u_i(t) \rangle_{A_i, t}^3. \quad (1)$$

The rotor area is divided in ten ring segments.  $A_i$  is the area of the  $i^{\text{th}}$  ring segment and  $\langle u_i(t) \rangle_{A_i, t}$  denotes the temporally and spatially averaged velocity in mean flow direction within the area  $A_i$ .  $P^*$  is estimated for 50 different hub locations in the range  $-0.5D \leq z \leq 0.5D$ , at hub height. We define the horizontal wake center as the  $z$ -position resulting in the minimum of

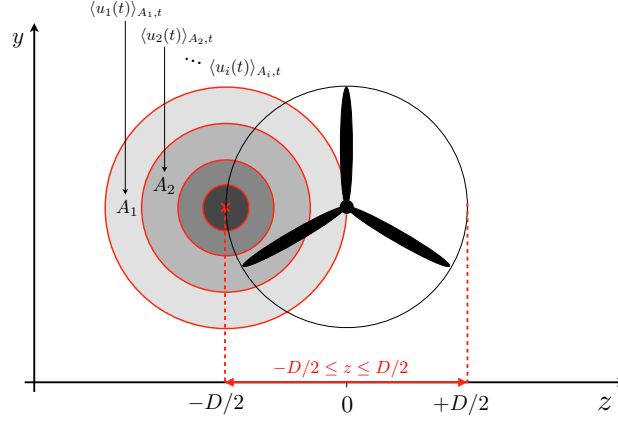


**Figure 4.** Illustration of the wake center detection method. The hub of a potential downstream turbine is located at the red  $\times$ .  $\langle u_i(t) \rangle_{A_i,t}$  is the spatially and temporarily averaged  $u$ -component of the velocity. The potential power  $P^*$  is calculated for each ring segment and then added up. This procedure is repeated for 50 horizontal hub locations  $\times$ , while the position resulting in the lowest value of  $P^*$  is interpreted as wake center.

$P^*$ . The procedure is illustrated in Figure 4.

### 2.3 Examined quantities

The turbulent kinetic energy (TKE) is defined by the fluctuations of the three velocity components as

$$5 \quad k = 0.5 (\langle u'(t)^2 \rangle + \langle v'(t)^2 \rangle + \langle w'(t)^2 \rangle) , \quad (2)$$

where  $u'(t)$  is the fluctuation around the mean of  $u(t)$  so that

$$u(t) = \langle u(t) \rangle + u'(t) . \quad (3)$$

For briefness, we write  $\langle u \rangle$  instead of  $\langle u(t) \rangle$ . As the third flow component  $w$  was not recorded, we assume  $w'(t) \approx v'(t)$   $\langle w'(t)^2 \rangle \approx \langle v'(t)^2 \rangle$ , so that Equation (2) becomes

$$10 \quad k = 0.5 (\langle u'(t)^2 \rangle + 2\langle v'(t)^2 \rangle) , \quad (4)$$

which will be used in further analyses. [Measurements where performed validating this approximation.](#)

For a thorough analysis of the wake turbulence, we examine velocity changes during a time lag  $\tau$  and refer to them as *velocity increments*,

$$u_\tau(t) := u(t) - u(t + \tau) . \quad (5)$$

15 Investigating their probability density function (PDF) allows for scale-dependent analyses of turbulent flows, including all higher order moments of  $u_\tau$ , hence all structure functions of order  $n$ ,  $S_\tau^n = \langle u_\tau^n \rangle$  of a velocity time series (Frisch, 1995). The

impact of certain properties of velocity increment PDFs on wind turbines is to date a widely discussed topic in wind energy research, see (e.g. Mücke et al., 2011; Milan et al., 2013; Berg et al., 2016; Schottler et al., 2017c). For more details, we refer the reader to Morales et al. (2012) or Schottler et al. (2017c). Following Chillà et al. (1996), the shape parameter

$$\lambda^2(\tau) = \frac{\ln(F(u_\tau)/3)}{4} \quad (6)$$

5 is used to quantify the shape of the distribution  $p(u_\tau)$ .  $F(u_\tau)$  is the flatness of the time series of velocity increments,

$$F(u_\tau) = \frac{\langle (u_\tau - \langle u_\tau \rangle)^4 \rangle}{\langle u_\tau^2 \rangle^2}. \quad (7)$$

Equation (6) becomes zero for a Gaussian distribution, larger values correspond to broader, more heavy-tailed PDF.  $\lambda^2$  is of practical relevance as it provides an analytical expression for the shape of  $p(u_\tau)$ . A discussion about the interpretation is given in Section 4. In this analysis, we compute  $\lambda^2$  for time scales  $\tau$  that relate to the rotor diameter  $D$  of the respective turbine.

10 Using Taylor's hypothesis of frozen turbulence (Mathieu and Scott, 2000), the length scale  $r = D$  is converted to the time scales  $\tau$ ,

$$\tau = r / \langle u \rangle = D / \langle u \rangle, \quad (8)$$

whereas  $\langle u \rangle$  refers to the respective time series, resulting in varying values of  $\tau$  within a wake.

In order to compute  $u_\tau(t)$  using Equation (5), evenly spaced data are needed. The procedure applied to uniformly re-sample  
15 the non-uniform LDA data is described in Appendix A. The approach results in a constant sampling rate for each wake.

### 3 Results

#### 3.1 The non-yawed wakes

At first, we investigate wakes without yaw misalignment,  $\gamma = 0^\circ$ . Figure 5 shows the contour plots of the velocity component in mean flow direction  $\langle u \rangle / u_{ref}$  for both turbines, respectively,  $6D$  downstream. The velocity deficits behind both turbines show a circular shape as expected, exceeding the rotor area, indicating a slight wake expansion. For both wakes, the minimum velocity is  $\langle u \rangle / u_{ref} = 0.64$ . Besides those general similarities, some differences are apparent. Both graphs show the tower wake, which is pronounced stronger for the ForWind turbine. This can be explained by the larger tower diameter relative to the rotor diameter as shown in Figure 3. Similarly, the four poles the ForWind turbine is placed on (cf. Figure 1) are likely to enhance this effect. Figure 5 also reveals that the wake behind the ForWind turbine is slightly displaced vertically towards the ground. This effect  
25 can be linked to the tower wake, creating an uneven vertical transport of momentum as recently demonstrated by Pierella and Saeiran (2017). Next, the NTNU wake shows areas of velocities exceeding  $\langle u \rangle / u_{ref} = 1.1$  at the edges of the velocity deficit, especially in the corners of the contour plot. Very likely, this is a blockage effect as the measurement plane is significantly larger for the NTNU turbine. This results in a higher blockage ratio (13% for the NTNU rotor, 5.4% for the ForWind rotor). As suggested by Chen and Liou (2011), blockage effects are expected for a cross-sectional blockage ratio exceeding 10%

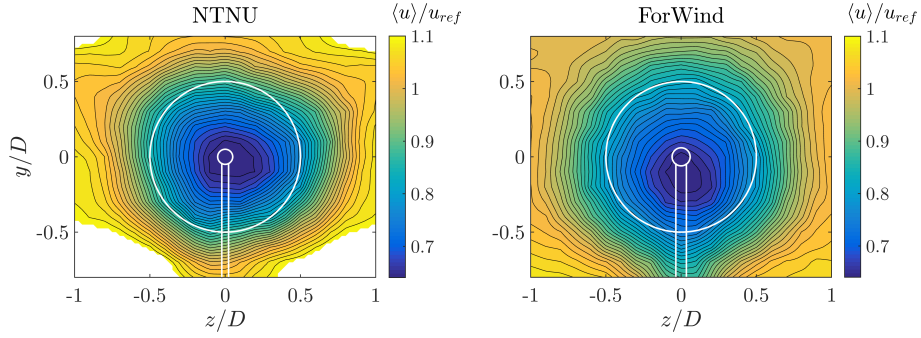


**Figure 5.**  $\langle u \rangle / u_{ref}$  at  $\gamma = 0^\circ$  for the NTNU turbine (left) and ForWind turbine (right). The white lines indicate the contours of the respective turbine. Values exceeding  $\langle u \rangle / u_{ref} = 1.1$  are masked.

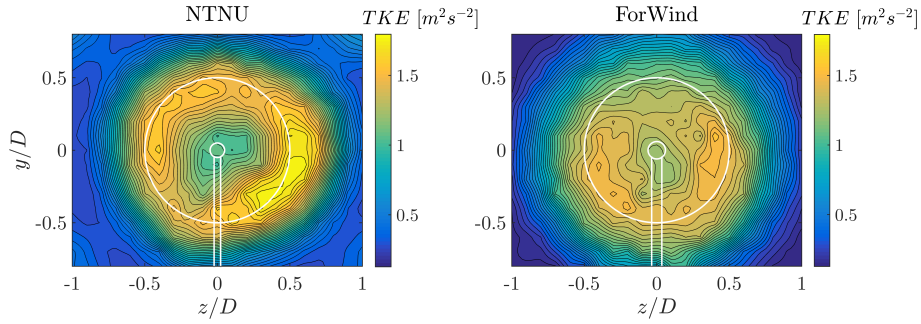


**Figure 6.** Turbulent kinetic energy (TKE) in  $m^2 s^{-2}$  according to Equation (4) for  $\gamma = 0^\circ$ . Left: NTNU turbine, right: ForWind turbine.

when using model wind turbines, which is confirmed here. In order to better compare both contour plots, values exceeding  $\langle u \rangle / u_{ref} = 1.1$  are masked.

To further analyze the wake flows, Figure 6 shows the contour plots of the turbulent kinetic energy (TKE) behind both turbines. The contours of the TKE appear as a circular shape, slightly larger than the rotor area. Behind the NTNU rotor, an outer ring of high TKE values appears more pronounced than in the center region. This observation is significantly less distinct for the ForWind turbine. The differences of the pronounced ring arise most likely from the different blade geometries. The airfoil of the NTNU turbine (NREL S826) has higher lift coefficients for the relevant angles of attack and Reynolds numbers compared to the ForWind rotor (SD7003 airfoil). A comparison of both airfoils is given in Schottler et al. (2017b). As a result, larger pressure differences between suction and pressure side of the blades are expected, resulting in more pronounced tip vortices shed from the NTNU rotor. Although those are already decayed at  $x/D = 6$  (Eriksen and Krogstad, 2017), the tip vortices are likely to be the origin for a pronounced TKE at blade tip locations for behind the NTNU rotor.

Further increasing in complexity and completeness of the wakes' stochastic description, Figure 7 shows the contour plots of the shape parameter  $\lambda^2$  behind both turbines. The length scale  $\tau$  is related to the rotor diameter  $D$  of the respective turbine. The scale is transferred from space to time using Taylor's Hypothesis, cf. Equation (8). In both cases, the contours of  $\lambda^2$  show

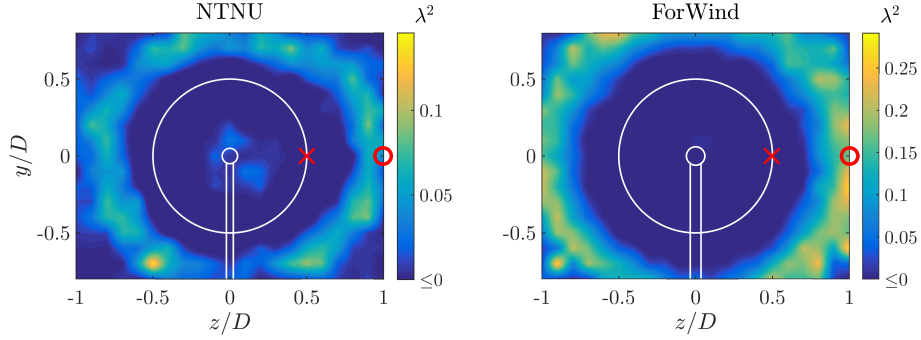


**Figure 7.**  $\lambda^2$  for both turbines at  $\gamma = 0^\circ$ . The time scales  $\tau$  correspond to the length scale of the rotor diameter, cf. Equation (8). The red markings  $\times$  and  $\circ$  show measurement positions for which  $p(u_\tau)$  were calculated as shown in Figure 8. Left: NTNU turbine, right: ForWind turbine. Note the different scaling.

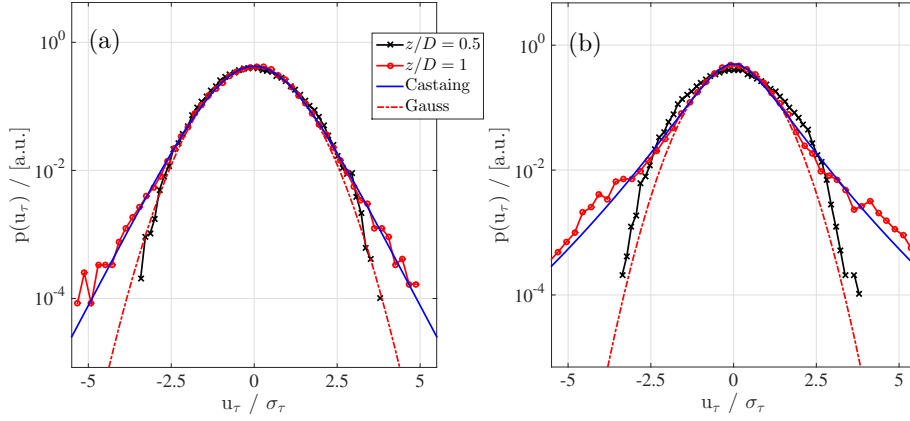


**Figure 8.**  $p(u_\tau)$  of the time series at two measurement position, ( $y = 0, z = D/2$ ) and ( $y = 0, z = D$ ) corresponding to the red marks in Figure 7. (a): NTNU turbine, (b): ForWind turbine, both at  $\gamma = 0^\circ$ . The time scales  $\tau$  are related to the length scales of rotor diameters by Taylor's Hypothesis using Equation (8). For  $z/D = 1$  (red curve) the Castaing distribution is shown with  $\lambda_{NTNU}^2 = 0.046$  and  $\lambda_{ForWind}^2 = 0.17$  (Castaing et al., 1990). A Gaussian fit is added to guide the eye.

a circular ring, whose diameter is significantly larger than the rotor diameter. In order to quantify the qualitative shapes of the contours shown in Figure 7, Figure 8 shows the increment PDFs of the respective time series,  $p(u_\tau)$ , at the positions indicated by the red marks ( $\circ/\times$ ) in Figure 7.  $u_\tau$  is normalized by the standard deviation,  $\sigma_\tau$ , for better visual comparison. As shown in black, the positions behind the rotor tips, where  $\lambda^2 \approx 0$ , reveal increment PDFs very close to a Gaussian, which holds for both turbines. For  $z = D$ , which lies within the ring of large  $\lambda^2$  values,  $p(u_\tau)$  strongly deviates from a Gaussian, showing a heavy-tailed distribution, indicating more frequent occurrences of extreme events. Exemplary, in both cases an event of  $5\sigma_\tau$  is underestimated by multiple orders of magnitude comparing a Gaussian distribution to the PDFs at  $z = D$ . Figure 8 further shows  $p(u_\tau)$  based on the model proposed by Castaing et al. (1990). Those distributions were evaluated based on

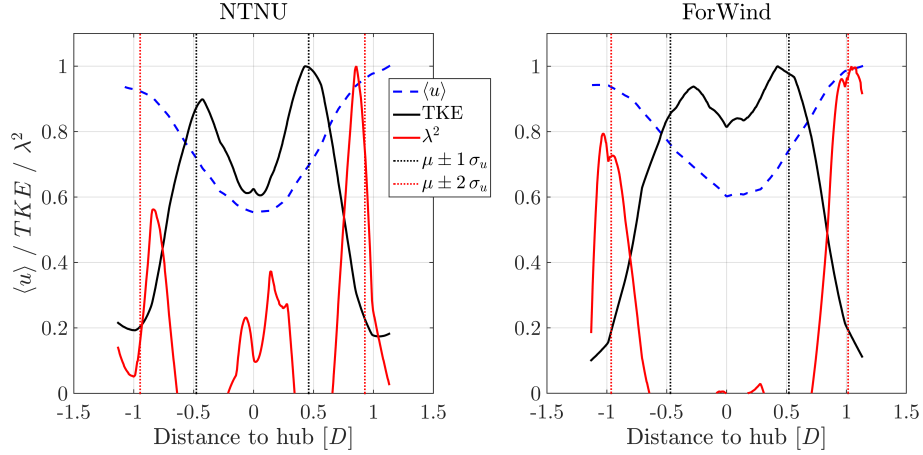


**Figure 9.** Diagonal cuts on the line  $y = z$  through the contour plots for  $\gamma = 0^\circ$ . Values are normalized to their respective maximum. The vertical dotted lines mark  $\mu \pm 1\sigma_u$  (black) and  $\mu \pm 2\sigma_u$  (red) of a Gaussian fit through the velocity deficit shown in blue.

the  $\lambda^2$  values computed by Equation (6) at  $z = D$ , visualizing exemplarily how well the distributions' shapes are grasped by  $\lambda^2$ . To show the difference in  $p(u_\tau)$  more intuitively, Figure ?? shows the increment time series  $u_\tau(t)/\sigma_\tau$  at  $z = D/2$  and  $z = D$ , exemplary for the ForWind turbine. It can be seen how Figure ??(a) is characterized by noisy fluctuations while Figure ??(b) shows sudden jumps e.g. extreme events  $u_\tau(t)$  at  $z = D/2$  (a) and  $z = D$  (b) behind the ForWind turbine, cf. Figures 7(b) and 8(b).  $\sigma_\tau$  is the standard deviation of  $u_\tau$ . Our results show that, depending on the examined quantity, different radial wake regions are of interest. To compare the varying spatial extensions of the three quantities' significant areas, Figure 9 shows diagonal cuts through the respective contour plots for the non-yawed cases along the line  $y = z$ . The area of pronounced TKE approximately coincides with the rotor area. The notable peaks are separated by  $\approx 0.86 D$  (NTNU) and  $\approx 0.77 D$  (ForWind), respectively, being significantly less pronounced behind the ForWind rotor as previously described. Clearly, the  $\lambda^2$  peaks span a much larger distance, being approximately  $1.7 D$  (NTNU) and  $2.0 D$  (ForWind). At their location, the velocity deficit has recovered to  $\geq 90\%$  of the free stream velocity in all cases. Thus, for a thorough description of wind turbine wakes, a much larger radial area is of interest as compared to a description restricted to mean values and the turbulent kinetic energy as often done in literature and wake models. An approximation of the lateral extension of high TKE and  $\lambda^2$  values based on a Gaussian fit through the velocity deficit is given by  $\mu \pm 1\sigma_u$  and  $\mu \pm 2\sigma_u$ , respectively, with  $\mu$  being the mean value and  $\sigma_u$  the standard deviation of the fit. For illustration, the dotted lines in Figure 9 mark the respective locations. It is shown that the radial areas of TKE and  $\lambda^2$  can be related in this way to the velocity deficit. To get a feeling of the impact on potential downstream turbine, Figure 10 compares  $p(u_\tau)$  in absolute terms at a free stream position,  $y/D = 0.8, z/D = 1$ , and at a position featuring high  $\lambda^2$  values,  $y/D = 0, z/D = 1$ , exemplary for the ForWind turbine. It becomes clear that velocity increments exceeding  $3ms^{-1}$  occur much more frequent within the ring of high  $\lambda^2$  values than in three free stream. Hereby we show that this radial position of the wake features significantly different flows than the free stream. To compare more visually, Figure 11 shows the

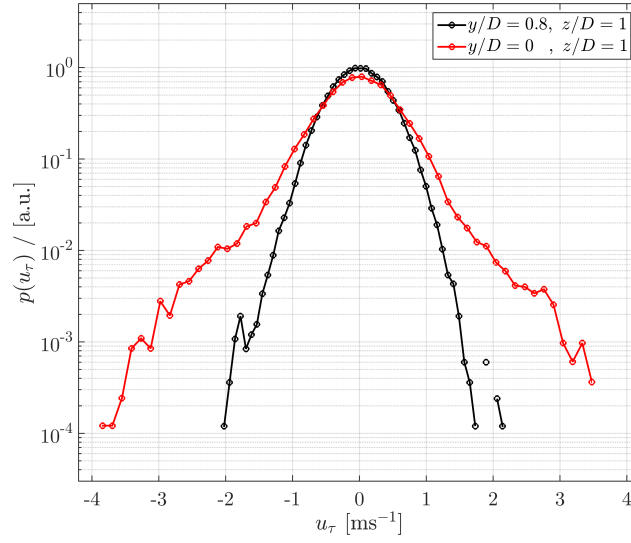


**Figure 10.**  $p(u_\tau)$  of the free stream at  $y/D = 0.8, z/D = 1$  and of  $y/D = 0, z/D = 1$ , exemplary for the ForWind turbine.

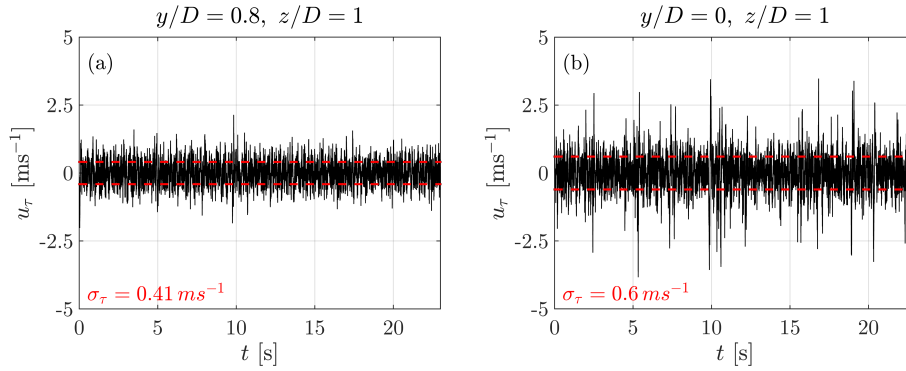


**Figure 11.** Time series of increments  $u_\tau(t)$  for the positions  $y/D = 0.8, z/D = 1$  (free stream, a) and  $y/D = 0, z/D = 1$ . The standard deviations  $\sigma_\tau$  are indicated in red.

corresponding time series  $u_\tau(t)$ . Clearly, the spiky signature of extreme events become obvious in Figure 11(b), confirming that no free stream condition is reached at  $z/D = 1$ .

### 3.2 Wakes during yaw-misalignment

During a yaw misalignment of  $\gamma = \pm 30^\circ$ , the velocity deficits behind both rotors are deflected and deformed as shown in Figure 12 by the contours of the main flow component  $\langle u \rangle / u_{ref}$ .

The wake is deflected sideways behind both turbines, whereas the lateral direction is dependent on the yaw angle's sign. This is expected due to a lateral thrust component of the rotor as a result of yaw misalignment, which has been observed and



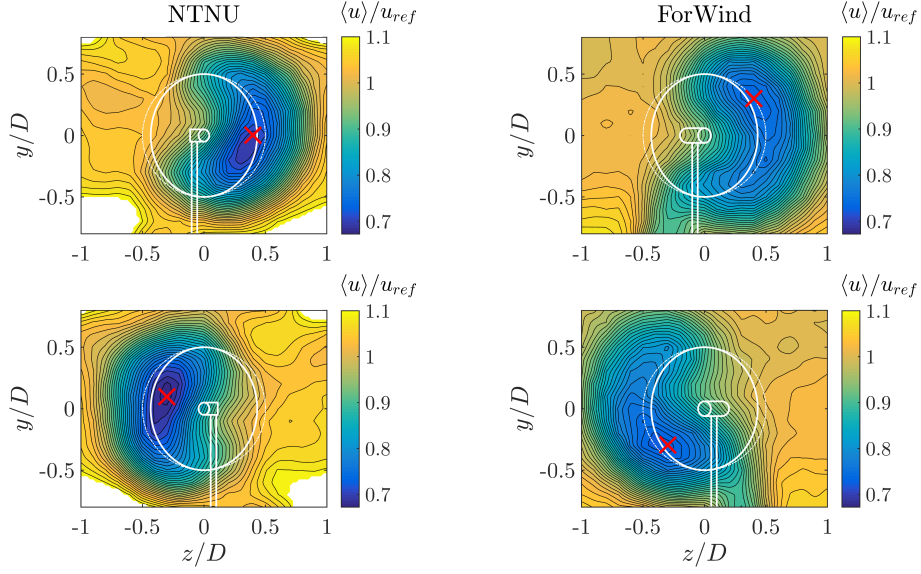


**Figure 12.**  $\langle u \rangle / u_{ref}$  during yaw misalignment. Top row:  $\gamma = -30^\circ$ , ~~but~~ bottom row:  $\gamma = 30^\circ$ . Left column: NTNU turbine, right column: ForWind turbine. The solid white lines indicate the contours of the respective turbine, while the dashed lines denote the rotor area without yaw misalignment. The red  $\times$  marks the position of minimum measured velocity  $\langle u \rangle$ . Values exceeding 1.1 are masked for better comparison.

**Table 2.** Wake center location as computed by the approach described in Section 2.2 with corresponding skew angles.

Turbine	Yaw angle [ $^\circ$ ]	Wake center [ $D$ ]	Skew angle [ $^\circ$ ]
NTNU	30	-0.28	$\approx -2.6$
NTNU	-30	0.32	$\approx 3.0$
ForWind	30	-0.38	$\approx -3.6$
ForWind	-30	0.38	$\approx 3.6$

described in numerous studies including (Medici and Alfredsson, 2006; Jiménez et al., 2010; Vollmer et al., 2016; Trujillo et al., 2016). The deflection of the velocity deficit is quantified using the approach described in Section 2.2, the results are listed in Table 2 including the resulting wake skew angles.

As Table 2 shows, the skew angles behind the ForWind turbine are equal apart from their sign for both directions of yaw misalignment. The NTNU rotor however, shows slightly different deflection angles for  $\gamma = 30^\circ$  and  $\gamma = -30^\circ$ , which is likely caused by blockage effects, that play a more significant role for the NTNU rotor due to the larger blockage ratio. This can also be seen in Figure 12, where speed-up effects are visible in the corners. In Schottler et al. (2017b), where the same setup was used<sup>1</sup>, the skew angle for the NTNU rotor decreased from  $x/D = 3$  to  $x/D = 6$ , which is a further indication for wall

<sup>1</sup>In Schottler et al. (2017b), the quantification was carried out for a sheared inflow. Other aspects of the setup were equal.

effects due to blockage, especially during yaw misalignment. Furthermore, both values show smaller angles as for the ForWind turbine. ~~In addition to the blockage effects, this is much likely caused by differences in thrust coefficient, cf. Table 1.~~

In Figure 12, minimum  $\langle u \rangle$  values are marked, showing a vertical transport of momentum in all cases. For  $\gamma = 30^\circ$ , the wake is moved upwards behind the NTNU turbines, and downwards behind the ForWind rotor. Directions are reversed for  $\gamma = -30^\circ$ . Similar observations have been made by Bastankhah and Porté-Agel (2016). The vertical transport is related to an interaction of a wake's rotation with the tower shadow/ground. Our results isolate this effect, as the direction of vertical transport is opposite comparing both turbines having an opposite direction of rotation. The fact that the vertical transport is stronger behind the ForWind rotor further supports this explanation as the tower wake is more pronounced due to the larger tower diameter and the structure the turbines is placed on.

A deformation of the velocity deficit to a curled "kidney" shape is observed for both turbines during yaw misalignment, whereas it is slightly more pronounced behind the ForWind turbine. The curled shape behind a wind turbine model in yaw has previously been observed by Howland et al. (2016) using a drag disc of 30 mm diameter and by Bastankhah and Porté-Agel (2016) using a rotating turbine model of 150 mm diameter. Figure 12 confirms these findings on two further scales. For a better comparison of the curled shape of the velocity deficit during yaw misalignment, we apply the following parametrization, exemplary shown in Figure 13(a) for the ForWind turbine at  $\gamma = 30^\circ$ : data points of horizontal cuts through the wake,  $\langle u \rangle_{y=\text{const.}}$ , are fitted by a polynomial. The procedure is repeated for values of  $y$  ranging from  $-0.4D$  to  $0.4D$ . The positions of the polynomials' minima (green marks), are fitted by a quadratic function (red line). Figure 13(b) shows the comparison of both turbines for  $\gamma = \pm 30^\circ$ . As already seen in Figure 12, the wakes behind the ForWind turbine are deflected further and the curled shape is pronounced stronger, which can be attributed to ~~the larger thrust coefficient and~~ blockage effects. Figure 13(b) also shows that the wakes behind both turbines are slightly tilted. Looking at the black curves (ForWind turbine), an asymmetry can be noticed as the curves are tilted towards the left, while the red curves are tilted towards the right. This is illustrated by the gray, dashed lines in Figure 13(b) which connect the points of intersection for  $\gamma = \pm 30^\circ$ . Similar asymmetries have been observed by Bastankhah and Porté-Agel (2016) for positive and negative yaw angles, which is explained by an interaction of a wake's rotation with the tower wake and the ground. By using turbines of opposite rotation direction, we can attribute the asymmetries in vertical transport and the tilt in opposite direction for  $\gamma = \pm 30^\circ$  to the rotation of rotor and wake. Not shown in detail here, the same effect was observed for different inflow conditions and other downstream distances, using the same setup and methods as in this study.

Adding TKE and  $\lambda^2$  contours during yaw misalignment, Figure 14 shows all three examined quantities, exemplary at a yaw misalignment of  $\gamma = -30^\circ$ , for both turbines. The shapes of the TKE contours are deformed similarly as for  $\langle u \rangle$ . A curled shape evolves and the differences between both turbines as described for  $\gamma = 0^\circ$  are still notable during yaw misalignment. Similarly, the circular rings of high  $\lambda^2$  values are deformed to a curled shape at  $\gamma = \pm 30^\circ$ . Thus, the general effect of heavy-tailed increment PDFs surrounding the velocity deficits in a wake is stable against yaw misalignment and the resulting inflow variations at the rotor blades. Further, this finding is confirmed in Large Eddy Simulations (LES) performed at the Universidad de la República, Uruguay, shown in Appendix B. Therewith, it is found to be a general effect as it is observed for all wakes considered, independent of yaw misalignment or turbine design. The red markings in Figure 14 show the approximation of the

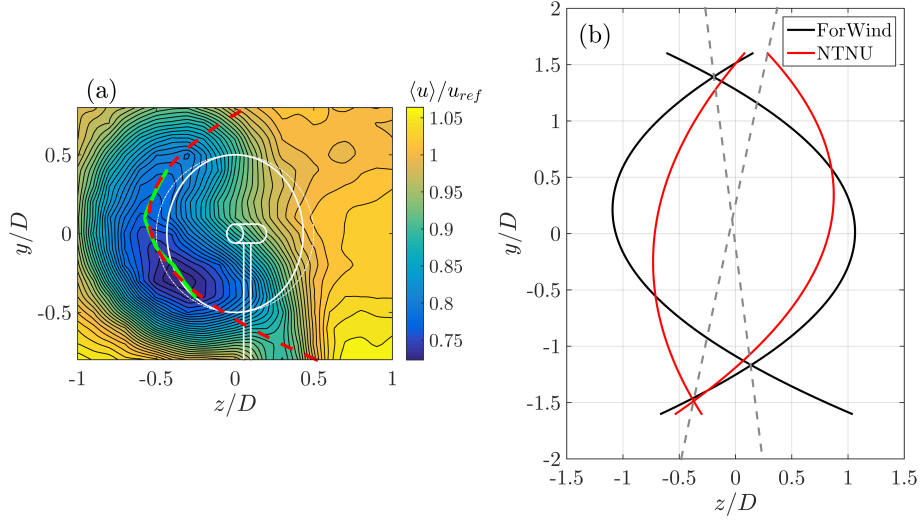


**Figure 13.** (a): Example of parameterizing the curled shape of the velocity deficit. The green markings show minimal velocities of a polynomial function used to fit the interpolated data points in a horizontal line,  $y = \text{const}$ . The red, dashed line shows a quadratic fit based on the green markings. (b): Visualization of the curled shapes of the velocity deficits. For both turbines, the cases  $\gamma = \pm 30^\circ$  are shown. Dashed lines show a visualization of the wakes tilt, connecting the respective intersections of the curves.

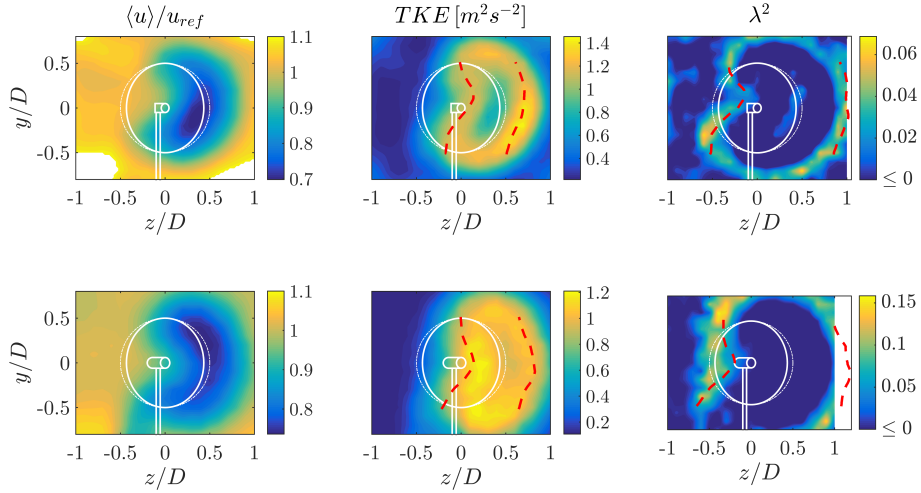


**Figure 14.**  $\langle u \rangle / u_{ref}$  (left column), TKE (center column) and  $\lambda^2$  (right column) for  $\gamma = -30^\circ$  behind the NTNU turbine (top row) and the ForWind turbine (bottom row). The time scale for  $\lambda^2$  corresponds to the length scale of the rotor diameter. The red marks show the approximation of the respective parameter's radial extension based on  $\mu \pm 1\sigma_u$  (TKE, middle column) and  $\mu \pm 2\sigma_u$  ( $\lambda^2$ , left column) as described in Section 3.1.

radial extension of the TKE and  $\lambda^2$  based on  $\mu \pm 1\sigma_u$  and  $\mu \pm 2\sigma_u$ .  $\mu$  and  $\sigma_u$  correspond to Gaussian fits of the velocity deficits

at various horizontal cuts ( $y=\text{const.}$ ) from  $y/D = -0.5$  to  $y/D = 0.5$ . It is shown that the methods results in quite good first order approximations, also during yaw misalignment.

## 4 Discussion

In this study the characterization of yawed and non-yawed wind turbine wakes is investigated and extended by taking into account a further turbulence measure, namely the intermittency parameter  $\lambda^2$ . We find heavy-tailed distributions of velocity increments in a ring area *surrounding* the velocity deficit and areas of high TKE in a wind turbine wake. Thus, the definition of a wake width strongly depends on the quantities taken into account as the ring area features significantly different statistics than the free stream. The heavy-tailed distributions are the statistical description of large velocity changes over given time scales and are transferred to turbines in terms of loads and power output. This has been shown experimentally (Schottler et al., 2017c), numerically (Mücke et al., 2011) and in a field study by Milan et al. (2013). Consequently, our findings should be considered in wind farm layout optimization approaches, where a wake's width affects-is a crucial parameter for radial turbine spacing. As layouts are being optimized regarding power and loads, the latter might be significantly affected by taking into account intermittency and the resulting increased wake width. Possibly, the ring of non-Gaussian velocity increments is a result of instable flow states, where the flow switches between a wake and free stream state. Behind a rotor, the wake characteristics dominate the flow. Outside the wake, free stream properties are dominant. In the transition zone, a switching between both flow states is believed to result in heavy-tailed velocity increments and therewith high  $\lambda^2$  values. Generally,  $\lambda^2$  will be larger for smaller scales  $\tau$ , which is a known feature of turbulence (Frisch, 1995).

Care should be taken when interpreting  $\lambda^2$  as an indicator for an increment PDF's shape. Here, we use the shape parameter as qualitative indicator. For a more quantitative analysis, one has to consider the increment PDF of a time series directly. This is done in Figure 8 exemplary for chosen points, however, in order include all time series of a wake, using  $\lambda^2$  allows for a much better visualization and comparison.

Figure 14 shows that the velocity deficit is deflected laterally during yaw misalignment, so that a potential in-line downstream turbine would exhibit a power increase as more undisturbed flow hits the rotor area at  $z/D \approx -0.5$ . Looking at the  $\lambda^2$  contours however shows, that areas of non-Gaussian velocity increments are now deflected onto the rotor area. This becomes important when assessing the applicability of active wake steering approaches, as a gain in power has to be balanced with a potential load increase, affecting maintenance costs and the lifetime of turbines overall.

It should be noted that it is to date not clear to what extent high TKE levels and intermittent force data are affecting common ways of fatigue and extreme load calculations. This important aspects needs to be addressed in future works. Possibly, it strongly dependents on details such as considered time scales. In our opinion, it is likely that non-Gaussian inflow is linked to drive train, gear box or pitch systems failures, especially because those inflow characteristics are not accounted for in standard models used in the design process.

The velocity deficit in mean flow direction  $\langle u \rangle$  deforms to a curled "kidney" shape during yaw misalignment. Consequently, horizontal cuts through the wake are insufficient when characterizing wakes behind yawed rotors, resulting in misleading and incomplete conclusions when quantifying wake deflections by yaw misalignment. The parametrization of the wake's curl

shown in Figure 13 should not be interpreted as quantification. Instead, we use the described approach to better compare multiple curled wakes as done in Figure 13(b). Our analyses include the velocity deficit in mean flow direction, the turbulent kinetic energy and the shape parameter  $\lambda^2$ . The turbulence intensity in the wake revealed very comparable results as the TKE, which is why we restrict our analyses to the TKE.

5 Besides the lateral deflection, a vertical transport of the velocity deficit is observed for both turbines during yaw misalignment. Using counter-rotating turbines, this effect could be attributed to the wake's rotation and its interaction with the tower wake. In full scale scenarios, the ground, wind shear and rotor tilt would further contribute to the effect. For potential floating turbines, a pitch motion will deflect the wake upwards, see Rockel et al. (2014). This vertical deflection will interact with the vertical transport shown in Figure 12. Consequently, the direction of yaw misalignment is believed to be of importance when applying  
10 the concept of wake steering to wind farm controls. This confirms findings by Fleming et al. (2014a) and Schottler et al. (2017a), reporting an asymmetric power output of a two-turbine case with respect to the upstream turbine's angle of yaw misalignment. One should bear in mind that the inflow turbulence intensities are different regarding both turbines. We want to point out that the influence of inflow turbulence on the wake deflection is studied in Bartl et al. (2018), showing no significant effects.

## 15 5 Conclusions

This work shows an experimental investigation of wind turbine wakes, using two different model wind turbines. The analyses include the main flow component, the turbulent kinetic energy and two-point statistics of velocity increments, quantified by the shape parameter  $\lambda^2$ . Yaw angles of  $\gamma = \{0^\circ, \pm 30^\circ\}$  are considered at a downstream distance of  $x/D = 6$ .

Generally, the results of  $\langle u \rangle$ , the TKE and  $\lambda^2$  compare well for both model turbines. Minor differences could be ascribed to the  
20 more prominent blockage (12.8% vs 5.4%) in the NTNU setup, confirming findings by Chen and Liou (2011) even for wake velocity measurements, who state blockage effects can be neglected for a blockage ratio  $\leq 10\%$ .

An outer ring of heavy-tailed velocity increments surrounds the velocity deficit and areas of high TKE in a wind turbine wake. The wake features significantly non-Gaussian velocity increment distributions in those areas, where the velocity deficit recovered nearly completely. For  $\gamma = 0^\circ$ , the ring has a diameter of approximately  $1.7D - 2D$ , depending on the turbine. Based  
25 on a Gaussian fit through the velocity deficit, the radial location of intermittent increments can be approximated by  $\mu \pm 2\sigma_u$ , making a wake considerably wider when taking two-point statistics into account. This observation becomes important in wind farm layout optimization and active wake steering approaches through yaw misalignment.

During yaw misalignment, the circular shape of a wake is deformed to a curled kidney-shape. A method for parameterizing the curl-shape was introduced. Further, the lateral wake deflection was quantified, resulting in skew angles of  $\pm 3.6^\circ$  at  $\pm 30^\circ$   
30 for the smaller rotor and  $3.0^\circ$  and  $-2.6^\circ$  for the larger rotor. Furthermore, vertical momentum transport in the wake during yaw misalignment was observed. The direction of vertical transport is dependent on the direction of yaw misalignment. Using counter-rotating turbines, the effect could be attributed to an interaction of a wake's rotation with the tower wake in this study.

*Data availability.* The experimental data set is available upon request.

## **Appendix A: Data preprocessing**

In order to study intermittency using the shape parameter  $\lambda^2$ , uniformly sampled data are needed when applying Equation (5). As the LDA measurement result in non-uniformly sampled data points, appropriate preprocessing is necessary. In the following, the procedure is described that results in uniformly sampled data points. It is exemplary applied to the data of an arbitrarily chosen wake.

The time separating two samples of a time series is  $\Delta t$ . For one time series,  $(\Delta t)^{-1}$  is plotted for all samples in Figure A1 (a). The corresponding histogram is shown in Figure A1 (b). The point corresponding to 40 % of all events is marked by the red dashed line and is referred to as  $F_S$ . In this example,  $F_S \approx 1.17$  kHz.

This procedure is repeated for all 357 time series contained in one plane of measurement. Figure A2 shows  $F_S$  for all time series, with the mean value indicated. The mean value of all  $F_S$  values in one plane will be used as sampling frequency to re-sample the time series in one plane uniformly, an exemplary result is shown in Figure A3. Data points are interpolated linearly onto a vector of uniformly spaced instants defined by the new sampling rate  $\langle F_S \rangle$ . It should be noted that the analyses of velocity increments were performed for different constant sampling rates without showing any significant effect on the results.

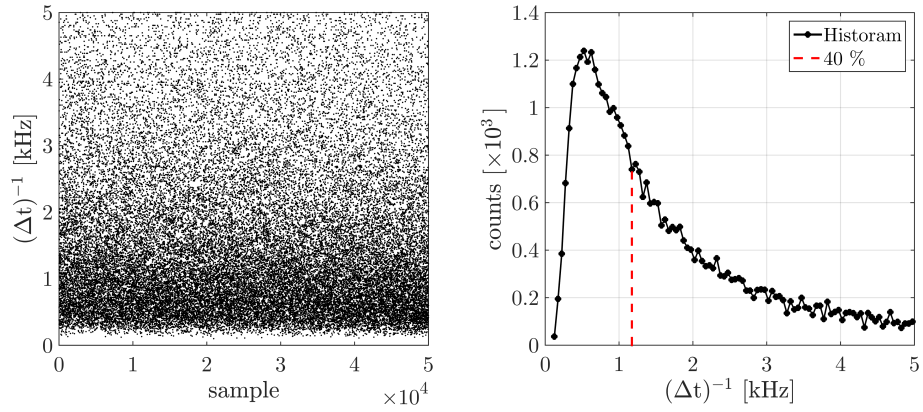


**Figure A1.**  $(\Delta t)^{-1}$  for all samples (a) with the respective histogram (b), where the maximum value is marked by the red, dashed line.

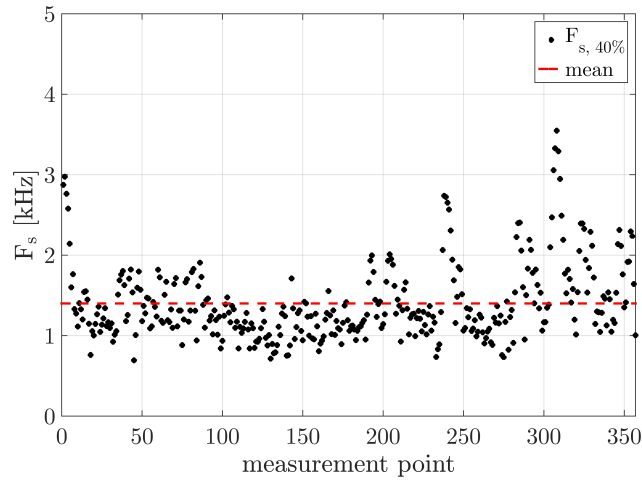


**Figure A2.**  $F_S$  for all 357 time series of one wake, the mean value is indicated in red, being  $\langle F_S \rangle = 1.4$  kHz.

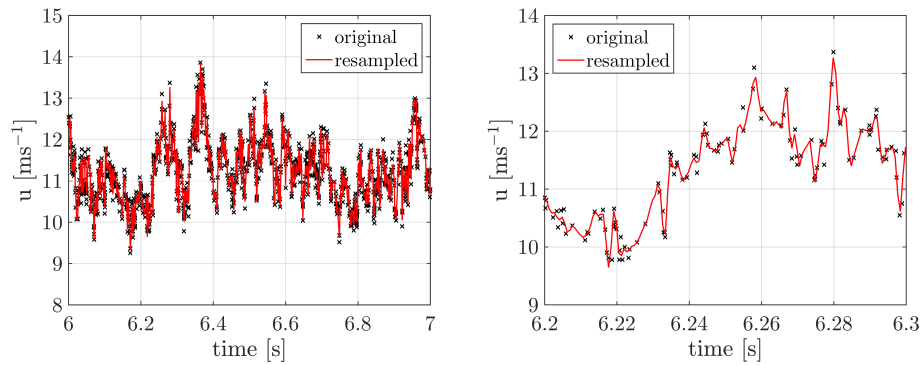


**Figure A3.** Examples of resampling the raw data  $u(t)$  uniformly with  $\langle F_S \rangle = 1.4$  kHz.



## Appendix B: LES simulations

Within the scope of the *blind test 5* project, LES simulations of the ForWind turbine in a very comparable setup were performed, where the inflow features a vertical shear as opposed to the experiments shown in this paper. The incompressible flow solver `caffa3d.MBRi` as described by Mendina et al. (2014) and Draper et al. (2016) was used to obtain the results shown in Figure 5 B1. The turbine was modeled by actuator lines. The top row shows  $x/D = 3$ ,  $x/D = 6$  is shown beneath. The contours of  $\langle u \rangle / u_{ref}$  and  $\lambda^2$  reveal very similar results compared to the experimental data. Qualitatively, it can be concluded that the outer ring of high  $\lambda^2$  values and thus heavy-tailed distributions of velocity increments, that surrounds the velocity deficit of a wake, can be correctly predicted in LES simulations.

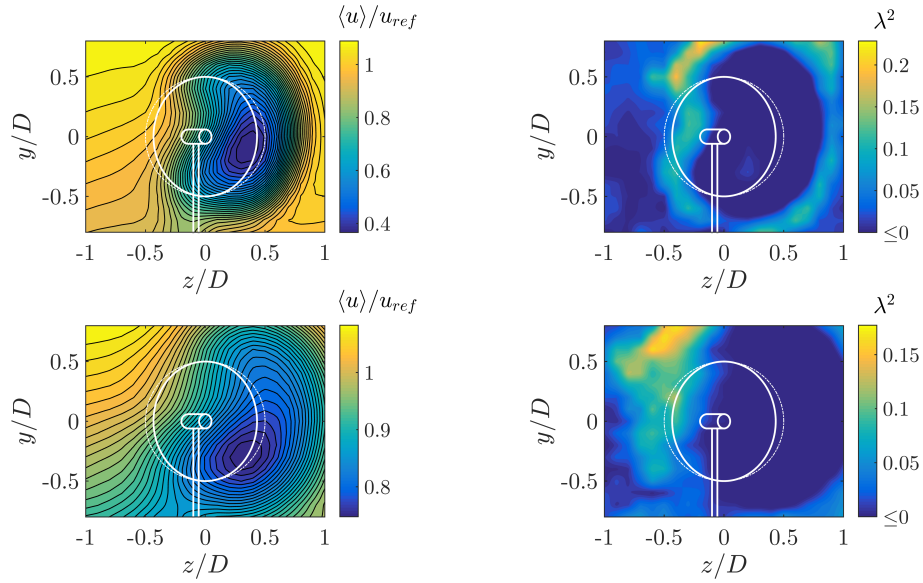


**Figure B1.** LES data of the wakes 3D (top row) and 6D (bottom row) behind the ForWind turbine at  $\gamma = 30^\circ$ . In contrast to the experiments presented in this paper, the inflow in the LES domain features a vertical shear with comparable turbulence intensity. The time scales of  $\tau$  for the  $\lambda^2$  calculations correspond to the length scale of the rotor diameter.

*Competing interests.* The authors declare no competing interests.

*Acknowledgements.* The authors thank Marín Draper and Andrés Guggeri, Universidad de la República, Uruguay for performing the LES simulation and providing the data. [Parts of this project is funded by the Ministry for Science and Culture of Lower Saxony through the funding initiative «Niedersächsisches Vorab».](#) The authors also thank the Reiner Lemoine Foundation for further funding.

## References

- Abdulrahim, A., Anik, E., and Uzol, O.: Experimental Investigation of the Wake Flow Field of a Model Wind Turbine Rotor with Tip Injection, in: 33rd Wind Energy Symposium, January, pp. 1–10, American Institute of Aeronautics and Astronautics, Reston, Virginia, <https://doi.org/10.2514/6.2015-0498>, <http://arc.aiaa.org/doi/10.2514/6.2015-0498>, 2015.
- 5 Amidror, I.: Scattered data interpolation methods for electronic imaging systems: a survey, *Journal of Electronic Imaging*, 11, 157, <https://doi.org/10.1117/1.1455013>, <http://electronicimaging.spiedigitallibrary.org/article.aspx?doi=10.1117/1.1455013>, 2002.
- Bak, C., Zahle, F., Bitsche, R., and Kim, T.: The DTU 10-MW reference wind turbine, *Danish wind power . . .*, <http://orbit.dtu.dk/services/downloadRegister/55645274/>, 2013.
- Barthelmie, R. J., Pryor, S., Frandsen, S. T., Hansen, K. S., Schepers, J., Rados, K., Schlez, W., Neubert, A., Jensen, L., and Neckelmann, S.:  
10 Quantifying the impact of wind turbine wakes on power output at offshore wind farms, *Journal of Atmospheric and Oceanic Technology*, 27, 1302–1317, 2010.
- Bartl, J. and Sætran, L.: Blind test comparison of the performance and wake flow between two in-line wind turbines exposed to different turbulent inflow conditions, *Wind Energy Science*, 2, 55–76, <https://doi.org/10.5194/wes-2-55-2017>, <http://www.wind-energ-sci-discuss.net/wes-2016-31/http://www.wind-energ-sci.net/2/55/2017/>, 2017.
- 15 Bartl, J., Mühle, F., Schottler, J., Sætran, L., Peinke, J., Adaramola, M., and Hölling, M.: Experiments on wind turbine wakes in yaw: Effects of inflow turbulence and shear, *Wind Energy Science*, submitted, 2017.
- Bartl, J., Mühle, F., Schottler, J., Sætran, L., Peinke, J., Adaramola, M., and Hölling, M.: Wind tunnel experiments on wind turbine wakes in yaw: Effects of inflow turbulence and shear, *Wind Energy Science Discussions*, pp. 1–22, <https://doi.org/10.5194/wes-2017-59>, <https://www.wind-energ-sci-discuss.net/wes-2017-59/>, 2018.
- 20 Bastankhah, M. and Porté-Agel, F.: Experimental and theoretical study of wind turbine wakes in yawed conditions, *Journal of Fluid Mechanics*, 806, 506–541, <https://doi.org/10.1017/jfm.2016.595>, <http://stacks.iop.org/1742-6596/625/i=1/a=012014>, 2016.
- Berg, J., Natarajan, A., Mann, J., and Patton, E. G.: Gaussian vs non-Gaussian turbulence: impact on wind turbine loads, *Wind Energy*, 17, n/a–n/a, <https://doi.org/10.1002/we.1963>, <http://doi.wiley.com/10.1002/we.1963>, 2016.
- Boettcher, F., Renner, C., Waldl, H. P., and Peinke, J.: On the statistics of wind gusts, *Boundary-Layer Meteorology*, 108, 163–173,  
25 <https://doi.org/10.1023/A:1023009722736>, 2003.
- Bottasso, C. L., Campagnolo, F., and Petrović, V.: Wind tunnel testing of scaled wind turbine models: Beyond aerodynamics, *Journal of Wind Engineering and Industrial Aerodynamics*, 127, 11–28, 2014.
- Burton, T., Sharpe, D., Jenkins, N., and Bossanyi, E.: *Wind Energy Handbook*, John Wiley and Sons, 2001.
- Campagnolo, F., Petrović, V., Bottasso, C., and Croce, A.: Wind tunnel testing of wake control strategies, in: *Proceedings of the American Control Conference*, vol. 2016-July, <https://doi.org/10.1109/ACC.2016.7524965>, 2016.
- 30 Castaing, B., Gagne, Y., and Hopfinger, E. J.: Velocity probability density functions of high Reynolds number turbulence, *Physica D: Non-linear Phenomena*, 46, 177–200, [https://doi.org/10.1016/0167-2789\(90\)90035-N](https://doi.org/10.1016/0167-2789(90)90035-N), 1990.
- Chen, T. and Liou, L.: Blockage corrections in wind tunnel tests of small horizontal-axis wind turbines, *Experimental Thermal and Fluid Science*, 35, 565–569, <https://doi.org/10.1016/j.expthermflusci.2010.12.005>, <http://dx.doi.org/10.1016/j.expthermflusci.2010.12.005http://linkinghub.elsevier.com/retrieve/pii/S0894177710002438>, 2011.
- 35 Chillà, F., Peinke, J., and Castaing, B.: Multiplicative Process in Turbulent Velocity Statistics: A Simplified Analysis, *Journal de Physique II*, 6, 455–460, <https://doi.org/10.1051/jp2:1996191>, 1996.

- Draper, M., Guggeri, A., and Usera, G.: Validation of the Actuator Line Model with coarse resolution in atmospheric sheared and turbulent inflow, *Journal of Physics: Conference Series*, 753, <https://doi.org/10.1088/1742-6596/753/8/082007>, 2016.
- Eriksen, P. E. and Krogstad, P. Å.: Development of coherent motion in the wake of a model wind turbine, *Renewable Energy*, 108, 449–460, <https://doi.org/10.1016/j.renene.2017.02.031>, <http://dx.doi.org/10.1016/j.renene.2017.02.031>, 2017.
- 5 España, G., Aubrun, S., Loyer, S., and Devinant, P.: Wind tunnel study of the wake meandering downstream of a modelled wind turbine as an effect of large scale turbulent eddies, *Journal of Wind Engineering and Industrial Aerodynamics*, 101, 24–33, 2012.
- Fleming, P., Gebraad, P. M., Lee, S., Wingerden, J.-W., Johnson, K., Churchfield, M., Michalakes, J., Spalart, P., and Moriarty, P.: Simulation comparison of wake mitigation control strategies for a two-turbine case, *Wind Energy*, 2014a.
- Fleming, P., Annoni, J., Shah, J. J., Wang, L., Ananthan, S., Zhang, Z., Hutchings, K., Wang, P., Chen, W., and Chen, L.: Field test  
10 of wake steering at an offshore wind farm, *Wind Energy Science*, 2, 229–239, <https://doi.org/10.5194/wes-2-229-2017>, <http://www.wind-energ-sci-discuss.net/wes-2017-4/><https://www.wind-energ-sci.net/2/229/2017/>, 2017.
- Fleming, P. a., Gebraad, P. M. O., Lee, S., van Wingerden, J. W., Johnson, K., Churchfield, M., Michalakes, J., Spalart, P., and Moriarty, P.: Evaluating techniques for redirecting turbine wakes using SOWFA, *Renewable Energy*, 70, 211–218, <https://doi.org/10.1016/j.renene.2014.02.015>, 2014b.
- 15 Frisch, U.: *Turbulence : the legacy of A.N. Kolmogorov*, vol. 1, Cambridge university press, <https://doi.org/10.1017/S0022112096210791>, 1995.
- Gebraad, P. M. O., Teeuwisse, F. W., van Wingerden, J. W., Fleming, P. A., Ruben, S. D., Marden, J. R., and Pao, L. Y.: Wind plant power optimization through yaw control using a parametric model for wake effects-a CFD simulation study, *Wind Energy*, 19, 95–114, <https://doi.org/10.1002/we.1822>, <http://doi.wiley.com/10.1002/we.1822>, 2014.
- 20 Howland, M. F., Bossuyt, J., Martínez-Tossas, L. A., Meyers, J., and Meneveau, C.: Wake structure in actuator disk models of wind turbines in yaw under uniform inflow conditions, *Journal of Renewable and Sustainable Energy*, 8, <https://doi.org/10.1063/1.4955091>, <http://dx.doi.org/10.1063/1.4955091>, 2016.
- Jiménez, Á., Crespo, A., and Migoya, E.: Application of a LES technique to characterize the wake deflection of a wind turbine in yaw, *Wind energy*, 13, 559–572, 2010.
- 25 Jonkman, J. M., Butterfield, S., Musial, W., and Scott, G.: *Definition of a 5-MW reference wind turbine for offshore system development*, National Renewable Energy Laboratory Golden, CO, 2009.
- Liu, L., Hu, F., Cheng, X.-L., and Song, L.-L.: Probability Density Functions of Velocity Increments in the Atmospheric Boundary Layer, *Boundary-Layer Meteorology*, 134, 243–255, <https://doi.org/10.1007/s10546-009-9441-z>, 2010.
- Mathieu, J. and Scott, J.: *An introduction to turbulent flow*, Cambridge University Press, 2000.
- 30 Medici, D. and Alfredsson, P.: Measurements on a wind turbine wake: 3D effects and bluff body vortex shedding, *Wind Energy*, 9, 219–236, 2006.
- Mendina, M., Draper, M., Kelm Soares, A. P., Narancio, G., and Usera, G.: A general purpose parallel block structured open source incompressible flow solver, *Cluster Computing*, 17, 231–241, <https://doi.org/10.1007/s10586-013-0323-2>, 2014.
- Milan, P., Wächter, M., and Peinke, J.: Turbulent character of wind energy, *Physical Review Letters*, 110, 1–5, <https://doi.org/10.1103/PhysRevLett.110.138701>, 2013.
- 35 Morales, A., Wächter, M., and Peinke, J.: Characterization of wind turbulence by higher-order statistics, *Wind Energy*, 15, 391–406, <https://doi.org/10.1002/we.478>, 2012.

- Mücke, T., Kleinhans, D., and Peinke, J.: Atmospheric turbulence and its influence on the alternating loads on wind turbines, *Wind Energy*, 14, 301–316, <https://doi.org/10.1002/we.422>, <http://dx.doi.org/10.1002/we.422>, 2011.
- Pierella, F. and Saetran, L.: Wind tunnel investigation on the effect of the turbine tower on wind turbines wake symmetry, *Wind Energy*, 17, 657–669, <https://doi.org/10.1002/we.2120>, <http://onlinelibrary.wiley.com/doi/10.1002/we.1608/fullhttp://doi.wiley.com/10.1002/we.2120>, 2017.
- 5 Rockel, S., Camp, E., Schmidt, J., Peinke, J., Cal, R. B., and Hölling, M.: Experimental study on influence of pitch motion on the wake of a floating wind turbine model, vol. 7, <https://doi.org/10.3390/en7041954>, 2014.
- Rockel, S., Peinke, J., Hölling, M., and Cal, R. B.: Wake to wake interaction of floating wind turbine models in free pitch motion: An eddy viscosity and mixing length approach, *Renewable Energy*, 85, 666–676, <https://doi.org/10.1016/j.renene.2015.07.012>, 2016.
- 10 Schottler, J., Hölling, A., Peinke, J., and Hölling, M.: Wind tunnel tests on controllable model wind turbines in yaw, 34th Wind Energy Symposium, p. 1523, 2016.
- Schottler, J., Hölling, A., Peinke, J., and Hölling, M.: Brief Communication : On the influence of vertical wind shear on the combined power output of two model wind turbines in yaw, pp. 1–5, 2017a.
- Schottler, J., Mühle, F., Bartl, J., Peinke, J., Adaramola, M. S., Saetran, L., and Hölling, M.: Comparative study on the wake deflection behind yawed wind turbine models, *Journal of Physics: Conference Series*, 854, 012 032, <https://doi.org/10.1088/1742-6596/854/1/012032>, <http://stacks.iop.org/1742-6596/854/i=1/a=012032?key=crossref.c68d7b8d172fd82bbd89c31f05132338>, 2017b.
- 15 Schottler, J., Reinke, N., Hölling, A., Whale, J., Peinke, J., and Hölling, M.: On the impact of non-Gaussian wind statistics on wind turbines – an experimental approach, *Wind Energy Science*, 2, 1–13, <https://doi.org/10.5194/wes-2-1-2017>, [http://www.wind-energ-sci-discuss.net/wes-2016-24/\\$\delimiter"026E30F\\$nhhttp://www.wind-energ-sci.net/2/1/2017/](http://www.wind-energ-sci-discuss.net/wes-2016-24/$\delimiter), 2017c.
- 20 Trujillo, J.-J., Seifert, J. K., Würth, I., Schlipf, D., and Kühn, M.: Full field assessment of wind turbine near wake deviation in relation to yaw misalignment, *Wind Energy Science Discussions*, pp. 1–17, <https://doi.org/10.5194/wes-2015-5>, <http://www.wind-energ-sci-discuss.net/wes-2015-5/>, 2016.
- van Kuik, G. A. M., Peinke, J., Nijssen, R., Lekou, D., Mann, J., Sørensen, J. N., Ferreira, C., van Wingerden, J. W., Schlipf, D., Gebraad, P., Polinder, H., Abrahamsen, A., van Bussel, G. J. W., Sørensen, J. D., Tavner, P., Bottasso, C. L., Muskulus, M., Matha, D., Lindeboom, H. J., Degraer, S., Kramer, O., Lehnhoff, S., Sonnenschein, M., Sørensen, P. E., Künneke, R. W., Morthorst, P. E., and Skytte, K.: Long-term research challenges in wind energy – a research agenda by the European Academy of Wind Energy, *Wind Energy Science*, 1, 1–39, <https://doi.org/10.5194/wes-1-1-2016>, <http://www.wind-energ-sci.net/1/1/2016/>, 2016.
- 25 Vollmer, L., Steinfeld, G., Heinemann, D., and Kühn, M.: Estimating the wake deflection downstream of a wind turbine in different atmospheric stabilities: an LES study, *Wind Energy Science*, 1, 129–141, <https://doi.org/10.5194/wes-1-129-2016>, <http://www.wind-energ-sci.net/1/129/2016/>, 2016.
- 30

# Wind tunnel experiments on wind turbine wakes in yaw: Redefining the wake width

Jannik Schottler<sup>1</sup>, Jan Bartl<sup>2</sup>, Franz Mühle<sup>3</sup>, Lars Sætran<sup>2</sup>, Joachim Peinke<sup>1,4</sup>, and Michael Hölling<sup>1</sup>

<sup>1</sup>ForWind, University of Oldenburg, Institute of Physics, Oldenburg, Germany

<sup>2</sup>Department of Energy and Process Engineering, Norwegian University of Science and Technology, Trondheim, Norway

<sup>3</sup>Faculty of Environmental Sciences and Natural Resource Management, Norwegian University of Life Sciences, Ås, Norway

<sup>4</sup>Fraunhofer IWES, Oldenburg, Germany

*Correspondence to:* Jannik Schottler (jannik.schottler@forwind.de)

**Abstract.** This paper presents an investigation of wakes behind model wind turbines, including cases of yaw misalignment. Two different turbines were used and their wakes are compared, isolating effects of boundary conditions and turbine specifications. Laser Doppler Anemometry was used to scan a full plane of a wake normal to the main flow direction, 6 rotor diameters downstream of the respective turbine. The wakes of both turbines are compared in terms of the time averaged main flow component, the turbulent kinetic energy and the distribution of velocity increments. The shape of the velocity increments' distributions is quantified by the shape parameter  $\lambda^2$ .

The results show that areas of strongly heavy-tailed distributed velocity increments are surrounding the velocity deficit in all cases examined. Thus, a wake is significantly wider when two-point statistics are included as opposed to a description limited to one-point quantities. As non-Gaussian distributions of velocity increments affect loads of downstream rotors, our findings impact the application of active wake steering through yaw misalignment as well as wind farm layout optimizations and should therefore be considered in future wake studies, wind farm layout and farm control approaches. Further, the velocity deficits behind both turbines are deformed to a kidney-like curled shape during yaw misalignment, for which parameterization methods are introduced. Moreover, the lateral wake deflection during yaw misalignment is investigated.

## 1 Introduction

Due to the installation of wind turbines in wind farm arrangements, the turbine wakes become inflow conditions of downstream rotors, causing *wake effects*. Those include a reduced wind velocity and increased turbulence levels. The former cause power losses of up to 20% (Barthelmie et al., 2010) in wind farms, while the latter are linked to increased loads of downstream turbines, affecting fatigue and life time (Burton et al., 2001). In order to mitigate wake effects, various concepts of active wake control strategies have been proposed and investigated. One concept is an active wake steering by an intentional yaw misalignment, where the velocity deficit behind a rotor is deflected laterally by misaligning it with the mean inflow direction. The possibility of wake re-direction by yawing was observed and investigated by means numeric simulations (e.g. Jiménez et al., 2010; Fleming et al., 2014b), in wind tunnel experiments (e.g. Medici and Alfredsson, 2006; Campagnolo et al., 2016) and in full-scale field measurements by Trujillo et al. (2016). Further, the potential of increasing the power yield in a wind farm

configuration was explored experimentally (Schottler et al., 2016), numerically (e.g. Fleming et al., 2014b; Gebraad et al., 2014) and in a field test in a full-scale wind farm (Fleming et al., 2017), showing promising results as the total power yield could be increased in the mentioned studies.

As the applicability of the concept to future wind farms require a thorough understanding of the wakes behind yawed wind turbines, this study examines the wakes behind model wind turbines during yaw misalignment. Experimental studies are necessary to validate numeric results, to tune engineering models and to gain a deeper understanding of the present effects in a controlled laboratory environment. However, when examining wake effects experimentally, varying turbine models are used. Those models strongly differ in their complexity and design, including blade design, geometry or control concepts. The simplest model is a drag disc concept, where a wind turbine is modeled by a porous disk in the flow as done by España et al. (2012) or Howland et al. (2016). Moreover, rotating turbine models have been used in numerous studies, where the design and complexity of the models vary significantly. Examples include (Medici and Alfredsson, 2006), (Bottasso et al., 2014), (Abdulahim et al., 2015), (Rockel et al., 2016) or (Bastankhah and Porté-Agel, 2016). In contrast to numerical studies, where the vast majority of the research community uses consistent turbine models (NREL 5 MW (Jonkman et al., 2009) or DTU 10 MW (Bak et al., 2013) reference turbines for example), experiments lack certain systematics and comparability due to varying turbine models, facilities and measurement techniques. The present study aims to compare the wakes of two different model wind turbines in the same facility, using comparable boundary conditions as far as possible. Therewith, a separation between general wake effects and turbine specific observations can be achieved.

We present wake analyses ranging from mean quantities to higher order statistics. Average mean flow components are of relevance when assessing the energy yield of potential downstream turbines. An investigation of turbulence parameters such as the turbulent kinetic energy (TKE) is linked to fluctuating inflow conditions, which is important for loads of downstream turbines and therewith their lifetime (Burton et al., 2001). To gain a deeper insight, we extend our analyses to two-point statistics. More precisely, velocity increments are analyzed, allowing for a scale dependent analysis of flows. Non-Gaussianity of the distributions of velocity increments has been reported not only in small scale turbulence (Frisch, 1995), but also in the atmospheric boundary layer (e.g. Boettcher et al., 2003; Liu et al., 2010; Morales et al., 2012). To what extent statistical characteristics of velocity increments are transferred to wind turbines is of current interest throughout the research community (van Kuik et al., 2016). Schottler et al. (2017c) found a transfer of intermittency from wind to torque, thrust and power data in a wind tunnel experiment using a model wind turbine. Similarly, Mücke et al. (2011) found a transfer of intermittency to torque data using a generic turbine model. Milan et al. (2013) reported intermittent power data in a full-scale wind farm. We thus believed that distributions of velocity increments in wakes are of importance for potential downstream turbines as non-Gaussian characteristics are likely to be transferred to wind turbines in terms of fluctuating loads and power output. Consequently, investigations of velocity increments in wakes become extremely relevant for active wake control concepts as well as for wind farm layout approaches. A further elaboration on the connection of non-Gaussian velocity increments and loads as well of power fluctuations is given in Section 4.

**Table 1.** Summary of main turbine characteristics. The tip speed ratio (TSR) is based on the free stream velocity  $u_{ref}$  at hub height. The Reynolds number at the blade tip,  $Re_{tip}$ , is based on the chord length at the blade tip and the effective velocity during turbine operation. For the ForWind turbine,  $0.96R$  was chosen as radial position to account for the rounded blade tips. The blockage corresponds to the ratio of the rotor’s swept area to the wind tunnel’s cross sectional area. The direction of rotation refers to observing the rotor from upstream, with (c)cw meaning (counter)clockwise. The thrust coefficients were measured at  $\gamma = 0^\circ$  and corrected for thrust on the tower and support structure.

Turbine	Rotor diameter	Hub diameter	Blockage	TSR	$Re_{tip}$	Rotation	$c_T$
ForWind	0.580 m	0.077 m	5.4 %	6	$\approx 6.4 \times 10^4$	cw	0.87
NTNU	0.894 m	0.090 m	13 %	6	$\approx 1.1 \times 10^5$	ccw	0.87

This work is organized as follows. Section 2 introduces the methods used throughout the study, including the experimental methods, a concept for quantifying a wake’s deflection and a definition of the examined parameters. Section 3 shows the result of the study. First, results of the non-yawed rotors are investigated and compared in Section 3.1. Wakes during yaw misalignment are analyzed in Section 3.2, including a quantification of the wake deflection. Section 4 discusses the findings before Section 5 summarizes this work and states the conclusions. This work is part of a joint experimental campaign by the NTNU in Trondheim and ForWind in Oldenburg. While this paper compares the wakes behind two different model wind turbines during one inflow condition, a second paper by Bartl et al. (2017) examines the influence of varying inflow conditions on the wake of one model wind turbine.

## 2 Method

### 10 2.1 Experimental methods

The experiments were performed in the wind tunnel of the Norwegian University of Science and Technology (NTNU) in Trondheim, Norway. The closed-loop wind tunnel has a closed test section of  $2.71 \text{ m} \times 1.81 \text{ m} \times 11.15 \text{ m}$  (width  $\times$  height  $\times$  length). The inlet to the test section was equipped with a turbulence grid having a solidity of 35% and a mesh size of 0.24 m. Further details about the grid are described by Bartl and Sætran (2017). Two different model wind turbines were used that vary in geometry, blade design and direction of rotation. Those deliberate distinctions allow for an isolation of general effects of wake properties. The turbines will be denoted *NTNU* and *ForWind*, respectively. Table 1 summarizes the main features and differences of both turbines, further details are described by Schottler et al. (2017b). Figure 1 shows technical drawings. As can be seen, the ForWind turbine was placed on four cylindrical poles to lift the rotor above the wind tunnel boundary layer to the same hub height as the NTNU turbine, being 820 mm above the wind tunnel floor. One turbine at a time was placed on a turning table allowing for yaw misalignment, denoted by the angle  $\gamma$ , which is positive for a clockwise rotation of the rotor when observed from above as sketched in Figure 2. For the NTNU turbine, the reference velocity measured in the empty wind tunnel was  $u_{ref,NTNU} = 10 \text{ m s}^{-1}$  at a turbulence intensity of  $TI = \sigma_u / \langle u \rangle = 0.1$ . For the ForWind turbine, the inflow



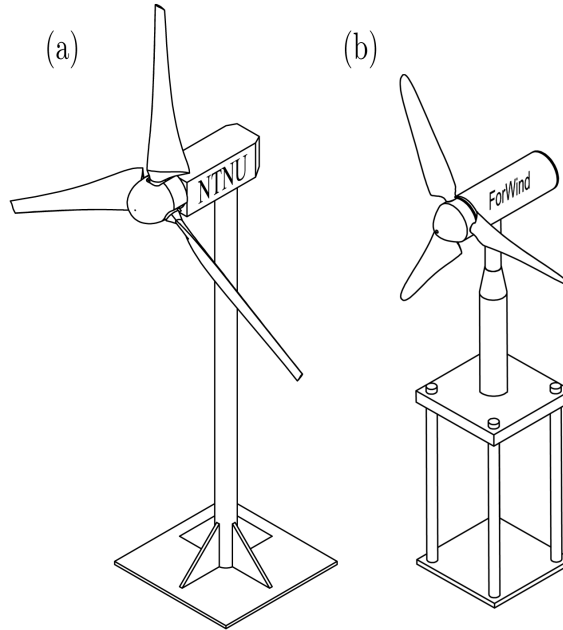


**Figure 1.** Technical drawings of the NTNU turbine (a) and the ForWind turbine (b).

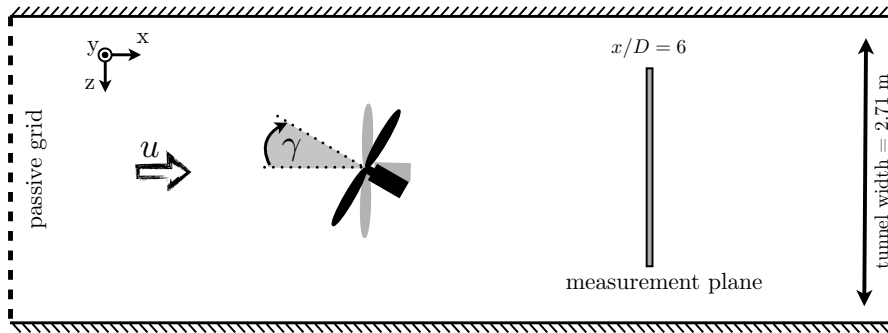


**Figure 2.** Sketch of the setup, top view.  $D$  denotes the respective rotor diameter as listed in Table 1.

velocity was  $u_{ref,ForWind} = 7.5 \text{ m s}^{-1}$  and  $TI = 0.05$ . In both cases,  $u(t)$  was homogeneous within  $\pm 6\%$  and the  $TI$  within  $\pm 3\%$  on a vertical line at the turbine's position.

In this study we consider two-dimensional cuts through the wake, normal to the main flow direction at a downstream distance of  $x/D = 6$  for both turbines as illustrated in Figure 2. Data were acquired using a Dantec FiberFlow two-component Laser Doppler Anemometer (LDA) system, recording the  $u$ - and  $v$ -component of the flow. The accuracy is stated to be 0.04% by the manufacturer. During turbine operation, the LDA system was traversed in the  $yz$ -plane, normal to the main flow direction. Each measured plane consists of 357 points, 21 in  $z$ -direction ranging from  $-D$  to  $+D$  and 17 points in  $y$ -direction, ranging from

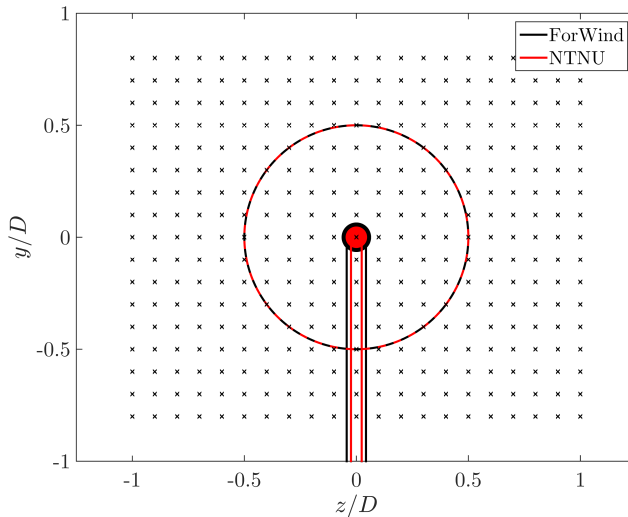


**Figure 3.** Non-dimensional measurement grid behind the rotor for  $\gamma = 0^\circ$ . The respective contours of the turbines are shown in black (ForWind) and red (NTNU). For the NTNU turbine, the wind tunnel walls are located at  $z/D = \pm 1.5$  and  $y/D = \pm 1.0$ , for the ForWind turbine at  $z/D = \pm 2.34$  and  $y/D = \pm 1.56$ .

$-0.8D$  to  $0.8D$ , see Figure 3. The resulting distance separating two points of measurement is thus  $0.1D$ . For one location,  $5 \times 10^4$  samples were recorded, resulting in time series of varying lengths of approximately 30 s. As can be seen, the NTNU turbine has a slimmer tower and nacelle relative to its rotor diameter when compared to the ForWind turbine. The grid of physically measured values was interpolated to a grid of  $401 \times 321 \approx 129000$  points for further analyses. The distance between the interpolated grid points is therewith reduced to  $0.005D$ . Natural neighbor interpolation is used, resulting in a smoother approximation of the distribution of data points (Amidror, 2002).

## 2.2 Wake center detection

In order to quantify the lateral wake position, we compute the power of a potential downstream turbine as described by Schottler et al. (2017b). A similar approach was shown by Vollmer et al. (2016). We define the potential power of a downstream turbine to be

$$P^* = \sum_{i=1}^{10} \rho A_i \langle u_i(t) \rangle_{A_i,t}^3. \quad (1)$$

The rotor area is divided in ten ring segments.  $A_i$  is the area of the  $i^{\text{th}}$  ring segment and  $\langle u_i(t) \rangle_{A_i,t}$  denotes the temporally and spatially averaged velocity in mean flow direction within the area  $A_i$ .  $P^*$  is estimated for 50 different hub locations in the range  $-0.5D \leq z \leq 0.5D$ , at hub height. We define the horizontal wake center as the  $z$ -position resulting in the minimum of  $P^*$ . The procedure is illustrated in Figure 4.

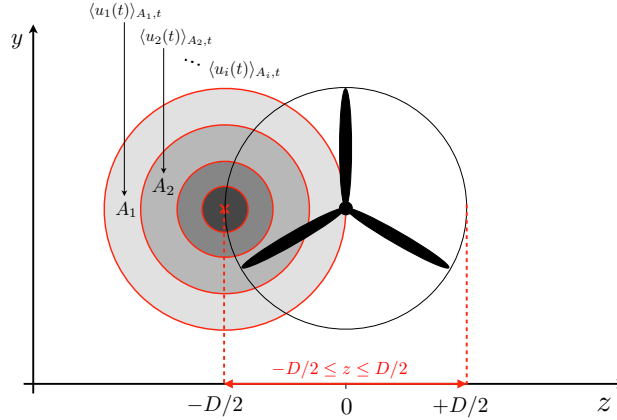


**Figure 4.** Illustration of the wake center detection method. The hub of a potential downstream turbine is located at the red  $\times$ .  $\langle u_i(t) \rangle_{A_{i,t}}$  is the spatially and temporarily averaged  $u$ -component of the velocity. The potential power  $P^*$  is calculated for each ring segment and then added up. This procedure is repeated for 50 horizontal hub locations  $\times$ , while the position resulting in the lowest value of  $P^*$  is interpreted as wake center.

### 2.3 Examined quantities

The turbulent kinetic energy (TKE) is defined by the fluctuations of the three velocity components as

$$k = 0.5 (\langle u'(t)^2 \rangle + \langle v'(t)^2 \rangle + \langle w'(t)^2 \rangle) , \quad (2)$$

where  $u'(t)$  is the fluctuation around the mean of  $u(t)$  so that

$$5 \quad u(t) = \langle u(t) \rangle + u'(t) . \quad (3)$$

For brevity, we write  $\langle u \rangle$  instead of  $\langle u(t) \rangle$ . As the third flow component  $w$  was not recorded, we assume  $\langle w'(t)^2 \rangle \approx \langle v'(t)^2 \rangle$  so that Equation (2) becomes

$$k = 0.5 (\langle u'(t)^2 \rangle + 2\langle v'(t)^2 \rangle) , \quad (4)$$

which will be used in further analyses. Measurements were performed validating this approximation.

10 For a thorough analysis of the wake turbulence, we examine velocity changes during a time lag  $\tau$  and refer to them as *velocity increments*,

$$u_\tau(t) := u(t) - u(t + \tau) . \quad (5)$$

Investigating their probability density function (PDF) allows for scale-dependent analyses of turbulent flows, including all higher order moments of  $u_\tau$ , hence all structure functions of order  $n$ ,  $S_\tau^n = \langle u_\tau^n \rangle$  of a velocity time series (Frisch, 1995). The  
15 impact of certain properties of velocity increment PDFs on wind turbines is to date a widely discussed topic in wind energy

research, see (e.g. Mücke et al., 2011; Milan et al., 2013; Berg et al., 2016; Schottler et al., 2017c). For more details, we refer the reader to Morales et al. (2012) or Schottler et al. (2017c). Following Chillà et al. (1996), the shape parameter

$$\lambda^2(\tau) = \frac{\ln(F(u_\tau)/3)}{4} \quad (6)$$

is used to quantify the shape of the distribution  $p(u_\tau)$ .  $F(u_\tau)$  is the flatness of the time series of velocity increments,

$$5 \quad F(u_\tau) = \frac{\langle (u_\tau - \langle u_\tau \rangle)^4 \rangle}{\langle u_\tau^2 \rangle^2}. \quad (7)$$

Equation (6) becomes zero for a Gaussian distribution, larger values correspond to broader, more heavy-tailed PDF.  $\lambda^2$  is of practical relevance as it provides an analytical expression for the shape of  $p(u_\tau)$ . A discussion about the interpretation is given in Section 4. In this analysis, we compute  $\lambda^2$  for time scales  $\tau$  that relate to the rotor diameter  $D$  of the respective turbine. Using Taylor's hypothesis of frozen turbulence (Mathieu and Scott, 2000), the length scale  $r = D$  is converted to the time  
10 scales  $\tau$ ,

$$\tau = r/\langle u \rangle = D/\langle u \rangle, \quad (8)$$

whereas  $\langle u \rangle$  refers to the respective time series, resulting in varying values of  $\tau$  within a wake.

In order to compute  $u_\tau(t)$  using Equation (5), evenly spaced data are needed. The procedure applied to uniformly re-sample the non-uniform LDA data is described in Appendix A. The approach results in a constant sampling rate for each wake.

## 15 3 Results

### 3.1 The non-yawed wakes

At first, we investigate wakes without yaw misalignment,  $\gamma = 0^\circ$ . Figure 5 shows the contour plots of the velocity component in mean flow direction  $\langle u \rangle/u_{ref}$  for both turbines, respectively,  $6D$  downstream. The velocity deficits behind both turbines show a circular shape as expected, exceeding the rotor area, indicating a slight wake expansion. For both wakes, the minimum velocity  
20 is  $\langle u \rangle/u_{ref} = 0.64$ . Besides those general similarities, some differences are apparent. Both graphs show the tower wake, which is pronounced stronger for the ForWind turbine. This can be explained by the larger tower diameter relative to the rotor diameter as shown in Figure 3. Similarly, the four poles the ForWind turbine is placed on (cf. Figure 1) are likely to enhance this effect. Figure 5 also reveals that the wake behind the ForWind turbine is slightly displaced vertically towards the ground. This effect can be linked to the tower wake, creating an uneven vertical transport of momentum as recently demonstrated by Pierella and  
25 Saetran (2017). Next, the NTNU wake shows areas of velocities exceeding  $\langle u \rangle/u_{ref} = 1.1$  at the edges of the velocity deficit, especially in the corners of the contour plot. Very likely, this is a blockage effect as the measurement plane is significantly larger for the NTNU turbine. This results in a higher blockage ratio (13% for the NTNU rotor, 5.4% for the ForWind rotor). As suggested by Chen and Liou (2011), blockage effects are expected for a cross-sectional blockage ratio exceeding 10% when using model wind turbines, which is confirmed here. In order to better compare both contour plots, values exceeding

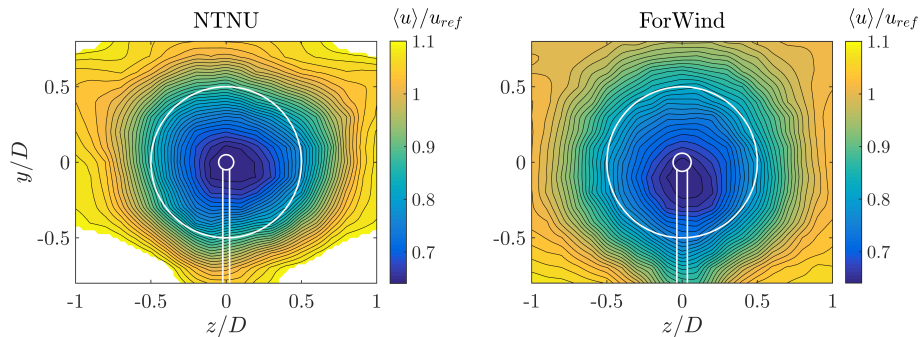


**Figure 5.**  $\langle u \rangle / u_{ref}$  at  $\gamma = 0^\circ$  for the NTNU turbine (left) and ForWind turbine (right). The white lines indicate the contours of the respective turbine. Values exceeding  $\langle u \rangle / u_{ref} = 1.1$  are masked.

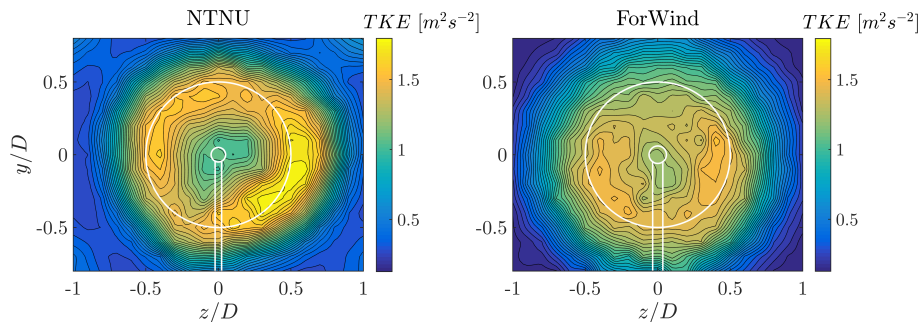


**Figure 6.** Turbulent kinetic energy (TKE) in  $m^2 s^{-2}$  according to Equation (4) for  $\gamma = 0^\circ$ . Left: NTNU turbine, right: ForWind turbine.

$\langle u \rangle / u_{ref} = 1.1$  are masked.

To further analyze the wake flows, Figure 6 shows the contour plots of the turbulent kinetic energy (TKE) behind both turbines. The contours of the TKE appear as a circular shape, slightly larger than the rotor area. Behind the NTNU rotor, an outer ring of high TKE values appears more pronounced than in the center region. This observation is significantly less distinct for the ForWind turbine. The differences of the pronounced ring arise most likely from the different blade geometries. The airfoil of the NTNU turbine (NREL S826) has higher lift coefficients for the relevant angles of attack and Reynolds numbers compared to the ForWind rotor (SD7003 airfoil). A comparison of both airfoils is given in Schottler et al. (2017b). As a result, larger pressure differences between suction and pressure side of the blades are expected, resulting in more pronounced tip vortices shed from the NTNU rotor. Although those are already decayed at  $x/D = 6$  (Eriksen and Krogstad, 2017), the tip vortices are likely to be the origin for a pronounced TKE at blade tip locations for behind the NTNU rotor.

Further increasing in complexity and completeness of the wakes' stochastic description, Figure 7 shows the contour plots of the shape parameter  $\lambda^2$  behind both turbines. The length scale  $\tau$  is related to the rotor diameter  $D$  of the respective turbine. The scale is transferred from space to time using Taylor's Hypothesis, cf. Equation (8). In both cases, the contours of  $\lambda^2$  show a circular ring, whose diameter is significantly larger than the rotor diameter. In order to quantify the qualitative shapes of the

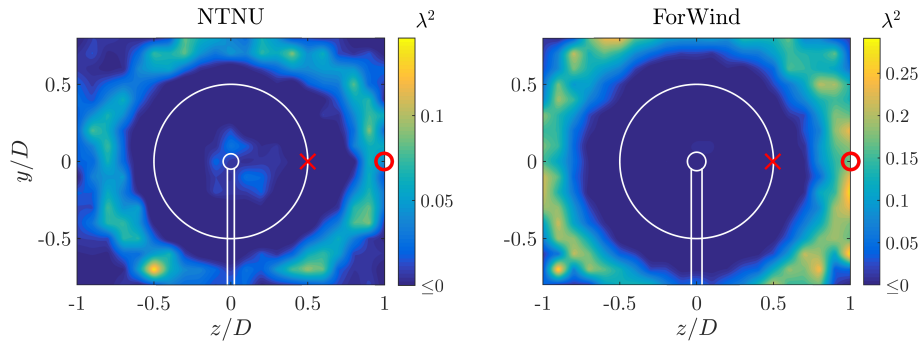


**Figure 7.**  $\lambda^2$  for both turbines at  $\gamma = 0^\circ$ . The time scales  $\tau$  correspond to the length scale of the rotor diameter, cf. Equation (8). The red markings  $\times$  and  $\circ$  show measurement positions for which  $p(u_\tau)$  were calculated as shown in Figure 8. Left: NTNU turbine, right: ForWind turbine. Note the different scaling.

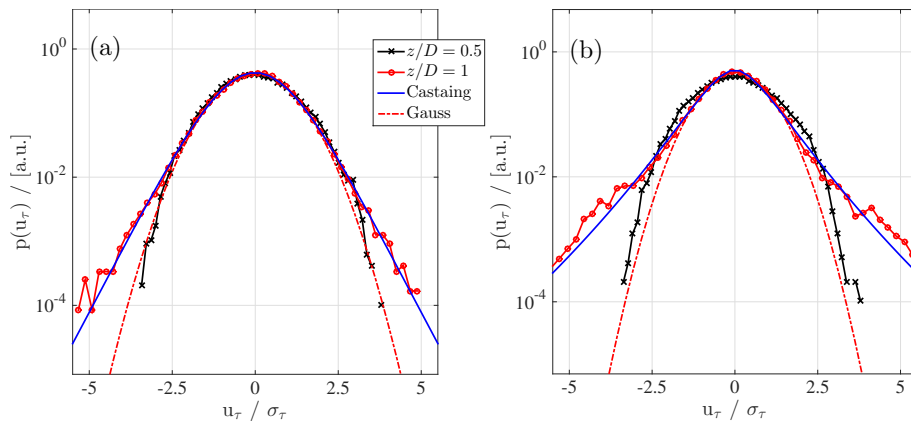


**Figure 8.**  $p(u_\tau)$  of the time series at two measurement position,  $(y = 0, z = D/2)$  and  $(y = 0, z = D)$  corresponding to the red marks in Figure 7. (a): NTNU turbine, (b): ForWind turbine, both at  $\gamma = 0^\circ$ . The time scales  $\tau$  are related to the length scales of rotor diameters by Taylor's Hypothesis using Equation (8). For  $z/D = 1$  (red curve) the Castaing distribution is shown with  $\lambda_{NTNU}^2 = 0.046$  and  $\lambda_{ForWind}^2 = 0.17$  (Castaing et al., 1990). A Gaussian fit is added to guide the eye.

contours shown in Figure 7, Figure 8 shows the increment PDFs of the respective time series,  $p(u_\tau)$ , at the positions indicated by the red marks ( $\circ/\times$ ) in Figure 7.  $u_\tau$  is normalized by the standard deviation,  $\sigma_\tau$ , for better visual comparison. As shown in black, the positions behind the rotor tips, where  $\lambda^2 \approx 0$ , reveal increment PDFs very close to a Gaussian distribution, which holds for both turbines. For  $z = D$ , which lies within the ring of large  $\lambda^2$  values,  $p(u_\tau)$  strongly deviates from a Gaussian, showing a heavy-tailed distribution. Figure 8 further shows  $p(u_\tau)$  based on the model proposed by Castaing et al. (1990). Those distributions were evaluated based on the  $\lambda^2$  values computed by Equation (6) at  $z = D$ , visualizing exemplary how well the distributions' shapes are grasped by  $\lambda^2$ . Our results show that, depending on the examined quantity, different radial wake regions are of interest. To compare the varying spatial extensions of the three quantities' significant areas, Figure 9 shows

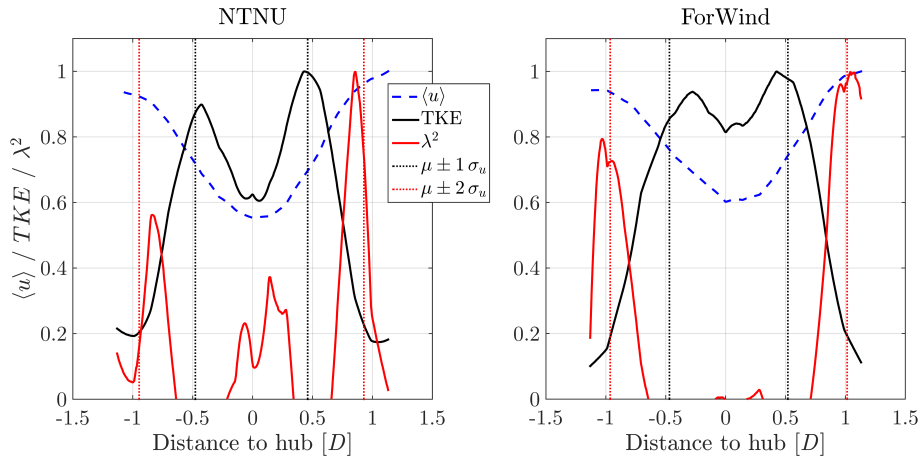


**Figure 9.** Diagonal cuts on the line  $y = z$  through the contour plots for  $\gamma = 0^\circ$ . Values are normalized to their respective maximum. The vertical dotted lines mark  $\mu \pm 1\sigma_u$  (black) and  $\mu \pm 2\sigma_u$  (red) of a Gaussian fit through the velocity deficit shown in blue.

diagonal cuts through the respective contour plots for the non-yawed cases along the line  $y = z$ . The area of pronounced TKE approximately coincides with the rotor area. The notable peaks are separated by  $\approx 0.86 D$  (NTNU) and  $\approx 0.77 D$  (ForWind), respectively, being significantly less pronounced behind the ForWind rotor as previously described. Clearly, the  $\lambda^2$  peaks span a much larger distance, being approximately  $1.7 D$  (NTNU) and  $2.0 D$  (ForWind). At their location, the velocity deficit has recovered to  $\geq 90\%$  of the free stream velocity in all cases. Thus, for a thorough description of wind turbine wakes, a much larger radial area is of interest as compared to a description restricted to mean values and the turbulent kinetic energy as often done in literature and wake models. An approximation of the lateral extension of high TKE and  $\lambda^2$  values based on a Gaussian fit through the velocity deficit is given by  $\mu \pm 1\sigma_u$  and  $\mu \pm 2\sigma_u$ , respectively, with  $\mu$  being the mean value and  $\sigma_u$  the standard deviation of the fit. For illustration, the dotted lines in Figure 9 mark the respective locations. It is shown that the radial areas of TKE and  $\lambda^2$  can be related in this way to the velocity deficit. To get a feeling of the impact on potential downstream turbine, Figure 10 compares  $p(u_\tau)$  in absolute terms at a free stream position,  $y/D = 0.8$ ,  $z/D = 1$ , and at a position featuring high  $\lambda^2$  values,  $y/D = 0$ ,  $z/D = 1$ , exemplary for the ForWind turbine. It becomes clear that velocity increments exceeding  $3ms^{-1}$  occur much more frequent within the ring of high  $\lambda^2$  values than in three free stream. Hereby we show that this radial position of the wake features significantly different flows than the free stream. To compare more visually, Figure 11 shows the corresponding time series  $u_\tau(t)$ . Clearly, the spiky signature of extreme events become obvious in Figure 11(b), confirming that no free stream condition is reached at  $z/D = 1$ .

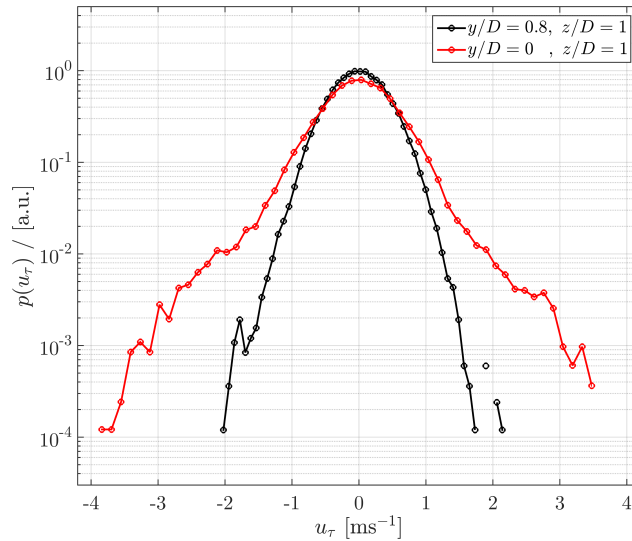


**Figure 10.**  $p(u_\tau)$  of the free stream at  $y/D = 0.8, z/D = 1$  and of  $y/D = 0, z/D = 1$ , exemplary for the ForWind turbine.

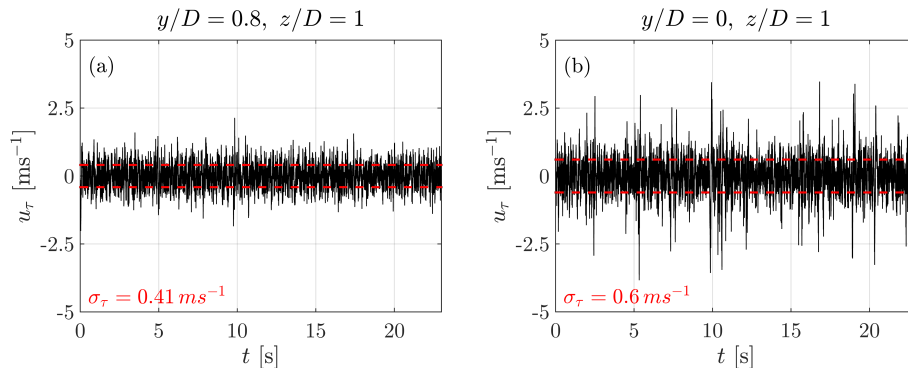


**Figure 11.** Time series of increments  $u_\tau(t)$  for the positions  $y/D = 0.8, z/D = 1$  (free stream, a) and  $y/D = 0, z/D = 1$ . The standard deviations  $\sigma_\tau$  are indicated in red.

### 3.2 Wakes during yaw-misalignment

During a yaw misalignment of  $\gamma = \pm 30^\circ$ , the velocity deficits behind both rotors are deflected and deformed as shown in Figure 12 by the contours of the main flow component  $\langle u \rangle / u_{ref}$ .

The wake is deflected sideways behind both turbines, whereas the lateral direction is dependent on the yaw angle's sign.

- 5 This is expected due to a lateral thrust component of the rotor as a result of yaw misalignment, which has been observed and described in numerous studies including (Medici and Alfredsson, 2006; Jiménez et al., 2010; Vollmer et al., 2016; Trujillo et al., 2016). The deflection of the velocity deficit is quantified using the approach described in Section 2.2, the results are listed in Table 2 including the resulting wake skew angles.



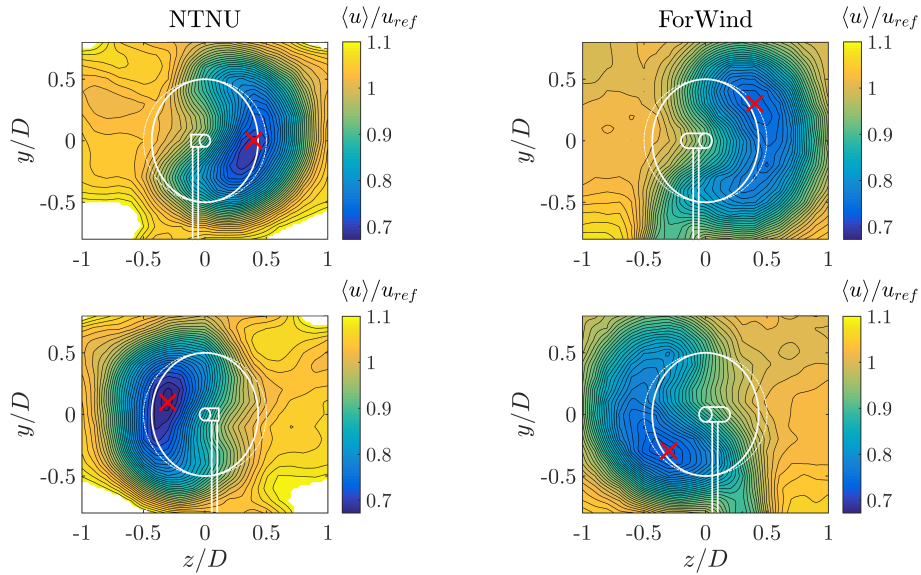


**Figure 12.**  $\langle u \rangle / u_{ref}$  during yaw misalignment. Top row:  $\gamma = -30^\circ$ , bottom row:  $\gamma = 30^\circ$ . Left column: NTNU turbine, right column: ForWind turbine. The solid white lines indicate the contours of the respective turbine, while the dashed lines denote the rotor area without yaw misalignment. The red  $\times$  marks the position of minimum measured velocity  $\langle u \rangle$ . Values exceeding 1.1 are masked for better comparison.

**Table 2.** Wake center location as computed by the approach described in Section 2.2 with corresponding skew angles.

Turbine	Yaw angle [ $^\circ$ ]	Wake center [ $D$ ]	Skew angle [ $^\circ$ ]
NTNU	30	-0.28	$\approx -2.6$
NTNU	-30	0.32	$\approx 3.0$
ForWind	30	-0.38	$\approx -3.6$
ForWind	-30	0.38	$\approx 3.6$

As Table 2 shows, the skew angles behind the ForWind turbine are equal apart from their sign for both directions of yaw misalignment. The NTNU rotor however, shows slightly different deflection angles for  $\gamma = 30^\circ$  and  $\gamma = -30^\circ$ , which is likely caused by blockage effects, that play a more significant role for the NTNU rotor due to the larger blockage ratio. This can also be seen in Figure 12, where speed-up effects are visible in the corners. In Schottler et al. (2017b), where the same setup was used<sup>1</sup>, the skew angle for the NTNU rotor decreased from  $x/D = 3$  to  $x/D = 6$ , which is a further indication for wall effects due to blockage, especially during yaw misalignment. Furthermore, both values show smaller angles as for the ForWind turbine.

In Figure 12, minimum  $\langle u \rangle$  values are marked, showing a vertical transport of momentum in all cases. For  $\gamma = 30^\circ$ , the wake is moved upwards behind the NTNU turbines, and downwards behind the ForWind rotor. Directions are reversed for

<sup>1</sup>In Schottler et al. (2017b), the quantification was carried out for a sheared inflow. Other aspects of the setup were equal.

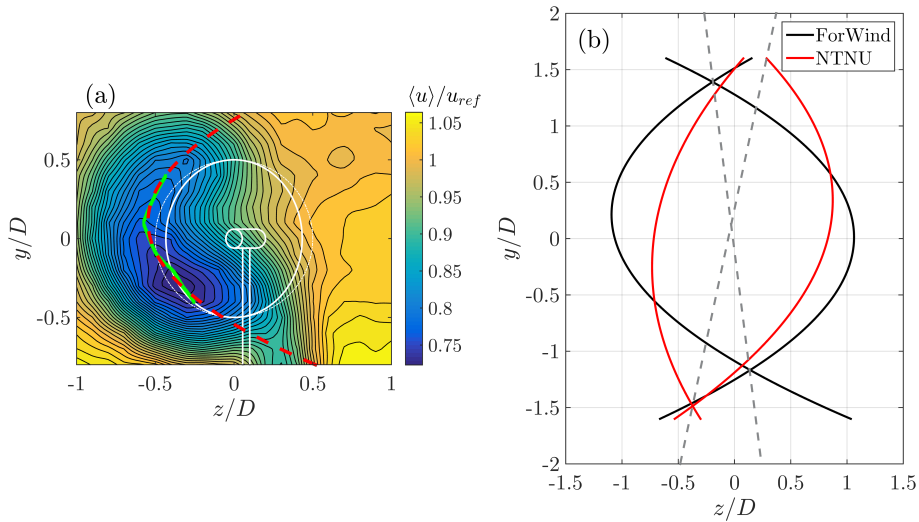


**Figure 13.** (a): Example of parameterizing the curled shape of the velocity deficit. The green markings show minimal velocities of a polynomial function used to fit the interpolated data points in a horizontal line,  $y = \text{const.}$ . The red, dashed line shows a quadratic fit based on the green markings. (b): Visualization of the curled shapes of the velocity deficits. For both turbines, the cases  $\gamma = \pm 30^\circ$  are shown. Dashed lines show a visualization of the wakes tilt, connecting the respective intersections of the curves.

$\gamma = -30^\circ$ . Similar observations have been made by Bastankhah and Porté-Agel (2016). The vertical transport is related to an interaction of a wake’s rotation with the tower shadow/ground. Our results isolate this effect, as the direction of vertical transport is opposite comparing both turbines having an opposite direction of rotation. The fact that the vertical transport is stronger behind the ForWind rotor further supports this explanation as the tower wake is more pronounced due to the larger tower diameter and the structure the turbines is placed on.

A deformation of the velocity deficit to a curled “kidney” shape is observed for both turbines during yaw misalignment, whereas it is slightly more pronounced behind the ForWind turbine. The curled shape behind a wind turbine model in yaw has previously been observed by Howland et al. (2016) using a drag disc of 30 mm diameter and by Bastankhah and Porté-Agel (2016) using a rotating turbine model of 150 mm diameter. Figure 12 confirms these findings on two further scales. For a better comparison of the curled shape of the velocity deficit during yaw misalignment, we apply the following parametrization, exemplary shown in Figure 13(a) for the ForWind turbine at  $\gamma = 30^\circ$ : data points of horizontal cuts through the wake,  $\langle u \rangle_{y=\text{const.}}$ , are fitted by a polynomial. The procedure is repeated for values of  $y$  ranging from  $-0.4D$  to  $0.4D$ . The positions of the polynomials’ minima (green marks), are fitted by a quadratic function (red line). Figure 13(b) shows the comparison of both turbines for  $\gamma = \pm 30^\circ$ . As already seen in Figure 12, the wakes behind the ForWind turbine are deflected further and the curled shape is pronounced stronger, which can be attributed to blockage effects. Figure 13(b) also shows that the wakes behind both turbines are slightly tilted. Looking at the black curves (ForWind turbine), an asymmetry can be noticed as the curves are tilted towards the left, while the red curves are tilted towards the right. This is illustrated by the gray, dashed lines in Figure 13(b) which connect the points of intersection for  $\gamma = \pm 30^\circ$ . Similar asymmetries have been observed by Bastankhah and Porté-Agel (2016) for

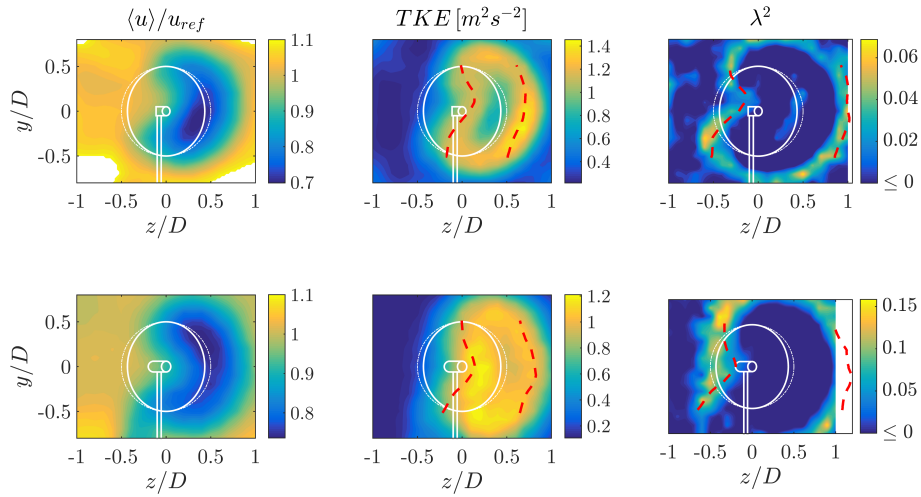


**Figure 14.**  $\langle u \rangle / u_{ref}$  (left column), TKE (center column) and  $\lambda^2$  (right column) for  $\gamma = -30^\circ$  behind the NTNU turbine (top row) and the ForWind turbine (bottom row). The time scale for  $\lambda^2$  corresponds to the length scale of the rotor diameter. The red marks show the approximation of the respective parameter's radial extension based on  $\mu \pm 1\sigma_u$  (TKE, middle column) and  $\mu \pm 2\sigma_u$  ( $\lambda^2$ , left column) as described in Section 3.1.

positive and negative yaw angles, which is explained by an interaction of a wake's rotation with the tower wake and the ground. By using turbines of opposite rotation direction, we can attribute the asymmetries in vertical transport and the tilt in opposite direction for  $\gamma = \pm 30^\circ$  to the rotation of rotor and wake. Not shown in detail here, the same effect was observed for different inflow conditions and other downstream distances, using the same setup and methods as in this study.

- 5 Adding TKE and  $\lambda^2$  contours during yaw misalignment, Figure 14 shows all three examined quantities, exemplary at a yaw misalignment of  $\gamma = -30^\circ$ , for both turbines. The shapes of the TKE contours are deformed similarly as for  $\langle u \rangle$ . A curled shape evolves and the differences between both turbines as described for  $\gamma = 0^\circ$  are still notable during yaw misalignment. Similarly, the circular rings of high  $\lambda^2$  values are deformed to a curled shape at  $\gamma = \pm 30^\circ$ . Thus, the general effect of heavy-tailed increment PDFs surrounding the velocity deficits in a wake is stable against yaw misalignment and the resulting inflow
- 10 variations at the rotor blades. Further, this finding is confirmed in Large Eddy Simulations (LES) performed at the Universidad de la República, Uruguay, shown in Appendix B. Therewith, it is found to be a general effect as it is observed for all wakes considered, independent of yaw misalignment or turbine design. The red markings in Figure 14 show the approximation of the radial extension of the TKE and  $\lambda^2$  based on  $\mu \pm 1\sigma_u$  and  $\mu \pm 2\sigma_u$ .  $\mu$  and  $\sigma_u$  correspond to Gaussian fits of the velocity deficits at various horizontal cuts ( $y = \text{const.}$ ) from  $y/D = -0.5$  to  $y/D = 0.5$ . It is shown that the methods results in quite good first
- 15 order approximations, also during yaw misalignment.

## 4 Discussion

In this study the characterization of yawed and non-yawed wind turbine wakes is investigated and extended by taking into account a further turbulence measure, namely the intermittency parameter  $\lambda^2$ . We find heavy-tailed distributions of velocity increments in a ring area *surrounding* the velocity deficit and areas of high TKE in a wind turbine wake. Thus, the definition of a wake width strongly depends on the quantities taken into account as the ring area features significantly different statistics than the free stream. The heavy-tailed distributions are the statistical description of large velocity changes over given time scales and are transferred to turbines in terms of loads and power output. This has been shown experimentally (Schottler et al., 2017c), numerically (Mücke et al., 2011) and in a field study by Milan et al. (2013). Consequently, our findings should be considered in wind farm layout optimization approaches, where a wake's width is a crucial parameter for radial turbine spacing. As layouts are being optimized regarding power and loads, the latter might be significantly affected by taking into account intermittency and the resulting increased wake width. Possibly, the ring of non-Gaussian velocity increments is a result of instable flow states, where the flow switches between a wake and free stream state. Behind a rotor, the wake characteristics dominate the flow. Outside the wake, free stream properties are dominant. In the transition zone, a switching between both flow states is believed to result in heavy-tailed velocity increments and therewith high  $\lambda^2$  values. Generally,  $\lambda^2$  will be larger for smaller scales  $\tau$ , which is a known feature of turbulence (Frisch, 1995).

Care should be taken when interpreting  $\lambda^2$  as an indicator for an increment PDF's shape. Here, we use the shape parameter as qualitative indicator. For a more quantitative analysis, one has to consider the increment PDF of a time series directly. This is done in Figure 8 exemplary for chosen points, however, in order include all time series of a wake, using  $\lambda^2$  allows for a much better visualization and comparison.

20

Figure 14 shows that the velocity deficit is deflected laterally during yaw misalignment, so that a potential in-line downstream turbine would exhibit a power increase as more undisturbed flow hits the rotor area at  $z/D \approx -0.5$ . Looking at the  $\lambda^2$  contours however shows, that areas of non-Gaussian velocity increments are now deflected onto the rotor area. This becomes important when assessing the applicability of active wake steering approaches, as a gain in power has to be balanced with a potential load increase, affecting maintenance costs and the lifetime of turbines overall.

It should be noted that it is to date not clear to what extent high TKE levels and intermittent force data are affecting common ways of fatigue and extreme load calculations. This important aspects needs to be addressed in future works. Possibly, it strongly depends on details such as considered time scales. In our opinion, it is likely that non-Gaussian inflow is linked to drive train, gear box or pitch systems failures, especially because those inflow characteristics are not accounted for in standard models used in the design process.

30

The velocity deficit in mean flow direction  $\langle u \rangle$  deforms to a curled "kidney" shape during yaw misalignment. Consequently, horizontal cuts through the wake are insufficient when characterizing wakes behind yawed rotors, resulting in misleading and incomplete conclusions when quantifying wake deflections by yaw misalignment. The parametrization of the wake's curl

shown in Figure 13 should not be interpreted as quantification. Instead, we use the described approach to better compare multiple curled wakes as done in Figure 13(b). Our analyses include the velocity deficit in mean flow direction, the turbulent kinetic energy and the shape parameter  $\lambda^2$ . The turbulence intensity in the wake revealed very comparable results as the TKE, which is why we restrict our analyses to the TKE.

5 Besides the lateral deflection, a vertical transport of the velocity deficit is observed for both turbines during yaw misalignment. Using counter-rotating turbines, this effect could be attributed to the wake's rotation and its interaction with the tower wake. In full scale scenarios, the ground, wind shear and rotor tilt would further contribute to the effect. For potential floating turbines, a pitch motion will deflect the wake upwards, see Rockel et al. (2014). This vertical deflection will interact with the vertical transport shown in Figure 12. Consequently, the direction of yaw misalignment is believed to be of importance when applying  
10 the concept of wake steering to wind farm controls. This confirms findings by Fleming et al. (2014a) and Schottler et al. (2017a), reporting an asymmetric power output of a two-turbine case with respect to the upstream turbine's angle of yaw misalignment. One should bear in mind that the inflow turbulence intensities are different regarding both turbines. We want to point out that the influence of inflow turbulence on the wake deflection is studied in Bartl et al. (2018), showing no significant effects.

## 15 5 Conclusions

This work shows an experimental investigation of wind turbine wakes, using two different model wind turbines. The analyses include the main flow component, the turbulent kinetic energy and two-point statistics of velocity increments, quantified by the shape parameter  $\lambda^2$ . Yaw angles of  $\gamma = \{0^\circ, \pm 30^\circ\}$  are considered at a downstream distance of  $x/D = 6$ .

Generally, the results of  $\langle u \rangle$ , the TKE and  $\lambda^2$  compare well for both model turbines. Minor differences could be ascribed to the  
20 more prominent blockage (12.8% vs 5.4%) in the NTNU setup, confirming findings by Chen and Liou (2011) even for wake velocity measurements, who state blockage effects can be neglected for a blockage ratio  $\leq 10\%$ .

An outer ring of heavy-tailed velocity increments surrounds the velocity deficit and areas of high TKE in a wind turbine wake. The wake features significantly non-Gaussian velocity increment distributions in those areas, where the velocity deficit recovered nearly completely. For  $\gamma = 0^\circ$ , the ring has a diameter of approximately  $1.7D - 2D$ , depending on the turbine. Based  
25 on a Gaussian fit through the velocity deficit, the radial location of intermittent increments can be approximated by  $\mu \pm 2\sigma_u$ , making a wake considerably wider when taking two-point statistics into account. This observation becomes important in wind farm layout optimization and active wake steering approaches through yaw misalignment.

During yaw misalignment, the circular shape of a wake is deformed to a curled kidney-shape. A method for parameterizing the curl-shape was introduced. Further, the lateral wake deflection was quantified, resulting in skew angles of  $\pm 3.6^\circ$  at  $\pm 30^\circ$   
30 for the smaller rotor and  $3.0^\circ$  and  $-2.6^\circ$  for the larger rotor. Furthermore, vertical momentum transport in the wake during yaw misalignment was observed. The direction of vertical transport is dependent on the direction of yaw misalignment. Using counter-rotating turbines, the effect could be attributed to an interaction of a wake's rotation with the tower wake in this study.

*Data availability.* The experimental data set is available upon request.

## **Appendix A: Data preprocessing**

In order to study intermittency using the shape parameter  $\lambda^2$ , uniformly sampled data are needed when applying Equation (5). As the LDA measurement result in non-uniformly sampled data points, appropriate preprocessing is necessary. In the following, the procedure is described that results in uniformly sampled data points. It is exemplary applied to the data of an arbitrarily chosen wake.

The time separating two samples of a time series is  $\Delta t$ . For one time series,  $(\Delta t)^{-1}$  is plotted for all samples in Figure A1 (a). The corresponding histogram is shown in Figure A1 (b). The point corresponding to 40 % of all events is marked by the red dashed line and is referred to as  $F_S$ . In this example,  $F_S \approx 1.17$  kHz.

10 This procedure is repeated for all 357 time series contained in one plane of measurement. Figure A2 shows  $F_S$  for all time series, with the mean value indicated. The mean value of all  $F_S$  values in one plane will be used as sampling frequency to re-sample the time series in one plane uniformly, an exemplary result is shown in Figure A3. Data points are interpolated linearly onto a vector of uniformly spaced instants defines by the new sampling rate  $\langle F_S \rangle$ . It should be noted that the analyses of velocity increments were performed for different constant sampling rates without showing any significant effect on the results.

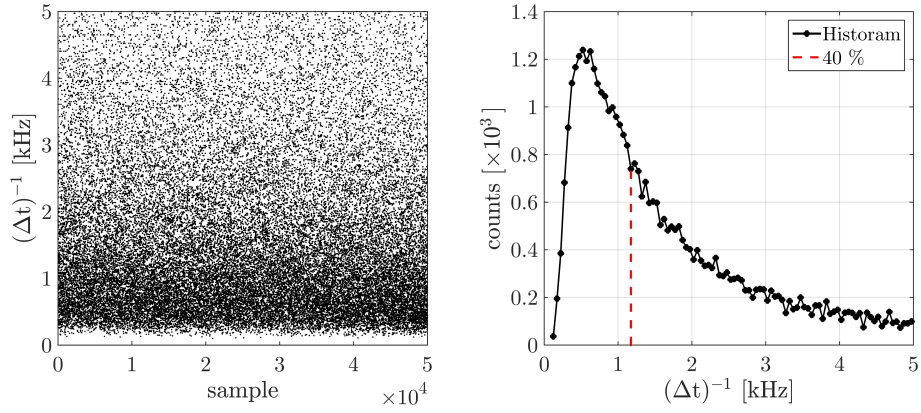


**Figure A1.**  $(\Delta t)^{-1}$  for all samples (a) with the respective histogram (b), where the maximum value is marked by the red, dashed line.

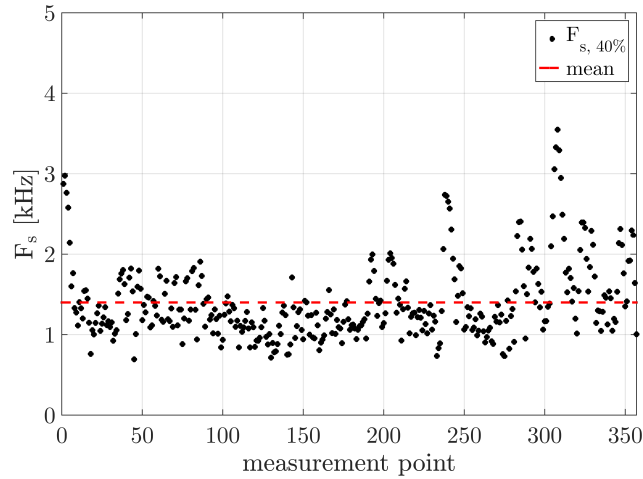


**Figure A2.**  $F_S$  for all 357 time series of one wake, the mean value is indicated in red, being  $\langle F_S \rangle = 1.4$  kHz.

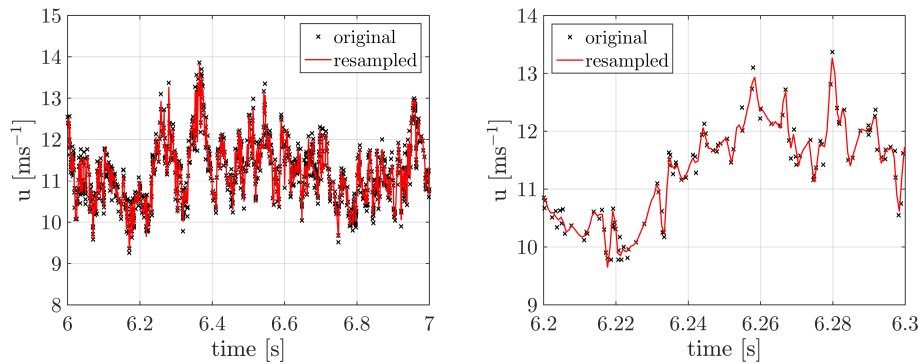


**Figure A3.** Examples of resampling the raw data  $u(t)$  uniformly with  $\langle F_S \rangle = 1.4$  kHz.

## Appendix B: LES simulations

Within the scope of the *blind test 5* project, LES simulations of the ForWind turbine in a very comparable setup were performed, where the inflow features a vertical shear as opposed to the experiments shown in this paper. The incompressible flow solver `caffa3d.MBRi` as described by Mendina et al. (2014) and Draper et al. (2016) was used to obtain the results shown in Figure 5 B1. The turbine was modeled by actuator lines. The top row shows  $x/D = 3$ ,  $x/D = 6$  is shown beneath. The contours of  $\langle u \rangle / u_{ref}$  and  $\lambda^2$  reveal very similar results compared to the experimental data. Qualitatively, it can be concluded that the outer ring of high  $\lambda^2$  values and thus heavy-tailed distributions of velocity increments, that surrounds the velocity deficit of a wake, can be correctly predicted in LES simulations.



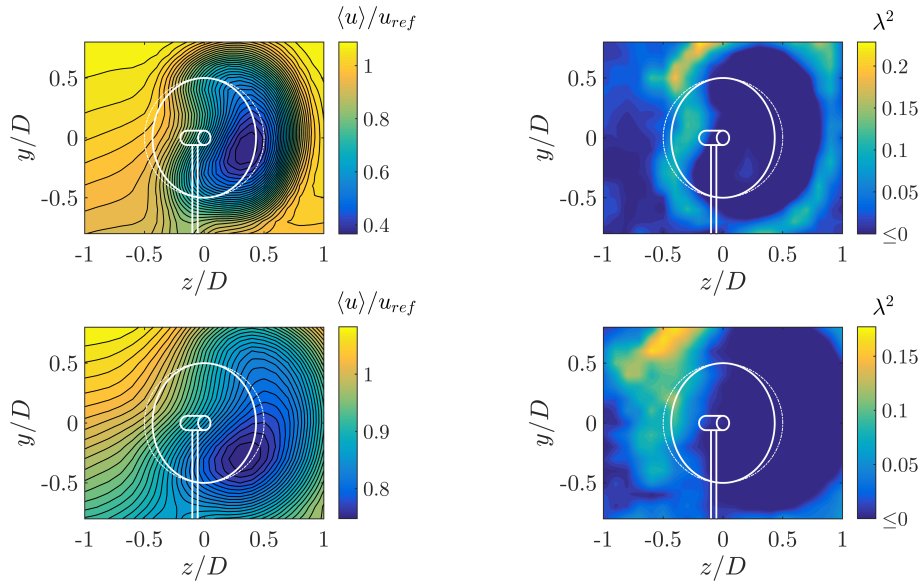


**Figure B1.** LES data of the wakes  $3D$  (top row) and  $6D$  (bottom row) behind the ForWind turbine at  $\gamma = 30^\circ$ . In contrast to the experiments presented in this paper, the inflow in the LES domain features a vertical shear with comparable turbulence intensity. The time scales of  $\tau$  for the  $\lambda^2$  calculations correspond to the length scale of the rotor diameter.

*Competing interests.* The authors declare no competing interests.

*Acknowledgements.* The authors thank Marín Draper and Andrés Guggeri, Universidad de la República, Uruguay for performing the LES simulation and providing the data. Parts of this project is funded by the Ministry for Science and Culture of Lower Saxony through the funding initiative «Niedersächsisches Vorab». The authors also thank the Reiner Lemoine Foundation for further funding.

## References

- Abdulrahim, A., Anik, E., and Uzol, O.: Experimental Investigation of the Wake Flow Field of a Model Wind Turbine Rotor with Tip Injection, in: 33rd Wind Energy Symposium, January, pp. 1–10, American Institute of Aeronautics and Astronautics, Reston, Virginia, <https://doi.org/10.2514/6.2015-0498>, <http://arc.aiaa.org/doi/10.2514/6.2015-0498>, 2015.
- 5 Amidror, I.: Scattered data interpolation methods for electronic imaging systems: a survey, *Journal of Electronic Imaging*, 11, 157, <https://doi.org/10.1117/1.1455013>, <http://electronicimaging.spiedigitallibrary.org/article.aspx?doi=10.1117/1.1455013>, 2002.
- Bak, C., Zahle, F., Bitsche, R., and Kim, T.: The DTU 10-MW reference wind turbine, *Danish wind power . . .*, <http://orbit.dtu.dk/services/downloadRegister/55645274/>, 2013.
- Barthelmie, R. J., Pryor, S., Frandsen, S. T., Hansen, K. S., Schepers, J., Rados, K., Schlez, W., Neubert, A., Jensen, L., and Neckelmann, S.:  
10 Quantifying the impact of wind turbine wakes on power output at offshore wind farms, *Journal of Atmospheric and Oceanic Technology*, 27, 1302–1317, 2010.
- Bartl, J. and Sætran, L.: Blind test comparison of the performance and wake flow between two in-line wind turbines exposed to different turbulent inflow conditions, *Wind Energy Science*, 2, 55–76, <https://doi.org/10.5194/wes-2-55-2017>, <http://www.wind-energ-sci-discuss.net/wes-2016-31/http://www.wind-energ-sci.net/2/55/2017/>, 2017.
- 15 Bartl, J., Mühle, F., Schottler, J., Sætran, L., Peinke, J., Adaramola, M., and Hölling, M.: Experiments on wind turbine wakes in yaw: Effects of inflow turbulence and shear, *Wind Energy Science*, submitted, 2017.
- Bartl, J., Mühle, F., Schottler, J., Sætran, L., Peinke, J., Adaramola, M., and Hölling, M.: Wind tunnel experiments on wind turbine wakes in yaw: Effects of inflow turbulence and shear, *Wind Energy Science Discussions*, pp. 1–22, <https://doi.org/10.5194/wes-2017-59>, <https://www.wind-energ-sci-discuss.net/wes-2017-59/>, 2018.
- 20 Bastankhah, M. and Porté-Agel, F.: Experimental and theoretical study of wind turbine wakes in yawed conditions, *Journal of Fluid Mechanics*, 806, 506–541, <https://doi.org/10.1017/jfm.2016.595>, <http://stacks.iop.org/1742-6596/625/i=1/a=012014>, 2016.
- Berg, J., Natarajan, A., Mann, J., and Patton, E. G.: Gaussian vs non-Gaussian turbulence: impact on wind turbine loads, *Wind Energy*, 17, n/a–n/a, <https://doi.org/10.1002/we.1963>, <http://doi.wiley.com/10.1002/we.1963>, 2016.
- Boettcher, F., Renner, C., Waldl, H. P., and Peinke, J.: On the statistics of wind gusts, *Boundary-Layer Meteorology*, 108, 163–173,  
25 <https://doi.org/10.1023/A:1023009722736>, 2003.
- Bottasso, C. L., Campagnolo, F., and Petrović, V.: Wind tunnel testing of scaled wind turbine models: Beyond aerodynamics, *Journal of Wind Engineering and Industrial Aerodynamics*, 127, 11–28, 2014.
- Burton, T., Sharpe, D., Jenkins, N., and Bossanyi, E.: *Wind Energy Handbook*, John Wiley and Sons, 2001.
- Campagnolo, F., Petrović, V., Bottasso, C., and Croce, A.: Wind tunnel testing of wake control strategies, in: *Proceedings of the American Control Conference*, vol. 2016-July, <https://doi.org/10.1109/ACC.2016.7524965>, 2016.
- 30 Castaing, B., Gagne, Y., and Hopfinger, E. J.: Velocity probability density functions of high Reynolds number turbulence, *Physica D: Non-linear Phenomena*, 46, 177–200, [https://doi.org/10.1016/0167-2789\(90\)90035-N](https://doi.org/10.1016/0167-2789(90)90035-N), 1990.
- Chen, T. and Liou, L.: Blockage corrections in wind tunnel tests of small horizontal-axis wind turbines, *Experimental Thermal and Fluid Science*, 35, 565–569, <https://doi.org/10.1016/j.expthermflusci.2010.12.005>, <http://dx.doi.org/10.1016/j.expthermflusci.2010.12.005http://linkinghub.elsevier.com/retrieve/pii/S0894177710002438>, 2011.
- 35 Chillà, F., Peinke, J., and Castaing, B.: Multiplicative Process in Turbulent Velocity Statistics: A Simplified Analysis, *Journal de Physique II*, 6, 455–460, <https://doi.org/10.1051/jp2:1996191>, 1996.

- Draper, M., Guggeri, A., and Usera, G.: Validation of the Actuator Line Model with coarse resolution in atmospheric sheared and turbulent inflow, *Journal of Physics: Conference Series*, 753, <https://doi.org/10.1088/1742-6596/753/8/082007>, 2016.
- Eriksen, P. E. and Krogstad, P. Å.: Development of coherent motion in the wake of a model wind turbine, *Renewable Energy*, 108, 449–460, <https://doi.org/10.1016/j.renene.2017.02.031>, <http://dx.doi.org/10.1016/j.renene.2017.02.031>, 2017.
- 5 España, G., Aubrun, S., Loyer, S., and Devinant, P.: Wind tunnel study of the wake meandering downstream of a modelled wind turbine as an effect of large scale turbulent eddies, *Journal of Wind Engineering and Industrial Aerodynamics*, 101, 24–33, 2012.
- Fleming, P., Gebraad, P. M., Lee, S., Wingerden, J.-W., Johnson, K., Churchfield, M., Michalakes, J., Spalart, P., and Moriarty, P.: Simulation comparison of wake mitigation control strategies for a two-turbine case, *Wind Energy*, 2014a.
- Fleming, P., Annoni, J., Shah, J. J., Wang, L., Ananthan, S., Zhang, Z., Hutchings, K., Wang, P., Chen, W., and Chen, L.: Field test  
10 of wake steering at an offshore wind farm, *Wind Energy Science*, 2, 229–239, <https://doi.org/10.5194/wes-2-229-2017>, <http://www.wind-energ-sci-discuss.net/wes-2017-4/><https://www.wind-energ-sci.net/2/229/2017/>, 2017.
- Fleming, P. a., Gebraad, P. M. O., Lee, S., van Wingerden, J. W., Johnson, K., Churchfield, M., Michalakes, J., Spalart, P., and Moriarty, P.: Evaluating techniques for redirecting turbine wakes using SOWFA, *Renewable Energy*, 70, 211–218, <https://doi.org/10.1016/j.renene.2014.02.015>, 2014b.
- 15 Frisch, U.: *Turbulence : the legacy of A.N. Kolmogorov*, vol. 1, Cambridge university press, <https://doi.org/10.1017/S0022112096210791>, 1995.
- Gebraad, P. M. O., Teeuwisse, F. W., van Wingerden, J. W., Fleming, P. A., Ruben, S. D., Marden, J. R., and Pao, L. Y.: Wind plant power optimization through yaw control using a parametric model for wake effects-a CFD simulation study, *Wind Energy*, 19, 95–114, <https://doi.org/10.1002/we.1822>, <http://doi.wiley.com/10.1002/we.1822>, 2014.
- 20 Howland, M. F., Bossuyt, J., Martínez-Tossas, L. A., Meyers, J., and Meneveau, C.: Wake structure in actuator disk models of wind turbines in yaw under uniform inflow conditions, *Journal of Renewable and Sustainable Energy*, 8, <https://doi.org/10.1063/1.4955091>, <http://dx.doi.org/10.1063/1.4955091>, 2016.
- Jiménez, Á., Crespo, A., and Migoya, E.: Application of a LES technique to characterize the wake deflection of a wind turbine in yaw, *Wind energy*, 13, 559–572, 2010.
- 25 Jonkman, J. M., Butterfield, S., Musial, W., and Scott, G.: *Definition of a 5-MW reference wind turbine for offshore system development*, National Renewable Energy Laboratory Golden, CO, 2009.
- Liu, L., Hu, F., Cheng, X.-L., and Song, L.-L.: Probability Density Functions of Velocity Increments in the Atmospheric Boundary Layer, *Boundary-Layer Meteorology*, 134, 243–255, <https://doi.org/10.1007/s10546-009-9441-z>, 2010.
- Mathieu, J. and Scott, J.: *An introduction to turbulent flow*, Cambridge University Press, 2000.
- 30 Medici, D. and Alfredsson, P.: Measurements on a wind turbine wake: 3D effects and bluff body vortex shedding, *Wind Energy*, 9, 219–236, 2006.
- Mendina, M., Draper, M., Kelm Soares, A. P., Narancio, G., and Usera, G.: A general purpose parallel block structured open source incompressible flow solver, *Cluster Computing*, 17, 231–241, <https://doi.org/10.1007/s10586-013-0323-2>, 2014.
- Milan, P., Wächter, M., and Peinke, J.: Turbulent character of wind energy, *Physical Review Letters*, 110, 1–5, <https://doi.org/10.1103/PhysRevLett.110.138701>, 2013.
- 35 Morales, A., Wächter, M., and Peinke, J.: Characterization of wind turbulence by higher-order statistics, *Wind Energy*, 15, 391–406, <https://doi.org/10.1002/we.478>, 2012.

- Mücke, T., Kleinhans, D., and Peinke, J.: Atmospheric turbulence and its influence on the alternating loads on wind turbines, *Wind Energy*, 14, 301–316, <https://doi.org/10.1002/we.422>, <http://dx.doi.org/10.1002/we.422>, 2011.
- Pierella, F. and Saetran, L.: Wind tunnel investigation on the effect of the turbine tower on wind turbines wake symmetry, *Wind Energy*, 17, 657–669, <https://doi.org/10.1002/we.2120>, <http://onlinelibrary.wiley.com/doi/10.1002/we.1608/fullhttp://doi.wiley.com/10.1002/we.2120>, 2017.
- 5 Rockel, S., Camp, E., Schmidt, J., Peinke, J., Cal, R. B., and Hölling, M.: Experimental study on influence of pitch motion on the wake of a floating wind turbine model, vol. 7, <https://doi.org/10.3390/en7041954>, 2014.
- Rockel, S., Peinke, J., Hölling, M., and Cal, R. B.: Wake to wake interaction of floating wind turbine models in free pitch motion: An eddy viscosity and mixing length approach, *Renewable Energy*, 85, 666–676, <https://doi.org/10.1016/j.renene.2015.07.012>, 2016.
- 10 Schottler, J., Hölling, A., Peinke, J., and Hölling, M.: Wind tunnel tests on controllable model wind turbines in yaw, 34th Wind Energy Symposium, p. 1523, 2016.
- Schottler, J., Hölling, A., Peinke, J., and Hölling, M.: Brief Communication : On the influence of vertical wind shear on the combined power output of two model wind turbines in yaw, pp. 1–5, 2017a.
- Schottler, J., Mühle, F., Bartl, J., Peinke, J., Adaramola, M. S., Saetran, L., and Hölling, M.: Comparative study on the wake deflection behind yawed wind turbine models, *Journal of Physics: Conference Series*, 854, 012 032, <https://doi.org/10.1088/1742-6596/854/1/012032>, <http://stacks.iop.org/1742-6596/854/i=1/a=012032?key=crossref.c68d7b8d172fd82bbd89c31f05132338>, 2017b.
- 15 Schottler, J., Reinke, N., Hölling, A., Whale, J., Peinke, J., and Hölling, M.: On the impact of non-Gaussian wind statistics on wind turbines – an experimental approach, *Wind Energy Science*, 2, 1–13, <https://doi.org/10.5194/wes-2-1-2017>, [http://www.wind-energ-sci-discuss.net/wes-2016-24/\\$\delimitator"026E30F\\\$nhttp://www.wind-energ-sci.net/2/1/2017/](http://www.wind-energ-sci-discuss.net/wes-2016-24/$\delimitator), 2017c.
- 20 Trujillo, J.-J., Seifert, J. K., Würth, I., Schlipf, D., and Kühn, M.: Full field assessment of wind turbine near wake deviation in relation to yaw misalignment, *Wind Energy Science Discussions*, pp. 1–17, <https://doi.org/10.5194/wes-2015-5>, <http://www.wind-energ-sci-discuss.net/wes-2015-5/>, 2016.
- van Kuik, G. A. M., Peinke, J., Nijssen, R., Lekou, D., Mann, J., Sørensen, J. N., Ferreira, C., van Wingerden, J. W., Schlipf, D., Gebraad, P., Polinder, H., Abrahamsen, A., van Bussel, G. J. W., Sørensen, J. D., Tavner, P., Bottasso, C. L., Muskulus, M., Matha, D., Lindeboom, H. J., Degraer, S., Kramer, O., Lehnhoff, S., Sonnenschein, M., Sørensen, P. E., Küenneke, R. W., Morthorst, P. E., and Skytte, K.: Long-term research challenges in wind energy – a research agenda by the European Academy of Wind Energy, *Wind Energy Science*, 1, 1–39, <https://doi.org/10.5194/wes-1-1-2016>, <http://www.wind-energ-sci.net/1/1/2016/>, 2016.
- 25 Vollmer, L., Steinfeld, G., Heinemann, D., and Kühn, M.: Estimating the wake deflection downstream of a wind turbine in different atmospheric stabilities: an LES study, *Wind Energy Science*, 1, 129–141, <https://doi.org/10.5194/wes-1-129-2016>, <http://www.wind-energ-sci.net/1/129/2016/>, 2016.
- 30